8-2022

Mesenchymal Stem Cell Fate on Carbon-Based Biomaterials: Implications for Bone Regeneration and Repair

Amber Frances MacDonald
amacdon4@vols.utk.edu

To the Graduate Council:

I am submitting herewith a dissertation written by Amber Frances MacDonald entitled "Mesenchymal Stem Cell Fate on Carbon-Based Biomaterials: Implications for Bone Regeneration and Repair." I have examined the final electronic copy of this dissertation for form and content and recommend that it be accepted in partial fulfillment of the requirements for the degree of Doctor of Philosophy, with a major in Comparative and Experimental Medicine.

Madhu, S, Dhar, Major Professor

We have read this dissertation and recommend its acceptance:

Madhu Dhar, David Anderson, Shawn Bourdo, Thomas Masi, Andrew Gross

Accepted for the Council:

Dixie L. Thompson

Vice Provost and Dean of the Graduate School

(Original signatures are on file with official student records.)

Mesenchymal Stem Cell Fate on Carbon-Based Biomaterials: Implications for Bone Regeneration and Repair

A Dissertation Presented for the
Doctor of Philosophy
Degree
The University of Tennessee, Knoxville

Amber F. MacDonald
August 2022

ACKNOWLEDGEMENTS

I first, and always, want to thank God for bringing me this far in my education. Being the first in my family to graduate from college, I have many times doubted myself, but I have learned along the way that with God all things are possible.

I next want to thank my mentor, Dr. Madhu Dhar, and my committee, Dr. David Anderson, Dr. Thomas Masi, Dr. Andrew Gross, and Dr. Shawn Bourdo. I also acknowledge my previous mentor when working on my Master of Science degree, Dr. Jay Whelan, who paved my foundation of science and research.

A special thank you to the laboratory of Dr. Madhu Dhar, who always supported me throughout this journey: Dr. Lisa Amelse, Dr. Steven Newby, Dr. Austin Bow, and Meaghan Harley-Troxell.

Among Bluefield College professors who inspired me to attend graduate school, I acknowledge: Dr. Doug Minnix, Dr. Scott Bryan, Dr. Rob Merritt, Ewell Vernon, and the late, Dr. Marsha Mead.

Last, I acknowledge my parents: my mother, Macel MacDonald and my father, the late Jack P. MacDonald. Without my mother's support, I would not have come to Tennessee. She taught me to value education when she did not have one of her own. As for my father, he would be beyond proud.

ABSTRACT

Treatment of traumatic bone injuries is actively relying on tissue engineering strategies for bone repair. In this research, we examined mesenchymal stem cells (MSCs) on carbon-based biomaterials, with a long-term goal of bone regeneration. MSCs are adult-derived cells that can differentiate into osteoblasts, and simultaneously stimulate osteoprogenitors in bone tissue environments. More specifically, carbon-based materials such as graphene, provides a bone-specific microenvironment for MSCs to undergo ossification. However, although the goal is new bone formation, signaling mechanisms to achieve bone differentiation can vary. Therefore, the over-arching focus of this research was to evaluate the osteogenic behavior of MSCs in the presence of graphene materials.

This dissertation contains five chapters. In chapter 1, we reviewed 3D-printing graphene scaffolds for tissue engineering. However, developing graphene scaffolds first requires understanding of MSC activity on graphene surfaces. Therefore, chapter 2 examines MSCs cultured on a low-oxidized graphene substrate, which supported several genes important to bone differentiation. In chapter 3, we examined the gene expression profile of MSCs cultured on graphene oxide (GO) and reduced graphene oxide (rGO), the major graphene derivatives. We found that genetic activity of MSCs was robustly upregulated on rGO in comparison to GO substrates. Afterwards, we shifted to the *in vivo* ovariectomized (OVX) rodent model, which mimics post-menopause osteoporosis. In chapter 4, we found that MSCs derived from OVX rats lacked normal bone mineralization in comparison to MSCs derived from healthy rats. RNA sequencing analysis revealed that several genes important to bone differentiation were not upregulated in OVX-MSCs. We therefore postulated that osteoporotic-bone injuries could be restored by delivering healthy MSCs on a graphene scaffold. In chapter 5, we created a mandible defect in both sham and OVX animals, which was filled with a 3D-printed rGO-MSC construct. After 60 days, we found similar bone regenerative potential between sham and OVX animals, suggesting that rGO-MSC scaffolds provides an optimal signaling environment within osteoporotic bone.

Overall, this information is a foundation of the cell signaling network between MSCs and graphene materials. Future models could potentially use graphene materials to prime MSCs into the bone differentiation pathway prior to *in vivo* applications.

TABLE OF CONTENTS

Chapter I: 3D-Printing Graphene Scaffolds for Tissue Engineering..……1

Abstract……..3
Introduction……4

Material Fabrication Techniques……...4

Material Properties for Tissue Engineering……...5

Carbon Nanomaterials……6
Graphene Nanomaterials……....6

3D-Printing of Graphene Scaffolds……....7
.
Graphene and Bone Regeneration……..……..9

Toxicity Challenges of Graphene Materials……..……12

Future Perspective and Conclusions…….……..……15

References…….…....16

Appendix…….……23

Chapter II: Genetic Profiling of Human Bone Marrow and Adipose Tissue-derived Mesenchymal Stem Cells Reveals Differences in Osteogenic Signaling Mediated by Graphene……..……..……27

Abstract……29
Introduction……..31

Materials and Methods……..……34
Tissue Procurement, Cell Isolation and Characterization……34
Preparation and Characterization of Graphene……35
Osteogenesis and Mineralization of MSCs……35
RNA Isolation……..……36
Human Osteogenesis PCR Array……37

Results……39

Discussion……48

Conclusion……..……55

References……57

Appendix……65

Chapter III: Comparing Osteogenic Gene Expression of Human MSCs on rGO and GO Substrates……76

Abstract……77
Introduction……78

Methods……79
Preparation of rGO and GO……79
Cell Culture on rGO and GO……79
RNA Isolation……79
Human Osteogenesis PCR Array……79

Results……80

Discussion……86

Conclusion……89

References……90

Appendix……93

Chapter IV: Next Generation RNA Sequencing Reveals Genetic Alterations during Chemically Induced Bone Differentiation of Mesenchymal Stem Cells from a Post-Menopause Animal Model ……98

Abstract……100
Introduction……101

Methods……102
Animal Model……102
Serum CTX-1/TRAP5b Ratio……103
Isolation of Rat MSCs……103
Characterization of Rat MSCs……104
Differentiation of Rat MSCs into Osteoblasts……104
RNA Extraction……104
RNA Sequencing……105

Results……106

Discussion……110

Conclusion……114

References……115

Appendix……119

Chapter V: 3D-Printed rGO Constructs Support Mandibular Defects in an Osteoporotic Rodent Model……133

Abstract……134
Introduction……135

Methods……135
Cell Isolation and Culture……135
Scaffold Design and Preparation……136
DiI Staining……136
Animal Model……137
Surgical Procedure……137
Micro-CT……138
Histology……139

Results……140

Discussion……141

Conclusions……144

References……145

Appendix……148

VITA……155

LIST OF FIGURES

Figure 1.1. The process of a computer-controlled 3D-printing system…….23

Figure 1.2. The structure of graphene, graphene oxide, and reduced graphene oxide……....24

Figure 1.3. Images of 3D-printed graphene scaffolds……....25

Figure 2.1. Atomic force microscopy……..65

Figure 2.2. Osteogenic differentiation assay……...66

Figure 2.3. Assessment of RNA quality……..…67

Figure 2.4. The effects of LOG on RUNX2, BGLAP, and ALPL gene expressions……68

Figure 2.5. Differentially expressed genes when AD-MSCs and BM-MSCs undergo osteogenesis on LOG……69

Figure 2.6. Propeller plots depicting potential gene targets and corresponding protein interactions……..70

Figure 2.7. Immunofluoresence assays…….71

Figure 4.1. (A) Final weight of control and ovariectomized animals on the day of sacrifice. **(B)** The ratio of C-telopeptide of type I collagen (CTX-1) to tartrate-resistant acid phosphate isoform 5b (TRAP5B) in serum protein collected from animals on the day of sacrifice……..119

Figure 4.2. Expression of MSC markers……..…120

Figure 4.3. Osteogenic differentiation assay……..121

Figure 4.4. The percentage of upregulated genes related to adhesion, extracellular matrix, and growth factors……..123

Figure 4.5. The percentage of upregulated genes related to Wnt/β-Catenin signaling …….124-125

Figure 4.6. The percentage of upregulated genes related to cell differentiation/signaling …….126

Figure 4.7. The percentage of upregulated genes related to mineralization…..……..127

Figure 4.8. The percentage of upregulated metallopeptidase (bone remodeling) genes …….128

Figure 5.1. 3D printing of scaffolds and cell attachment……..……146

Figure 5.2. Diagram of surgical procedure……...147

Figure 5.3. (A) Average consumption of low calcium diet between sham (n=6) and OVX (n=6) animals prior to surgery **(B)** Final weight of sham and OVX animals on the day of surgery and sacrifice……148

Figure 5.4. Average percentage of newly formed bone within the former defects as measured by Micro-CT……....150

Figure 5.5. Representative von Kossa-MacNeal's tetrachrome staining images of mandibular defects treated with rGO-cell constructs in sham and OVX animals……...151

Figure 5.6. Representative Masson's Trichrome staining images of mandibular defects treated with rGO-cell constructs in sham and OVX animals……..152

CHAPTER I:

3D-PRINTING GRAPHENE SCAFFOLDS FOR TISSUE ENGINEERING

This chapter is in submission to *Pharmaceutics* by Amber F. MacDonald:

Amber F. MacDonald[a], Meaghan E. Harley-Troxell[a], Steven D. Newby[a], Madhu S. Dhar[a]

Affiliations:
[a] College of Veterinary Medicine, University of Tennessee, Knoxville, Tennessee 37996, USA

Corresponding author:
Madhu Dhar, Ph.D., College of Veterinary Medicine, University of Tennessee, 2407 River Dr. Knoxville, Tennessee 37996, USA; email: mdhar@utk.edu; phone: 865-974-5703; Fax: 865-974-5773

ABSTRACT

Graphene-based materials have recently gained attention for regenerating various tissue defects including bone, nerve, cartilage, and muscle. However, graphene constructs have mainly been studied as 2-dimensional (2D) substrates when biological organs are within a 3-dimensional (3D) environment. Therefore, developing 3D graphene scaffolds is the next clinical standard, yet most have been fabricated as foams which limits control of consistent morphology and porosity. To overcome this issue, 3D-printing technology is revolutionizing tissue engineering, due to its speed, accuracy, reproducibility, and overall ability to personalize treatment whereby scaffolds are printed to the exact dimensions of a tissue defect. However, 3D-printed graphene scaffolds have surprisingly only begun within the last few years. In this review, we briefly discuss the different fabrication techniques for 3D scaffolds, the novelty of graphene materials, and its application for 3D printing in tissue engineering. This information will help tissue engineering scientists to study graphene-based materials as 3D-printing candidates for traumatic tissue injuries.

INTRODUCTION

There is a growing demand to engineer functional tissue using 3-dimensional (3D) biological substitutes. Tissue engineering is a field composed of many scientific disciplines including biomedical engineering, cellular molecular biology, material science, and biochemistry. The concept of tissue engineering evolved in the 1990s whereby stem cells and materials could be implanted *in vivo* to restore injured tissues.[1] Since all tissues are derived from stem cells, conventional tissue engineering strategies have centered around stem cell-based therapies. However, preparation of exogenous stem cells is a process that can take months—between isolation, expansion, characterization, and ensuring quality control (i.e. lack of viral contamination). Even then, stem-cell therapies are not FDA approved and have many concerns over regulation and safety. Alternatively, scaffold materials that both supports a defect and attracts endogenous stem cells to the injured area is the future of tissue engineering. Graphene materials have recently gained attraction for engineering new tissues. However, most graphene studies have relied on 2-dimensional (2D) surfaces, when native tissues are within a 3-dimensional (3D) environment. Hence, the fabrication of novel biomaterials (including graphene derivatives) relies on 3D construction, which is feasible through many techniques, including 3D printing. In this review, we briefly discuss the different fabrication techniques for 3D scaffolds, the novelty of graphene materials, and its applications for 3D printing in tissue engineering.

Material Fabrication Techniques

There are several fabrication techniques to produce scaffolds which are categorized as either conventional or rapid prototyping (as summarized by Eltom et al., 2019).[2] Conventional techniques include electrospinning, solvent casting, leaching, and phase separation.[3-5] However, with conventional techniques there is poor control over architecture, pore network, and pore size, drawing challenges to consistently reproduce scaffolds with identical parameters.[6, 7] On the other side, rapid prototyping uses computer software, more commonly known as computer aided design (CAD), which designs scaffolds for production by a 3D printing machine. Figure 1.1 describes the steps between software design and the final product of a 3D printed scaffold. The

design is then converted into a digital format using a Standard Tessellation Language (STL) file format. Using the STL file, the software 'slices' the design into multiple layers which are given values that denote how each layer is printed. The next step is G-coding which communicates to the machine on how to move during printing. These files are then transferred to a 3D printer and the material of interest is subsequently printed into a 3D construct. A common 3D printing technique is fused deposition modeling (FDM) whereby a thermoplastic polymer is melted above its glass transition temperature, extruded through the printer's nozzle, and re-solidifies upon cooling on the print bed.[8-10]

In tissue engineering, fabricating 3D printed scaffolds has gained much popularity due to its speed, accuracy, reproducibility, and overall ability to personalize treatment whereby scaffolds are printed to the exact dimensions of a tissue defect. Most recently, there is new excitement of 3D printing directly into a patient's body. For example, when diseased tissues are extracted during surgery, 3D printing technology could directly fill the open cavity for faster recovery and less pain post-surgery.

Material Properties for Tissue Engineering

Although 3D printing is revolutionizing personalized treatment, the material needed to print the scaffold is a long-debated topic that depends on the desired tissue source to be repaired. These materials range anywhere from hydrogels, to nanoparticles, bio-metals, bio-ceramics, and bio-degradable polymers. There are many material properties that influence tissue regeneration such as porosity, wettability, stiffness, strength, elasticity, biodegradability, and cytocompatibility. Materials must withstand water absorption without rapid deterioration, but yet gradually degrade overtime so that (1) new tissue can independently function and (2) does not create a permanent implant. Additionally, many tissues require a 3D porous structure that allows blood vessel infiltration for constant nutrient transport as cells are building new tissue.[11] The optimal pore size may vary between different tissues, but typically ranges between 100 – 500 µm.[12, 13] Thus, fabricating a porous structure is one variable that can be conveniently controlled by 3D printing technology.

Finally, tissue engineering materials must demonstrate properties of cytocompatibility, including cell adherence, cell viability, and stimulation of cell differentiation. Studies have shown that 3D scaffolds support cytocompatibility better than their 2D control counterpart.[14-17] Overall, testing 3D-printed structures *in vitro* is a stronger predictor of tissue reconstruction outcomes before implanting *in vivo*. Since carbon nanomaterials are under study for treating multiple tissue defects, the remainder of this review will specifically focus on graphene materials and its future as a 3D-printed scaffold.

Carbon Nanomaterials

Carbon-based nanomaterials have gained attention for treating various tissue defects.[18-20] Nanomaterials refers to extremely small particles (generally 1-100 nm by dimension), but yet are very strong and light weight. Particles <100 nm Ø can enter cells, while those smaller than 40 nm Ø can enter the nucleus.[21] Intracellular components such as DNA, RNA, proteins, and lipids control the cell's behavior and yet are very small nanometer structures. Therefore, nano-sized materials provide an attractive environment for optimal cell function.

Graphene Materials

Carbon nanomaterials include fullerenes, carbon nanotubes, nanodiamonds, carbon-based quantum dots, and graphene.[22] Of these, graphene is relatively the youngest and has rapidly emerged as a superstar due to its versatile properties in several industries from electronics to sporting equipment and medical science. Graphene comes from graphite, a gray crystalline mineral from rocks of South America, Asia, and North America. Graphite is easily recognized as the material within pencils, traditionally (but mistakenly) referred to as "pencil lead". Graphite's 3D structure contains millions of graphene layers that are weakly attached by van der Waals forces.[23] The carbon atoms are arranged as flat hexagonal rings, with each carbon covalently bonded to three other carbons. But despite its long-time existence, a graphene monolayer was not isolated until 2004 by Professor Sir Andre Geim and Professor Sir Kostya Novoselov, University of Manchester. Since then, graphene materials have been extensively studied in

engineering several tissues including bone [24-27], cartilage [28-30], nerve [31-33], skin [34-36], and heart.[37-39]

However, pristine graphene is hydrophobic (due to hydrocarbon contamination following air exposure) thereby lacking dispersion in water which raises aggregation/toxicity concerns when delivered *in vivo*.[40] This limitation has resulted in functionalizing graphite with hydrophilic groups that contain oxygen. Interestingly, this idea was discovered long before graphene when Benjamin Brodie oxidized graphite in 1859.[41] Today, the most common method to oxidize graphite is by the Hummer's method (a mixture of sulfuric acid, sodium nitrate, and potassium permanganate). Hereafter, graphite oxide layers are sonicated in water to exfoliate monolayers of graphene oxide (GO) (Figure 1.2). Unlike graphene, GO disperses in water and contains hydroxyl, carboxyl, and epoxy functional groups which allows it to be combined with other polymers or molecules for therapeutic use.[42] Typically, the C:O ratio in GO is 3 to 1.[43] However, its exact composition can vary depending on the graphite source and the method of production. Therefore, the amount and distribution of oxygen functional groups may be similar, but not identical between GO sources.[44]

Other functionalized graphene derivatives include reduced graphene oxide (rGO) which is an intermediate structure between graphene and GO, since it partially restores some properties lost during oxidation.[6] When GO is chemically reduced, some (but not all) of the oxygen functional groups are removed (Figure 1.2). In other words, rGO is the result of *reducing* the number of oxygen atoms found in GO. Reports estimate that rGO restores 80% sp^2 structure with the remaining sp^3 bonds derived from residual oxygen (C:O = 13:1).[8] The reason for deoxygenation is because GO desensitizes the natural conductivity property of pristine graphene.[45] Therefore, rGO is favored for treating cardiac and neural defects as these tissues generate electrical signals.

3D Printing of Graphene Scaffolds

Many tissue engineering studies have fabricated graphene materials as a 2D cell culture substrate, with results indicating cell compatibility by enhancing gene/protein expression, proliferation, and differentiation.[46-49] However, a 2D cell culture substrate

does not mimic the natural 3D tissue microenvironment. Developing 3D graphene scaffolds is the new standard, but most have been fabricated as foams which limits control of morphology such as the number of pores, the pore diameter, and the fiber diameter.[50-55] Therefore, it is attractive to 3D print graphene scaffolds, but surprisingly this progress has only begun within the last few years. The flaky texture of graphene resembles sawdust particles, and consequently is not a candidate for direct printing. Therefore, graphene materials must be incorporated within an ink that sustains a 3D shape upon printing.

Zhu et al., 2015 was one of the first studies to successfully 3D-print a graphene construct with a microlattice architecture (as shown in Figure 1.3B).[56] The intent of this study was to overcome the challenge of developing a printable graphene-based ink while maintaining its intrinsic properties (i.e. large surface area, stiffness, etc.). An ink gel was developed by combining a GO suspension with a silica filler which was loaded and extruded via the three-axis positioning stage (ABL 9000, Aerotech). The resulting construct was a porous GO aerogel with a cube like structure. However, it should also be noted that aerogels are very low-density solids and easily collapse. But nonetheless, this study showed future potential of 3D printing graphene materials with other polymers more suitable for tissue engineering scaffolds. For example, Wei et al., 2015 printed rGO with thermoplastic polymers such as acrylonitrile-butadiene-styrene (ABS) or polylactic acid (PLA).[8] rGO-ABS was prepared in concentrations of 0.4, 0.8, 1.6, 2.3, 3.8, 5.6, and 7.4 wt%. The majority of these concentrations extruded smoothly from the 3D printer (HOF1-X1, China), but 7.4% rGO-ABS clogged the printer's nozzle. However, it was noted that a more powerful homogenizing technique could allow more loading of rGO material. It was also recorded that the glass transition temperature (T_g) of pure ABS alone was ~105.8°C, but shifted to ~110°C with presence of rGO. When printing any novel material, the correct Tg is necessary so that the material is softened (yet not melted) for extrusion and subsequent cooling at room temperature.[57] Finally, Jiang et al., 2018 successfully designed a porous GO hydrogel via 3D printing.[58] The ink was prepared by adding $CaCl_2$ into a GO suspension whereby the Ca^{2+} ions could crosslink with the functional groups of GO to form a hydrogel. This method prevented any clogging within the nozzle, defied any collapsing, and maintained its shape upon

printing. Overall, these studies were the first attempts to directly print a graphene material using a 3D printing designed system.

More recently, Vijayavenkataraman et al., 2019 printed rGO scaffolds with the specific intent of engineering neural tissue.[59] rGO was mixed within polycaprolactone (PCL), but the exact concentration was unclear. Scaffolds were fabricated with the electrohydrodynamic jet (EHD-jet) printing system with the average fiber diameter (~46 µm) and pore size (~125 µm) consistent between both PCL and rGO-PCL scaffolds. As expected, the rGO-PCL scaffolds demonstrated better electrical conductivity (1.35 ± 0.3 mS/m) in comparison to its PCL control (0.09 ± 0.005 µS/cm). Interestingly, when PC12 cells were seeded, the rGO-PCL scaffolds stimulated more cell proliferation than PCL alone and supported expression of neural markers such as GAP43, β3-tubulin, and NF200. Overall, this data showed that rGO can be fabricated as a porous 3D scaffold, is cytocompatible, and should be further studied *in vivo* as a neural guide conduit.

Similarly, Seyedsalehi et al., 2020 mixed rGO within PCL at concentrations of either 0.5%, 1%, or 3% and successfully printed 3D scaffolds (strand size = 300 µm, pore size = 420 µm) with high consistency and repeatability (Figure 1.3A).[6] Structures were printed using the 4th Generation 3D Bioplotter using parameters of: cartridge temperature (100°C), platform temperature (10°C), pressure (0.6 MPa), and speed (1.4 mm/s). Many material properties were examined including wettability, swelling, degradation, deformation behavior, compressive modulus, compressive strength, and cytocompatibility. After 14 days in simulated body fluid, it was found that PCL alone was hydrophobic, whereas the addition of rGO increased water uptake, swelling, and accelerated the rate of degradation. Interestingly, 0.5% rGO-PCL scaffolds had the best mechanical performance with compressive modulus and compressive strength enhanced by 150% and 185%, respectively. However, increasing rGO content to 1% and 3% deteriorated mechanical performance as the rGO sheets formed irreversible aggregates. Finally, all rGO concentrations had no adverse effects on human adipose derived stem cells and supported cell viability *in vitro*. Overall, this study supported that combining small amounts of rGO within 3D printed scaffolds reinforces biomechanical properties necessary for regenerating tissues and organs.

Alternatively, other laboratories have coated graphene onto 3D scaffolds to enhance mechanical strength and cytocompatibility.[14,60] For example, Li et al., 2020 first fabricated 3D printed alginate (Alg) scaffolds before coating with rGO.[14] An Alg/Gel ink was printed using the 3D Bioplotter machine under parameters of room temperature, platform temperature (5°C), speed (10 mm/s), strand spacing (1.5 mm), and extrusion air pressure (5 bar). Once printed, the Alg scaffolds were immersed in a GO solution until a uniform composition was achieved and thereafter reduced in ascorbic acid to ultimately produce a 3D rGO-Alg scaffold. Porosity size varied from ~100 -1,000 µm due to multi-angled layers throughout the print. However, it is believed that various pore sizes are beneficial for tissue engineering as cell signaling is optimal at smaller pore sizes, while oxygen/nutrient transport is optimal at larger pore sizes.[14, 61, 62] Compared to Alg-only scaffolds, the coating of rGO increased the modulus by ~4 fold and demonstrated electrical conductivity. Interestingly, the proliferation of human adipose derived stem cells on 3D rGO-Alg scaffolds was ~85% higher than cells grown on 2D rGO substrates. Additionally, expression of alkaline phosphatase (a bone mineralization marker) was 5 times greater on 3D rGO-Alg scaffolds than on 2D rGO substrates. Overall, this data supports that rGO is supportive of cell attachment, proliferation, and osteogenic differentiation. Furthermore, it also supports the necessity of printing 3D scaffolds that mimic a natural tissue environment.

Graphene and Bone Regeneration

3D construction of graphene scaffolds is the next step for clinical translation in tissue engineering. This research is important as the last decade of traditional 2D cell culture systems have shown graphene substrates supports stem cell differentiation into various lineages. These cell lineages are influenced by the concentration of graphene, its functionalization, shape, and the stem cell source.[63, 64] But more specifically, multiple laboratories have found that graphene derivatives predominantly supports bone differentiation.[51, 65-80] A PubMed search using the phrase “graphene and bone” had more than double the publications of graphene and nerve, heart, muscle, and cartilage. Overall, the mechanical strength of graphene combined with its ability to support osteogenesis of stem cells, makes it a forefront candidate in bone tissue engineering.

Although graphene materials have rapidly emerged as a bone substitute, few studies have examined the mechanisms behind its ability to induce osteogenesis. Some theories suggest the carbon arrangement imitates an organic bone ECM microenvironment, attracting cells to attach, self-renew, and differentiate.[46] Nonetheless, spontaneous bone differentiation on 2D graphene substrates has been supported by calcium deposition and upregulation of bone-specific markers (i.e. ALPL, RUNX2, BMP2, SPP1, BGLAP, BMP2, and COL I). These studies demonstrate the end result of osteogenic differentiation, but the underlying signaling pathways are still under investigation. Wei et al., 2017 found that bone marrow-derived mesenchymal stem cells (BM-MSCs) cultured on GO nanosheets had increased expression of β-catenin, thereby suggesting involvement of the Wnt/β-catenin pathway during osteogenic differentiation.[81] Xie et al., 2019 found that human dental pulp MSCs cultured on pristine graphene achieved osteogenesis via the integrin/focal adhesion kinase axis, thereby signaling SMAD phosphorylation, RUNX2 transcription, and production of SPP1 and BGLAP proteins.[80] Supportively, MacDonald et al., 2021 found that when human adipose-derived MSCs (AD-MSCs) and BM-MSCs were cultured on low oxygen graphene (LOG), multiple genes were involved during bone differentiation including genes related to cell adhesion, extracellular matrix, transcriptional regulation, BMP and SMAD signaling, growth factors, and angiogenic factors.[47] These results were also encouraging as stem cell therapies derived from adipose tissue are much easier to obtain than stem cells derived from bone marrow. Therefore, any substrate material, such as graphene, that can nudge AD-MSCs into the bone lineage, is the preferred clinical strategy.

Despite this excitement, a major question is determining the best concentration of graphene that specifically sustains bone differentiation without collateral damage. BM-MSCs cultured on GO (0.1 µg/mL) had increased proliferation rates; however, at high GO concentrations (10 µg/mL), the BM-MSCs shrank and subsequently had reduced cell proliferation after just 3 days of culturing.[81] Similarly, Sun et al., 2021 found that silk fibroin/nanohydroxyapatite/GO (SF/nHA/GO) scaffolds loaded with urine-derived stem cells, had reduced osteogenic differentiation when GO concentrations exceeded 0.5%.[82] However, a different study found that 0.1% GO (combined with chitosan and

hydroxyapatite), was an optimal concentration for cell adhesion, proliferation, and differentiation of MC3T3-E1 cells, a preosteoblast cell line.[83] In vivo, this concentration showed both osteogenic induction and no adverse reactions in a rat cranial defect model. Overall, before graphene is clinically applied as a bone biomaterial, it is very important to clearly understand the optimal concentration for all derivatives including pristine graphene, GO, and rGO. Additionally, the concentration could also change based on the stem cell source, the shape and surface topography, and when the graphene source is combined with other polymers or drugs.

Despite this ongoing challenge, graphene materials have versatile ways in influencing bone regeneration. For example, graphene can indirectly support bone regeneration as a delivery vehicle that controls the release of potent BMP2 growth factors.[84-87] This helps to minimize the side effects of BMP2 reagents, but yet still provide a sustained stimulation of stem cells over time. GO was also used as a drug delivery platform to achieve a steady release of baicalin, a flavonoid compound widely used for both its osteoinductive and anti-inflammatory properties.[88] The surface area of graphene materials allows the immobilization of growth factors for targeted drug delivery that not only influences bone regeneration, but other tissues such as nerve and cartilage.[29, 64, 89-91] In other strategies, Hou et al., 2020 studied a 3D-printed graphene-PCL scaffold to conjunctively induce both cytotoxicity of Saos-2 cells (a human osteosarcoma cell line) and attract new bone regeneration. It was proposed that the gradual release of graphene could induce apoptosis of cancer cells, while the remaining PCL layers provided the biomechanical environment to sustain the recruitment of healthy stem cells.[63] Overall, graphene materials have versatile properties for supporting bone regeneration including as a direct stimulator of new bone material, a delivery vehicle for other pharmaceutics, or targeting cancers of the bone.

Toxicity Challenges of Graphene Materials

Despite the excitement of graphene materials and its use as a 3D scaffold for tissue engineering, its therapeutic use is still a novel idea and has yet to face a human clinical trial. As with any new substance, the primary question to address will always be safety. Information regarding toxicity of graphene is still uncertain, including any carcinogenic

potential. Yet, medical research has raced to examine its physiological effects for various diseases.

There are a growing number of *in vivo* reports regarding toxicity of graphene materials.[92-97] An early study described by Yang et al., 2010 evaluated GO sheets coated and functionalized with polyethlene glycol (PEGylated nanographene sheets or NGS-PEG) in mouse tumor models.[98] After 40 days, systematic injection of NGS-PEG (20 mg/kg) specifically targeted the tumor site with no signs of toxicity or accumulation in the kidney, liver, heart, spleen, intestine, or lungs. Interestingly, when NGS-PEG was combined with photothermal therapy, the tumors were completely ablated, suggesting graphene's potential for complementing current cancer treatments. However, it is important to note there was no control for NGS only, which may have had different toxicity outcomes.

Wang et al., 2011, evaluated GO toxicity in mice after 30 days of exposure to one of three concentrations: 0.1 mg, 0.25 mg, or 0.4 mg.[99] Results showed no mortality of mice exposed to 0.1 mg or 0.25 mg of GO. However, 4 of 9 mice died following GO injection at 0.4 mg. Histopathology results found GO conglomeration in the lung tissues, thus resulting in airway blockage and subsequent suffocation. When comparing lung tissues of all treatment groups, the mice exhibited a dose-dependent series of granulomas after just 7 days of exposure. In other words, increasing GO concentration severely increased toxicity reactions of the lungs. Overall, these results suggested that GO exposures could promote lung diseases.

A similar study from a separate laboratory also examined GO toxicity in mice following a low dose (1 mg/kg body weight) and a high dose (10 mg/kg body weight) via IV injection.[100] After 14 days, the 1 mg/kg dose of GO had no pathological changes in all organs tested (lungs, liver, spleen, and kidney). However, at 10 mg/kg, there was a high accumulation of GO in the lungs with pathological changes (i.e. granulomatous lesions, pulmonary edema, inflammatory cell infiltration, and fibrosis). The authors concluded that GO was biocompatible in most tissues, but higher dosages draws concern for abnormal changes within lung tissues.

With growing pulmonary toxicity concerns, Singh et al., 2012 compared the lungs of mice injected with either GO or graphene that was functionalized with amine groups (G-NH2).[101] After 15 min., GO (250 µg/kg) stimulated vascular occlusion in lung tissue, while animals treated with G-NH2 (250 µg) had no signs of any occlusive pathology and instead demonstrated normal, healthy lung tissue. It was concluded that G-NH2 is not pro-thrombotic and is a safe graphene derivative, unlike other variations of graphene materials.

Schinwald et al., 2012 evaluated the risk of graphene nanoplatelets (GP) (average thickness of ~10 nm) following either inhalation or intrapleural injection in mice.[102] For inhalation, 50 µg of GP was added onto the tongue and held until at least 2 full breaths were completed. After 24 hr, granulomatous lesions were present in the bronchiolar lumen of mice exposed to GP, but normal lung pathology was observed in both the vehicle and carbon control groups. Additionally, there was an increase of the total number of inflammatory cells (i.e. neutrophils, esoinophils) in the lavage fluid, and continued to show an inflammatory response one-week post-exposure. Secondly, an intrapleural injection of GP (5 µg) resulted in particle aggregations in pleural macrophages, indicating frustrated phagocytosis, an elevation of pro-inflammatory cytokine markers, and pleural thickening of the chest wall. Overall, the authors concluded that GP imposes a risk to the respiratory system, but acknowledged that the layer thickness is a key factor, and should be manufactured small enough that allows phagocytosis by macrophages.

Most recently, Tabish et al., 2018 studied the toxicity of graphene nanopores (GNP) after a single IP injection or multiple injections (total of 14) over 27 days at doses of 5 mg/kg or 15 mg/kg in a rat model.[21] All doses (whether low or high, single or multiple) showed concerns in all tissues tested (liver, kidney, heart, small intestine, brain, testis, and lung), including tumor development within neural tissue of the brain. The pathological changes were presumably due to accumulation and low clearance of GNPs in the rat. Overall, more long-term *in vivo* studies are necessary to minimize adverse effects of graphene materials. The proper dosage and administration route must be carefully examined before any introduction of graphene materials in the clinic.

Future Perspective and Conclusions

Conventional strategies of repairing tissue defects have relied on exogenous stem cells and 2D substrates. However, stem-cell based therapies have many limitations with future strategies turning to 3D structures that both supports and attracts cell differentiation within the injury site. Graphene, a novel biomaterial is under thorough research for repairing various tissues such as bone, cartilage, nerve, and heart. However, *in vitro* work of graphene has mainly been studied as a 2D monolayer or a 3D foam, whereby scaffold morphology is poorly controlled. With the revolution of 3D-printing technology, questions have asked whether graphene scaffolds can be 3D printed. Currently, there is a paucity of studies that have attempted 3D-printed graphene scaffolds for tissue engineering. These studies have mainly surfaced in the last few years, but it is expected that more developments will evolve in the future. Finally, 2D-graphene substrates have predominantly been studied in supporting new bone differentiation. Therefore, 3D-printed graphene scaffolds is the next step for clinical application in bone tissue engineering. However, understanding the optimal concentration of all graphene derivatives that balances both bone differentiation and minimizes toxicity is necessary prior to transplantation. Overall, there is great excitement over 3D-printed graphene scaffolds, but much work is necessary before standardization within tissue engineering.

REFERENCES

1. Langer, R.; Vacanti, J. P., Tissue engineering. *Science* **1993,** *260* (5110), 920-6.
2. Eltom, A.; Zhong, G.; Muhammad, A., Scaffold Techniques and Designs in Tissue Engineering Functions and Purposes: A Review. *Advances in Materials Science and Engineering* **2019,** *2019*, 3429527.
3. Jun, I.; Han, H.-S.; Edwards, J. R.; Jeon, H., Electrospun Fibrous Scaffolds for Tissue Engineering: Viewpoints on Architecture and Fabrication. *International journal of molecular sciences* **2018,** *19* (3), 745.
4. Sola, A.; Bertacchini, J.; D'Avella, D.; Anselmi, L.; Maraldi, T.; Marmiroli, S.; Messori, M., Development of solvent-casting particulate leaching (SCPL) polymer scaffolds as improved three-dimensional supports to mimic the bone marrow niche. *Mater Sci Eng C Mater Biol Appl* **2019,** *96*, 153-165.
5. Ehterami, A.; Masoomikarimi, M.; Bastami, F.; Jafarisani, M.; Alizadeh, M.; Mehrabi, M.; Salehi, M., Fabrication and Characterization of Nanofibrous Poly (L-Lactic Acid)/Chitosan-Based Scaffold by Liquid-Liquid Phase Separation Technique for Nerve Tissue Engineering. *Mol Biotechnol* **2021,** *63* (9), 818-827.
6. Seyedsalehi, A.; Daneshmandi, L.; Barajaa, M.; Riordan, J.; Laurencin, C. T., Fabrication and characterization of mechanically competent 3D printed polycaprolactone-reduced graphene oxide scaffolds. *Scientific Reports* **2020,** *10* (1), 22210.
7. Kundu, J.; Pati, F.; Shim, J. H.; Cho, D. W., 10 - Rapid prototyping technology for bone regeneration. In *Rapid Prototyping of Biomaterials*, Narayan, R., Ed. Woodhead Publishing: **2014**; pp 254-284.
8. Wei, X.; Li, D.; Jiang, W.; Gu, Z.; Wang, X.; Zhang, Z.; Sun, Z., 3D Printable Graphene Composite. *Scientific Reports* **2015,** *5* (1), 11181.
9. Manjunath, K. S.; Sridhar, K.; Gopinath, V.; Sankar, K.; Sundaram, A.; Gupta, N.; Shiek, A.; Shantanu, P. S., Facile manufacturing of fused-deposition modeled composite scaffolds for tissue engineering-an embedding model with plasticity for incorporation of additives. *Biomed Mater* **2020,** *16* (1), 015028.
10. Percoco, G.; Uva, A. E.; Fiorentino, M.; Gattullo, M.; Manghisi, V. M.; Boccaccio, A., Mechanobiological Approach to Design and Optimize Bone Tissue Scaffolds 3D Printed with Fused Deposition Modeling: A Feasibility Study. *Materials (Basel)* **2020,** *13* (3).
11. Xia, B.; Deng, Y.; Lv, Y.; Chen, G., Stem cell recruitment based on scaffold features for bone tissue engineering. *Biomater Sci* **2021,** *9* (4), 1189-1203.
12. Bružauskaitė, I.; Bironaitė, D.; Bagdonas, E.; Bernotienė, E., Scaffolds and cells for tissue regeneration: different scaffold pore sizes-different cell effects. *Cytotechnology* **2016,** *68* (3), 355-369.
13. Oh, S. H.; Park, I. K.; Kim, J. M.; Lee, J. H., In vitro and in vivo characteristics of PCL scaffolds with pore size gradient fabricated by a centrifugation method. *Biomaterials* **2007,** *28* (9), 1664-1671.
14. Li, J.; Liu, X.; Crook, J. M.; Wallace, G. G., 3D Printing of Cytocompatible Graphene/Alginate Scaffolds for Mimetic Tissue Constructs. *Frontiers in bioengineering and biotechnology* **2020,** *8*, 824-824.
15. Duval, K.; Grover, H.; Han, L.-H.; Mou, Y.; Pegoraro, A. F.; Fredberg, J.; Chen, Z., Modeling Physiological Events in 2D vs. 3D Cell Culture. *Physiology (Bethesda)* **2017,** *32* (4), 266-277.
16. Bonnier, F.; Keating, M. E.; Wróbel, T. P.; Majzner, K.; Baranska, M.; Garcia-Munoz, A.; Blanco, A.; Byrne, H. J., Cell viability assessment using the Alamar blue assay: a comparison of 2D and 3D cell culture models. *Toxicol In Vitro* **2015,** *29* (1), 124-31.

17. Baker, B. M.; Chen, C. S., Deconstructing the third dimension: how 3D culture microenvironments alter cellular cues. *J Cell Sci* **2012,** *125* (Pt 13), 3015-24.
18. Harrison, B. S.; Atala, A., Carbon nanotube applications for tissue engineering. *Biomaterials* **2007,** *28* (2), 344-353.
19. Maiti, D.; Tong, X.; Mou, X.; Yang, K., Carbon-Based Nanomaterials for Biomedical Applications: A Recent Study. *Frontiers in Pharmacology* **2019,** *9* (1401).
20. Veetil, J. V.; Ye, K., Tailored carbon nanotubes for tissue engineering applications. *Biotechnol Prog* **2009,** *25* (3), 709-721.
21. Tabish, T. A.; Pranjol, M. Z. I.; Jabeen, F.; Abdullah, T.; Latif, A.; Khalid, A.; Ali, M.; Hayat, H.; Winyard, P. G.; Whatmore, J. L.; Zhang, S., Investigation into the toxic effects of graphene nanopores on lung cancer cells and biological tissues. *Applied Materials Today* **2018,** *12*, 389-401.
22. Patel, K.; Singh, R.; Kim, H.-W., Carbon based-nanomaterials as an emerging platform for theranostics. *Materials Horizons* **2018,** *6*.
23. Geetha Bai, R.; Muthoosamy, K.; Manickam, S.; Hilal-Alnaqbi, A., Graphene-based 3D scaffolds in tissue engineering: fabrication, applications, and future scope in liver tissue engineering. *Int J Nanomedicine* **2019,** *14*, 5753-5783.
24. Bahrami, S.; Baheiraei, N.; Shahrezaee, M., Biomimetic reduced graphene oxide coated collagen scaffold for in situ bone regeneration. *Scientific Reports* **2021,** *11* (1), 16783.
25. Arnold, A. M.; Holt, B. D.; Daneshmandi, L.; Laurencin, C. T.; Sydlik, S. A., Phosphate graphene as an intrinsically osteoinductive scaffold for stem cell-driven bone regeneration. *Proceedings of the National Academy of Sciences* **2019,** *116* (11), 4855.
26. Daneshmandi, L.; Barajaa, M.; Tahmasbi Rad, A.; Sydlik, S. A.; Laurencin, C. T., Graphene-Based Biomaterials for Bone Regenerative Engineering: A Comprehensive Review of the Field and Considerations Regarding Biocompatibility and Biodegradation. *Advanced Healthcare Materials* **2021,** *10* (1), 2001414.
27. Prasadh, S.; Suresh, S.; Wong, R., Osteogenic Potential of Graphene in Bone Tissue Engineering Scaffolds. *Materials (Basel, Switzerland)* **2018,** *11* (8), 1430.
28. Gong, M.; Sun, J.; Liu, G.; Li, L.; Wu, S.; Xiang, Z., Graphene oxide–modified 3D acellular cartilage extracellular matrix scaffold for cartilage regeneration. *Materials Science and Engineering: C* **2021,** *119*, 111603.
29. Zhou, M.; Lozano, N.; Wychowaniec, J. K.; Hodgkinson, T.; Richardson, S. M.; Kostarelos, K.; Hoyland, J. A., Graphene oxide: A growth factor delivery carrier to enhance chondrogenic differentiation of human mesenchymal stem cells in 3D hydrogels. *Acta Biomaterialia* **2019,** *96*, 271-280.
30. Shamekhi, M. A.; Mirzadeh, H.; Mahdavi, H.; Rabiee, A.; Mohebbi-Kalhori, D.; Baghaban Eslaminejad, M., Graphene oxide containing chitosan scaffolds for cartilage tissue engineering. *International Journal of Biological Macromolecules* **2019,** *127*, 396-405.
31. Bei, H. P.; Yang, Y.; Zhang, Q.; Tian, Y.; Luo, X.; Yang, M.; Zhao, X., Graphene-Based Nanocomposites for Neural Tissue Engineering. *Molecules (Basel, Switzerland)* **2019,** *24* (4), 658.
32. Grijalvo, S.; Díaz, D. D., Graphene-based hybrid materials as promising scaffolds for peripheral nerve regeneration. *Neurochemistry International* **2021,** *147*, 105005.
33. Qian, Y.; Wang, X.; Song, J.; Chen, W.; Chen, S.; Jin, Y.; Ouyang, Y.; Yuan, W.-E.; Fan, C., Preclinical assessment on neuronal regeneration in the injury-related microenvironment of graphene-based scaffolds. *npj Regenerative Medicine* **2021,** *6* (1), 31.
34. Safina, I.; Bourdo, S. E.; Algazali, K. M.; Kannarpady, G.; Watanabe, F.; Vang, K. B.; Biris, A. S., Graphene-based 2D constructs for enhanced fibroblast support. *PLoS One* **2020,** *15* (5), e0232670.

35. Hussein, K. H.; Abdelhamid, H. N.; Zou, X.; Woo, H.-M., Ultrasonicated graphene oxide enhances bone and skin wound regeneration. *Materials Science and Engineering: C* **2019,** *94*, 484-492.
36. Lasocka, I.; Jastrzębska, E.; Szulc-Dąbrowska, L.; Skibniewski, M.; Pasternak, I.; Kalbacova, M. H.; Skibniewska, E. M., The effects of graphene and mesenchymal stem cells in cutaneous wound healing and their putative action mechanism. *International journal of nanomedicine* **2019,** *14*, 2281-2299.
37. Sekuła-Stryjewska, M.; Noga, S.; Dźwigońska, M.; Adamczyk, E.; Karnas, E.; Jagiełło, J.; Szkaradek, A.; Chytrosz, P.; Boruczkowski, D.; Madeja, Z.; Kotarba, A.; Lipińska, L.; Zuba-Surma, E. K., Graphene-based materials enhance cardiomyogenic and angiogenic differentiation capacity of human mesenchymal stem cells in vitro – Focus on cardiac tissue regeneration. *Materials Science and Engineering: C* **2021,** *119*, 111614.
38. Karimi Hajishoreh, N.; Baheiraei, N.; Naderi, N.; Salehnia, M., Reduced graphene oxide facilitates biocompatibility of alginate for cardiac repair. *Journal of Bioactive and Compatible Polymers* **2020,** *35* (4-5), 363-377.
39. Bahrami, S.; Baheiraei, N.; Mohseni, M.; Razavi, M.; Ghaderi, A.; Azizi, B.; Rabiee, N.; Karimi, M., Three-dimensional graphene foam as a conductive scaffold for cardiac tissue engineering. *Journal of Biomaterials Applications* **2019,** *34* (1), 74-85.
40. Kozbial, A.; Li, Z. T.; Sun, J. N.; Gong, X.; Zhou, F.; Wang, Y. J.; Xu, H. C.; Liu, H. T.; Li, L., Understanding the intrinsic water wettability of graphite. *Carbon* **2014,** *74*, 218-225.
41. Brodie, B. C., *On the atomic weight of graphite*. [publisher not identified]: [London?], 1859.
42. Halim, A.; Luo, Q.; Ju, Y.; Song, G., A Mini Review Focused on the Recent Applications of Graphene Oxide in Stem Cell Growth and Differentiation. *Nanomaterials (Basel, Switzerland)* **2018,** *8* (9).
43. Tiginyanu, I.; Ursaki, V.; Popa, V., 11 - Ultra-thin membranes for sensor applications. In *Nanocoatings and Ultra-Thin Films*, Makhlouf, A. S. H.; Tiginyanu, I., Eds. Woodhead Publishing: **2011**; pp 330-354.
44. Araújo, M.; Soares, O.; Fernandes, A.; Pereira, M.; Freire, C., Tuning the surface chemistry of graphene flakes: new strategies for selective oxidation. *RSC Adv.* **2017,** *7*, 14290-14301.
45. Shahdeo, D.; Roberts, A.; Abbineni, N.; Gandhi, S., Chapter Eight - Graphene based sensors. In *Comprehensive Analytical Chemistry*, Hussain, C. M., Ed. Elsevier: **2020**; Vol. 91, pp 175-199.
46. Newby, S. D.; Masi, T.; Griffin, C. D.; King, W. J.; Chipman, A.; Stephenson, S.; Anderson, D. E.; Biris, A. S.; Bourdo, S. E.; Dhar, M., Functionalized Graphene Nanoparticles Induce Human Mesenchymal Stem Cells to Express Distinct Extracellular Matrix Proteins Mediating Osteogenesis. *International journal of nanomedicine* **2020,** *15*, 2501-2513.
47. MacDonald, A. F.; Trotter, R. D.; Griffin, C. D.; Bow, A. J.; Newby, S. D.; King, W. J.; Amelse, L. L.; Masi, T. J.; Bourdo, S. E.; Dhar, M. S., Genetic profiling of human bone marrow and adipose tissue-derived mesenchymal stem cells reveals differences in osteogenic signaling mediated by graphene. *Journal of Nanobiotechnology* **2021,** *19* (1), 285.
48. Lee, Y. J.; Seo, T. H.; Lee, S.; Jang, W.; Kim, M. J.; Sung, J. S., Neuronal differentiation of human mesenchymal stem cells in response to the domain size of graphene substrates. *J Biomed Mater Res A* **2018,** *106* (1), 43-51.
49. Lee, E. A.; Kwak, S.-Y.; Yang, J.-K.; Lee, Y.-S.; Kim, J.-H.; Kim, H. D.; Hwang, N. S., Graphene oxide film guided skeletal muscle differentiation. *Materials Science and Engineering: C* **2021,** *126*, 112174.
50. Li, N.; Zhang, Q.; Gao, S.; Song, Q.; Huang, R.; Wang, L.; Liu, L.; Dai, J.; Tang, M.; Cheng, G., Three-dimensional graphene foam as a biocompatible and conductive scaffold for neural stem cells. *Sci Rep* **2013,** *3*, 1604.

51. Crowder, S. W.; Prasai, D.; Rath, R.; Balikov, D. A.; Bae, H.; Bolotin, K. I.; Sung, H. J., Three-dimensional graphene foams promote osteogenic differentiation of human mesenchymal stem cells. *Nanoscale* **2013,** *5* (10), 4171-6.
52. Tasnim, N.; Thakur, V.; Chattopadhyay, M.; Joddar, B., The Efficacy of Graphene Foams for Culturing Mesenchymal Stem Cells and Their Differentiation into Dopaminergic Neurons. *Stem Cells Int* **2018,** *2018*, 3410168.
53. Amani, H.; Mostafavi, E.; Arzaghi, H.; Davaran, S.; Akbarzadeh, A.; Akhavan, O.; Pazoki-Toroudi, H.; Webster, T. J., Three-Dimensional Graphene Foams: Synthesis, Properties, Biocompatibility, Biodegradability, and Applications in Tissue Engineering. *ACS Biomater Sci Eng* **2019,** *5* (1), 193-214.
54. Bahremandi Tolou, N.; Salimijazi, H.; Kharaziha, M.; Faggio, G.; Chierchia, R.; Lisi, N., A three-dimensional nerve guide conduit based on graphene foam/polycaprolactone. *Mater Sci Eng C Mater Biol Appl* **2021,** *126*, 112110.
55. Shin, Y. C.; Kang, S. H.; Lee, J. H.; Kim, B.; Hong, S. W.; Han, D. W., Three-dimensional graphene oxide-coated polyurethane foams beneficial to myogenesis. *J Biomater Sci Polym Ed* **2018,** *29* (7-9), 762-774.
56. Zhu, C.; Han, T. Y.-J.; Duoss, E. B.; Golobic, A. M.; Kuntz, J. D.; Spadaccini, C. M.; Worsley, M. A., Highly compressible 3D periodic graphene aerogel microlattices. *Nature Communications* **2015,** *6* (1), 6962.
57. Becker, H.; Locascio, L. E., Polymer microfluidic devices. *Talanta* **2002,** *56* (2), 267-287.
58. Jiang, Y.; xu, Z.; Huang, T.; Liu, Y.; Guo, F.; Xi, J.; Gao, W.; Gao, C., Direct 3D Printing of Ultralight Graphene Oxide Aerogel Microlattices. *Advanced Functional Materials* **2018,** *28*, 1707024.
59. Vijayavenkataraman, S.; Thaharah, S.; Zhang, S.; Lu, W. F.; Fuh, J. Y. H., 3D-Printed PCL/rGO Conductive Scaffolds for Peripheral Nerve Injury Repair. *Artif Organs* **2019,** *43* (5), 515-523.
60. Li, J.; Liu, X.; Crook, J. M.; Wallace, G. G., Development of a porous 3D graphene-PDMS scaffold for improved osseointegration. *Colloids and Surfaces B: Biointerfaces* **2017,** *159*, 386-393.
61. Yang, S.; Leong, K. F.; Du, Z.; Chua, C. K., The design of scaffolds for use in tissue engineering. Part II. Rapid prototyping techniques. *Tissue Eng* **2002,** *8* (1), 1-11.
62. Murphy, C. M.; O'Brien, F. J., Understanding the effect of mean pore size on cell activity in collagen-glycosaminoglycan scaffolds. *Cell adhesion & migration* **2010,** *4* (3), 377-381.
63. Hou, Y.; Wang, W.; Bartolo, P., Novel Poly(varepsilon-caprolactone)/Graphene Scaffolds for Bone Cancer Treatment and Bone Regeneration. *3D Print Addit Manuf* **2020,** *7* (5), 222-229.
64. Tupone, M. G.; Panella, G.; d'Angelo, M.; Castelli, V.; Caioni, G.; Catanesi, M.; Benedetti, E.; Cimini, A., An Update on Graphene-Based Nanomaterials for Neural Growth and Central Nervous System Regeneration. *Int J Mol Sci* **2021,** *22* (23).
65. Lee, J. H.; Shin, Y. C.; Jin, O. S.; Kang, S. H.; Hwang, Y. S.; Park, J. C.; Hong, S. W.; Han, D. W., Reduced graphene oxide-coated hydroxyapatite composites stimulate spontaneous osteogenic differentiation of human mesenchymal stem cells. *Nanoscale* **2015,** *7* (27), 11642-51.
66. Xie, H.; Cao, T.; Gomes, J. V.; Castro Neto, A. H.; Rosa, V., Two and three-dimensional graphene substrates to magnify osteogenic differentiation of periodontal ligament stem cells. *Carbon* **2015,** *93*, 266-275.
67. Yang, X.; Zhao, Q.; Chen, Y.; Fu, Y.; Lu, S.; Yu, X.; Yu, D.; Zhao, W., Effects of graphene oxide and graphene oxide quantum dots on the osteogenic differentiation of stem cells from human exfoliated deciduous teeth. *Artif Cells Nanomed Biotechnol* **2019,** *47* (1), 822-832.

68. Nayak, T. R.; Andersen, H.; Makam, V. S.; Khaw, C.; Bae, S.; Xu, X.; Ee, P. L.; Ahn, J. H.; Hong, B. H.; Pastorin, G.; Özyilmaz, B., Graphene for controlled and accelerated osteogenic differentiation of human mesenchymal stem cells. *ACS Nano* **2011,** *5* (6), 4670-8.
69. Kim, J.; Kim, Y. R.; Kim, Y.; Lim, K. T.; Seonwoo, H.; Park, S.; Cho, S. P.; Hong, B. H.; Choung, P. H.; Chung, T. D.; Choung, Y. H.; Chung, J. H., Graphene-incorporated chitosan substrata for adhesion and differentiation of human mesenchymal stem cells. *J Mater Chem B* **2013,** *1* (7), 933-938.
70. Mo, X.; Wei, Y.; Zhang, X.; Cai, Q.; Shen, Y.; Dai, X.; Meng, S.; Liu, X.; Liu, Y.; Hu, Z.; Deng, X., Enhanced Stem Cell Osteogenic Differentiation by Bioactive Glass Functionalized Graphene Oxide Substrates. *Journal of Nanomaterials* **2016,** *2016*, 5613980.
71. Hermenean, A.; Codreanu, A.; Herman, H.; Balta, C.; Rosu, M.; Mihali, C. V.; Ivan, A.; Dinescu, S.; Ionita, M.; Costache, M., Chitosan-Graphene Oxide 3D scaffolds as Promising Tools for Bone Regeneration in Critical-Size Mouse Calvarial Defects. *Sci Rep* **2017,** *7* (1), 16641.
72. Lee, J. H.; Shin, Y. C.; Lee, S. M.; Jin, O. S.; Kang, S. H.; Hong, S. W.; Jeong, C. M.; Huh, J. B.; Han, D. W., Enhanced Osteogenesis by Reduced Graphene Oxide/Hydroxyapatite Nanocomposites. *Sci Rep* **2015,** *5*, 18833.
73. Zhou, Q.; Yang, P.; Li, X.; Liu, H.; Ge, S., Bioactivity of periodontal ligament stem cells on sodium titanate coated with graphene oxide. *Sci Rep* **2016,** *6*, 19343.
74. Lyu, C. Q.; Lu, J. Y.; Cao, C. H.; Luo, D.; Fu, Y. X.; He, Y. S.; Zou, D. R., Induction of Osteogenic Differentiation of Human Adipose-Derived Stem Cells by a Novel Self-Supporting Graphene Hydrogel Film and the Possible Underlying Mechanism. *ACS Appl Mater Interfaces* **2015,** *7* (36), 20245-54.
75. Radunovic, M.; De Colli, M.; De Marco, P.; Di Nisio, C.; Fontana, A.; Piattelli, A.; Cataldi, A.; Zara, S., Graphene oxide enrichment of collagen membranes improves DPSCs differentiation and controls inflammation occurrence. *J Biomed Mater Res A* **2017,** *105* (8), 2312-2320.
76. Kim, J.; Kim, H. D.; Park, J.; Lee, E. S.; Kim, E.; Lee, S. S.; Yang, J. K.; Lee, Y. S.; Hwang, N. S., Enhanced osteogenic commitment of murine mesenchymal stem cells on graphene oxide substrate. *Biomater Res* **2018,** *22*, 1.
77. Shie, M. Y.; Chiang, W. H.; Chen, I. P.; Liu, W. Y.; Chen, Y. W., Synergistic acceleration in the osteogenic and angiogenic differentiation of human mesenchymal stem cells by calcium silicate-graphene composites. *Mater Sci Eng C Mater Biol Appl* **2017,** *73*, 726-735.
78. Di Carlo, R.; Di Crescenzo, A.; Pilato, S.; Ventrella, A.; Piattelli, A.; Recinella, L.; Chiavaroli, A.; Giordani, S.; Baldrighi, M.; Camisasca, A.; Zavan, B.; Falconi, M.; Cataldi, A.; Fontana, A.; Zara, S., Osteoblastic Differentiation on Graphene Oxide-Functionalized Titanium Surfaces: An In Vitro Study. *Nanomaterials* **2020,** *10* (4).
79. Zhang, J.; Eyisoylu, H.; Qin, X. H.; Rubert, M.; Müller, R., 3D bioprinting of graphene oxide-incorporated cell-laden bone mimicking scaffolds for promoting scaffold fidelity, osteogenic differentiation and mineralization. *Acta Biomater* **2021,** *121*, 637-652.
80. Xie, H.; Cao, T.; Franco-Obregón, A.; Rosa, V., Graphene-Induced Osteogenic Differentiation Is Mediated by the Integrin/FAK Axis. *International Journal of Molecular Sciences* **2019,** *20* (3).
81. Wei, C.; Liu, Z.; Jiang, F.; Zeng, B.; Huang, M.; Yu, D., Cellular behaviours of bone marrow-derived mesenchymal stem cells towards pristine graphene oxide nanosheets. *Cell Prolif* **2017,** *50* (5).
82. Sun, J.; Li, L.; Xing, F.; Yang, Y.; Gong, M.; Liu, G.; Wu, S.; Luo, R.; Duan, X.; Liu, M.; Zou, M.; Xiang, Z., Graphene oxide-modified silk fibroin/nanohydroxyapatite scaffold loaded with urine-derived stem cells for immunomodulation and bone regeneration. *Stem Cell Res Ther* **2021,** *12* (1), 591.

83. Liu, S.; Li, Z.; Wang, Q.; Han, J.; Wang, W.; Li, S.; Liu, H.; Guo, S.; Zhang, J.; Ge, K.; Zhou, G., Graphene Oxide/Chitosan/Hydroxyapatite Composite Membranes Enhance Osteoblast Adhesion and Guided Bone Regeneration. *ACS Appl Bio Mater* **2021,** *4* (11), 8049-8059.
84. Wang, Q.; Wang, M.; Wang, K.; Sun, Y.; Zhang, H.; Lu, X.; Duan, K., Molecular mechanisms of interactions between BMP-2 and graphene: Effects of functional groups and microscopic morphology. *Applied Surface Science* **2020,** *525*, 146636.
85. Fu, C.; Yang, X.; Tan, S.; Song, L., Enhancing Cell Proliferation and Osteogenic Differentiation of MC3T3-E1 Pre-osteoblasts by BMP-2 Delivery in Graphene Oxide-Incorporated PLGA/HA Biodegradable Microcarriers. *Sci Rep* **2017,** *7* (1), 12549.
86. Zhong, C.; Feng, J.; Lin, X.; Bao, Q., Continuous release of bone morphogenetic protein-2 through nano-graphene oxide-based delivery influences the activation of the NF-κB signal transduction pathway. *Int J Nanomedicine* **2017,** *12*, 1215-1226.
87. La, W.-G.; Jung, M.-J.; Yoon, J.-K.; Bhang, S. H.; Jang, H.-K.; Lee, T.-J.; Yoon, H.-H.; Shin, J.-Y.; Kim, B.-S., Bone morphogenetic protein-2 for bone regeneration – Dose reduction through graphene oxide-based delivery. *Carbon* **2014,** *78*, 428-438.
88. Guo, B.; Feng, X.; Wang, Y.; Wang, X.; He, Y., Biomimetic and immunomodulatory baicalin-loaded graphene oxide-demineralized bone matrix scaffold for in vivo bone regeneration. *J Mater Chem B* **2021,** *9* (47), 9720-9733.
89. Weaver, C. L.; Cui, X. T., Directed Neural Stem Cell Differentiation with a Functionalized Graphene Oxide Nanocomposite. *Adv Healthc Mater* **2015,** *4* (9), 1408-16.
90. Ghaemi, A.; Javadi, S.; Heidari, M. K.; Rashedi, H.; Yazdian, F.; Omidi, M.; Tavakoli, Z.; Sheikhpour, M., Graphene-based materials in drug delivery and growth factor release: A critical review. *Wound Medicine* **2020,** *31*, 100193.
91. Yoon, H.; Bhang, S.; Kim, T.; Yu, T.; Hyeon, T.; Kim, B. S., Dual Roles of Graphene Oxide in Chondrogenic Differentiation of Adult Stem Cells: Cell-Adhesion Substrate and Growth Factor-Delivery Carrier. *Advanced Functional Materials* **2014,** *24*.
92. Seabra, A. B.; Paula, A. J.; de Lima, R.; Alves, O. L.; Durán, N., Nanotoxicity of graphene and graphene oxide. *Chem Res Toxicol* **2014,** *27* (2), 159-68.
93. Sharma, G.; Nagpal, A., Hairy intraoral flaps: An uncommon complication of surgical therapy in oral cancer. *Saudi Journal of Oral Sciences* **2014,** *1* (2), 123-124.
94. Ma, Y.; Shen, H.; Tu, X.; Zhang, Z., Assessing in vivo toxicity of graphene materials: current methods and future outlook. *Nanomedicine (Lond)* **2014,** *9* (10), 1565-80.
95. Chong, Y.; Ma, Y.; Shen, H.; Tu, X.; Zhou, X.; Xu, J.; Dai, J.; Fan, S.; Zhang, Z., The in vitro and in vivo toxicity of graphene quantum dots. *Biomaterials* **2014,** *35* (19), 5041-5048.
96. Zhang, L.; Ouyang, S.; Zhang, H.; Qiu, M.; Dai, Y.; Wang, S.; Wang, Y.; Ou, J., Graphene oxide induces dose-dependent lung injury in rats by regulating autophagy. *Exp Ther Med* **2021,** *21* (5), 462.
97. Tsai, M. H.; Chao, H. R.; Jiang, J. J.; Su, Y. H.; Cortez, M. S. P.; Tayo, L. L.; Lu, I. C.; Hsieh, H.; Lin, C. C.; Lin, S. L.; Mansor, W. N. W.; Su, C. K.; Huang, S. T.; Hsu, W. L., Toxicity of Low-dose Graphene Oxide Nanoparticles in an in-vivo Wild Type of Caenorhabditis elegans Model. *AEROSOL AND AIR QUALITY RESEARCH* **2021,** *21* (5).
98. Yang, K.; Zhang, S.; Zhang, G.; Sun, X.; Lee, S.-T.; Liu, Z., Graphene in Mice: Ultrahigh In Vivo Tumor Uptake and Efficient Photothermal Therapy. *Nano Letters* **2010,** *10* (9), 3318-3323.
99. Wang, K.; Ruan, J.; Song, H.; Zhang, J.; Wo, Y.; Guo, S.; Cui, D., Biocompatibility of Graphene Oxide. *Nanoscale Res Lett* **2011,** *6* (1), 8-8.
100. Zhang, X.; Yin, J.; Peng, C.; Hu, W.; Zhu, Z.; Li, W.; Fan, C.; Huang, Q., Distribution and biocompatibility studies of graphene oxide in mice after intravenous administration. *Carbon* **2011,** *49* (3), 986-995.

101. Singh, S. K.; Singh, M. K.; Kulkarni, P. P.; Sonkar, V. K.; Grácio, J. J. A.; Dash, D., Amine-Modified Graphene: Thrombo-Protective Safer Alternative to Graphene Oxide for Biomedical Applications. *ACS Nano* **2012,** *6* (3), 2731-2740.
102. Schinwald, A.; Murphy, F. A.; Jones, A.; MacNee, W.; Donaldson, K., Graphene-based nanoplatelets: a new risk to the respiratory system as a consequence of their unusual aerodynamic properties. *ACS Nano* **2012,** *6* (1), 736-46.

APPENDIX

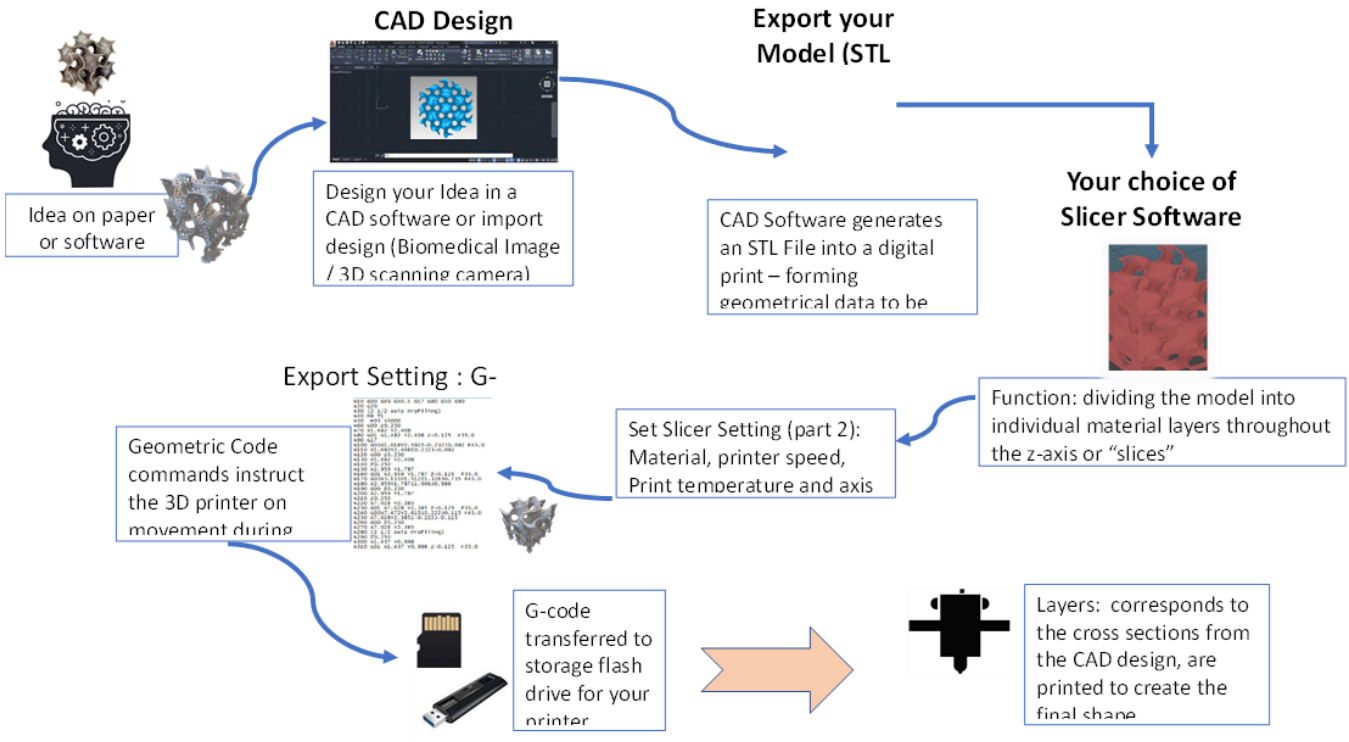

Figure 1.1. The process of a computer-controlled 3D-printing system.

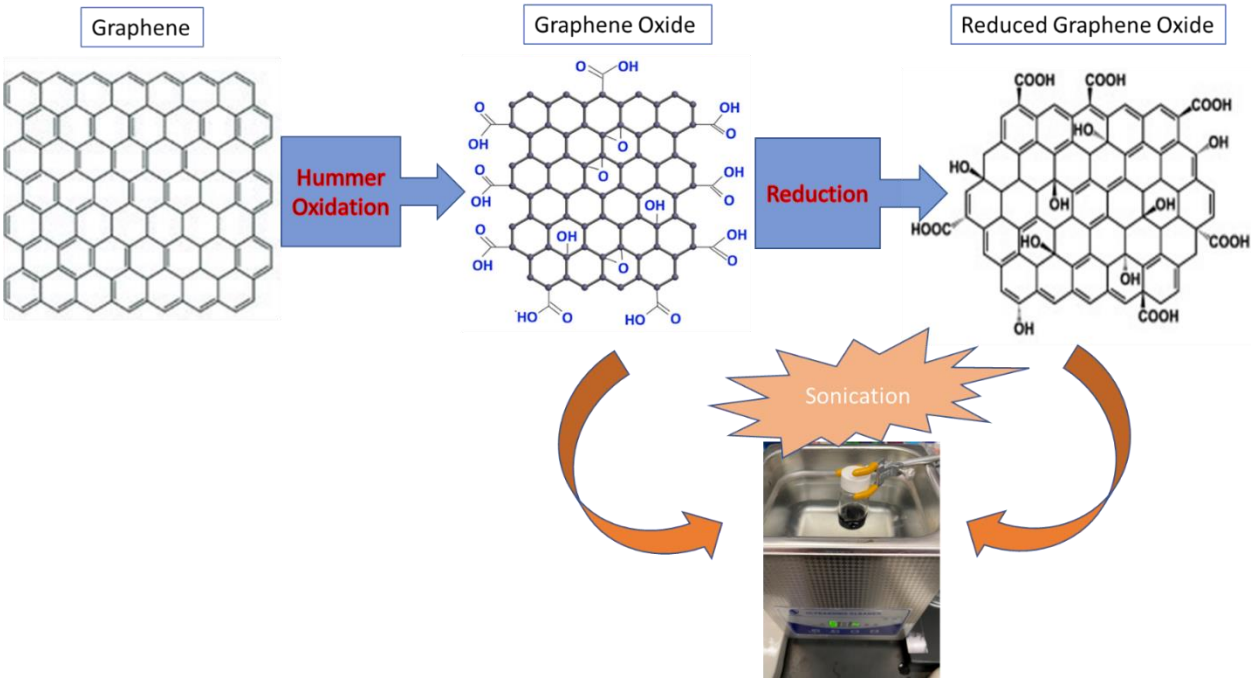

Figure 1.2. The structure of graphene, graphene oxide, and reduced graphene oxide.

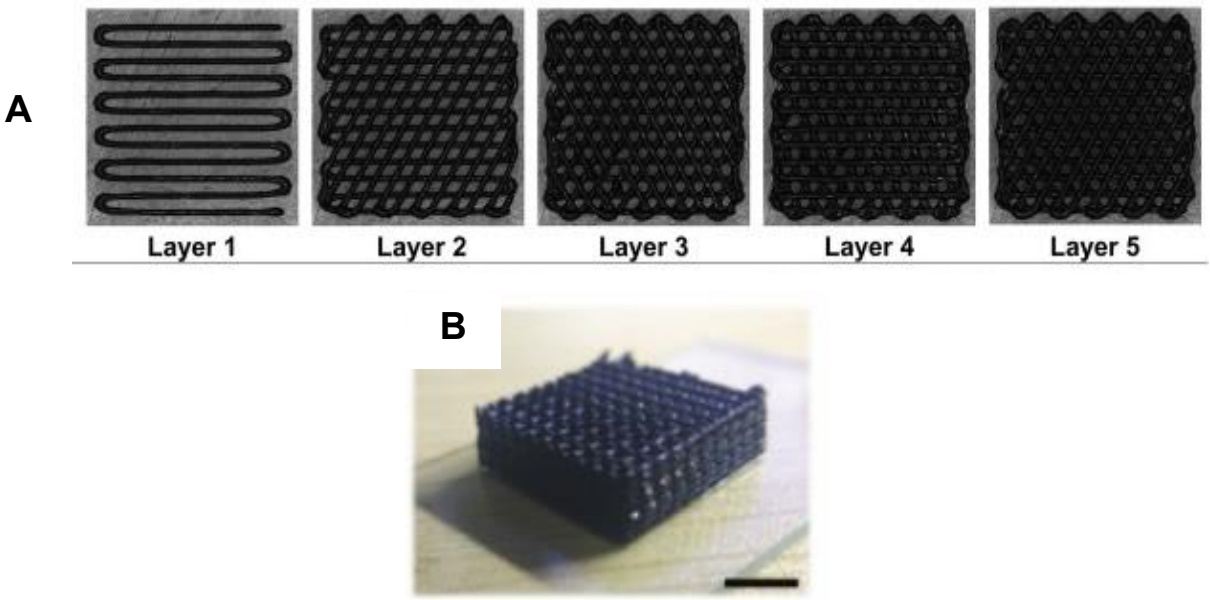

Figure 1.3. Images of 3D-printed graphene scaffolds. (A) Images of each printed layer of a PCL-rGO scaffold, adapted by Seyedsalehi et al., 2020. **(B)** Image of a 3D-printed GO aerogel with a micro lattice architecture, adapted by Zhu et al., 2015.

Table 1.1 Summary of 3D-Printed Graphene Studies. GO (graphene oxide); rGO (reduced graphene oxide); ABS (Acrylonitrile-butadiene-styrene); PLA (Polylactic acid); PCL (polycaprolactone).

Author, Year	Graphene Source	Polymer	3D-Printer Model	Printing Parameters	Overall Purpose
Zhu, 2015	GO	Silica	3-axis positioning stage (ABL 9000, Aerotech)	N/A	To demonstrate a 3D-printing strategy for graphene
Wei, 2015	rGO	ABS Or PLA	HOF1-X1	**rGO-ABS** Chamber Temp: 230°C Platform Temp: 80°C Nozzle: 130°C Speed: 20 mm/s **rGO-PLA** Chamber Temp: 190° Platform Temp: 60°C Nozzle:130°C Speed: 20 mm/s	To demonstrate graphene is 3D printable
Jiang, 2018	GO	GO was crosslinked with Ca^{2+} ions to form a hydrogel	TH-206H	Room Temp Pressure: 2-3 bar Speed: 4-10 mm s^{-1}	To enhance the functionality of 3D-printed graphene structures
Vijayavenkataraman, 2019	rGO	PCL	Electrohydrodynamic jet (EHD-jet)	N/A	To create a nerve guide conduit for neural regeneration
Seyedsalehi, 2020	rGO	PCL	4th Generation 3D Bioplotter	Temp: 100°C Platform Temp: 10°C Pressure: 0.6 MPa Speed: 1.4 mm/s	To evaluate printability, mechanical, and biological properties
Hou, 2020	Graphene	PCL	3DDiscovery™ Evolution	Temp: 90°C Screw Rotation Velocity: 8 rpm Deposit Velocity: 12 mm/s Pressure: 6 bar	To create a scaffold that targeted both osteosarcoma and recruited healthy stem cells for bone regeneration

CHAPTER II:
GENETIC PROFILING OF HUMAN BONE MARROW AND ADIPOSE TISSUE-DERIVED MESENCHYMAL STEM CELLS REVEALS DIFFERENCES IN OSTEOGENIC SIGNALING MEDIATED BY GRAPHENE

This chapter was originally published by Amber F. MacDonald:

Amber F. MacDonald[a], Ruby D. Trotter [b], Christopher D. Griffin [b], Austin J. Bow[a], Steven D. Newby[a], William J. King [b], Lisa L. Amelse[a], Thomas J. Masi [c], Shawn E. Bourdo [b], Madhu S. Dhar[a, *]

Affiliations:
[a] College of Veterinary Medicine, University of Tennessee, Knoxville, TN, 37996, USA
[b] Center for Integrative Nanotechnology Sciences, University of Arkansas at Little Rock, Little Rock, AR, 72204, USA
[c] University of Tennessee Graduate School of Medicine, Knoxville, TN, 37996, USA

Corresponding author:
Madhu Dhar, Ph.D., College of Veterinary Medicine, University of Tennessee, 2407 River Dr. Knoxville, Tennessee 37996, USA; email: mdhar@utk.edu; phone: 865-974-5703; Fax: 865-974-5773

This article was published by Journal of Nanobiotechnology 2021; 19: 285
doi: 10.1186/s12951-021-01024-x

ABSTRACT

Background: In the last decade, graphene surfaces have consistently supported osteoblast development of stem cells, holding promise as a therapeutic implant for degenerative bone diseases. However, until now no study has specifically examined the genetic changes when stem cells undergo osteogenic differentiation on graphene.

Results: In this study, we provide a detailed overview of gene expressions when human mesenchymal stem cells (MSCs) derived from either adipose tissue (AD-MSCs) or bone marrow (BM-MSCs), are cultured on graphene. Genetic expressions were measured using osteogenic RT^2 profiler PCR arrays and compared either over time (7 or 21 days) or between each cell source at each time point. Genes were categorized as either transcriptional regulation, osteoblast-related, extracellular matrix, cellular adhesion, BMP and SMAD signaling, growth factors, or angiogenic factors. Results showed that both MSC sources cultured on low oxygen graphene surfaces achieved osteogenesis by 21 days and expressed specific osteoblast markers. However, each MSC source cultured on graphene did have genetically different responses. When compared between each other, we found that genes of BM-MSCs were robustly expressed, and more noticeable after 7 days of culturing, suggesting BM-MSCs initiate osteogenesis at an earlier time point than AD-MSCs on graphene. Additionally, we found upregulated angiogenic markers in both MSCs sources, suggesting graphene could simultaneously attract the ingrowth of blood vessels in vivo. Finally, we identified several novel targets, including distal-less homeobox 5 (DLX5) and phosphate-regulating endopeptidase homolog, X-linked (PHEX).

Conclusions: Overall, this study shows that graphene genetically supports differentiation of both AD-MSCs and BM-MSCs but may involve different signaling mechanisms to achieve osteogenesis. Data further demonstrates the lack of aberrant signaling due to cell-graphene interaction, strengthening the application of specific form and concentration of graphene nanoparticles in bone tissue engineering.

Keywords: Angiogenic signaling; Focused arrays; Human mesenchymal stem cells; Osteogenesis; Osteogenic signaling

BACKGROUND

In the United States, there are approximately 1 million new cases of severe bone defects that require medical intervention. Traditionally these defects are filled with autologous bone grafts, in which bone removed from the hip or ribs is implanted into the defected area. Unfortunately, this method causes many limitations as the procedure alone is highly invasive, increases the risk of infection, causes donor site morbidity, and overall is not appropriate for geriatric patients. An alternative and extensively investigated medical strategy is bone tissue engineering. Bone tissue engineering requires viable or osteoprogenitor cells and natural/synthetic biomaterials which together are used in the fabrication of novel scaffold constructs [1]. Biomaterials developed for bone are manufactured with specific functions: (1) to deliver and home stem cells to the injury site, (2) to induce osteoblast differentiation of the externally delivered osteoprogenitors cells, (3) to induce osteoblast differentiation of the endogenous progenitor cells, and (4) should be mechanically strong, flexible, and gradually resorb as new bone is formed over time.

Since graphene's discovery in 2004, graphene-based nanocomposite scaffolds have gained significant appreciation in biomedicine, specifically bone tissue engineering. Graphene is a single isolated layer of graphite, having a two-dimensional structure consisting of carbon atoms orchestrated as hexagonal rings. It has been called "the wonder material" due to its superthin, yet super-strong and flexible features. In addition to single layer graphene, few-layer graphene can also be utilized for many of the same applications that single-layer graphene has been touted. Many variations of graphene have been developed that differ largely on the oxygen content – from pristine with little

to no oxygen in the carbon network to graphene oxide (GO) with the highest amounts of incorporated oxygen. There are many terms that can refer to variation in the chemical makeup, including reduced graphene oxide (rGO) and highly reduced graphene oxide (hrGO). These modifications are necessary for many applications since the pristine form of graphene is hydrophobic and consequently, cannot be dissolved or readily dispersed in water or bodily fluids. Aside from simple oxygen functionalization, many other functionalities and treatments can be incorporated to make graphene highly dispersible and less toxic [2-5]. We have coined distinct terms for the oxygen functionalized graphene based on the oxygen content, i.e. low and high oxygen content graphene as LOG and HOG, respectively [6, 7].

Graphene was first recognized to be biocompatible and a potential bone biomaterial in 2010 after recognizing that human osteoblasts and mesenchymal stem cells (MSCs) adhered and proliferated on graphene better than on silicon dioxide substrates [8]. Since then, multiple laboratories (including ours) have recognized graphene and its derivatives as valid osteoinductive and osteoconductive nanomaterials *in vitro* and *in vivo* [9, 10]. Our research group has demonstrated that a low-oxygen content graphene (LOG) material was cytocompatible and supported the adherence, proliferation and osteogenic differentiation of goat bone marrow derived MSCs (BM-MSCs) *in vitro* [9]. We then confirmed the osteoinductive and osteoconductive potential of LOG with goat adipose derived MSCs (AD-MSCs) *in vivo* [10]. Likewise, we most recently demonstrated that LOG exhibited similar effects on human AD-MSCs *in vitro*, i.e. MSCs underwent osteogenic differentiation without any chemical induction. Human MSCs exposed to graphene surfaces expressed specific integrin heterodimers and the

corresponding ECM proteins, suggesting that the structure and topography of LOG surface potentially induces the expression of bone – specific ECM and thus, promotes MSCs to undergo osteogenic differentiation [11].

Even though graphene-based nanomaterials are being used in bone tissue engineering and their biological role in osteoblast differentiation of MSCs has been demonstrated in multiple studies, *in vitro* and *in vivo*, the signals that are triggered i.e. the knowledge of the signal transduction pathways that the cells undergo during this process is limited [12, 13].

Adult MSCs can be isolated from a variety of tissues including, bone marrow, adipose tissue, dental pulp, umbilical cord blood, Wharton's jelly, and the placenta. Even though bone marrow and adipose tissue are the most commonly used tissue sources of MSCs, their efficacy in regenerative medicine is varied. This is primarily due to the donor-to-donor variation as well as the variations in isolation and *in vitro* cell culturing protocols of expansion [14-16]. The application of either bone marrow or adipose tissue – derived MSCs in bone tissue engineering can be further affected by the interaction between MSCs and the nanomaterials used. Hence, in order to assess the efficacy of nanomaterial/cell constructs and to improve the fabrication of the nanomaterials, it is important to evaluate differences in cell signaling in presence of the nanomaterials.

This study was carried out to understand the genetic expressions that graphene regulates on human MSCs i.e. to identify molecular targets that specifically communicate osteogenic differentiation of MSCs. The study design also provided us with the opportunity to compare and contrast the osteogenic response between bone marrow and adipose tissue – derived MSCs. All graphene and MSC studies report

conclusions from single reactions of osteoblastic markers [17-19], but this method provides minuscule insight on how graphene nanomaterials influence cell behavior during osteogenesis. Therefore, the objective of this study was to measure and compare changes in gene expression during osteogenesis of human MSCs derived from adipose tissue and bone marrow on a LOG surface. Based on previous literature and data from our laboratory, we hypothesized that using osteogenic focused arrays and monitoring changes in osteogenesis over a specific time period, we will be able to evaluate the key pathways that MSCs go through in presence of functionalized form of graphene.

MATERIALS AND METHODS

Tissue Procurement, Cell isolation and Characterization

Human adipose tissue – derived MSCs were isolated, characterized and cryobanked as described earlier [11]. Prior to cell isolation, patient consent was obtained and approved by an IRB protocol at the University of Tennessee Medical Center in Knoxville. Adipose tissue was collected from patients undergoing pannulectomies. Following cell expansion, human adipose-derived MSCs (AD-MSCs) were confirmed for cell morphology, protein markers, and trilineage differentiation, as described earlier [11, 20]. Human bone-marrow derived MSCs (BM-MSCs) were commercially purchased from American Type Culture Collection (ATCC) (Manassas, VA). Cells were expanded and cryopreserved as per ATCC's recommendations. MSCs were confirmed for their adherence to tissue culture plastic and ability for tri-lineage differentiation *in vitro*. Cells from passages 2-6 were used in all experiments described.

Preparation and Characterization of Graphene

Processing conditions

Pristine graphene was purchased commercially from Angstron Materials (Dayton, Ohio) and oxidized within an acidic mixture (6:2:3 ratio of sulfuric acid, nitric acid, and water) as described earlier [6, 10]. The final product was a low-oxygen functionalized form of graphene (LOG) with approximately 6-10% oxygen content and was confirmed to be the form used in previous studies [6, 10]. LOG was dispersed in ethanol/water by sonication. Aliquots of the dispersion were used to coat the dishes for cell culture.

Deposition of graphene

Non-tissue cultured treated dishes were coated with LOG to produce uniform surfaces with very little exposed plastic. For all experiments, the LOG concentration was 0.2 mg/cm^2 of dish surface.

Surface topography

Surface roughness/topography was investigated using atomic force microscopy (AFM). A Bruker Dimension AFM using a Budget Sensors Tap300Al-G tip (300 kHz and 40 N/m) in tapping mode. Random spots were chosen for analysis on a 100 mm petri dish and scan sizes of 50 mm x 50 mm were collected. An average of 7 spots and standard deviation was determined. NanoScope Analysis 1.5 (Bruker) software was used to analyze the surface images to determine average roughness (Ra) and root-mean-square (Rq).

Osteogenesis and mineralization of MSCs

AD-MSCs and BM-MSCs were grown to 70-80% confluency in growth media (DMEM F12+10%FBS+1%penicillin-streptomycin-antimycotic) and incubated in an atmosphere

of 5% CO_2 at 37°C. For experimental conditions, cells were harvested with 0.05% trypsin and seeded at 1 X 10^5/well of a 12 well plate and 1 X 10^6/100 mm cell culture dish coated with LOG. Cells were cultured on LOG for either 7 or 21 days and were maintained in growth media without any osteo-differentiation inducers throughout the study. At specified time points, cells were either stained with Alizarin red and quantitated as reported earlier [11] or collected for RNA experiments (described below). To ensure that AD-MSCs generated in our lab and commercial BM-MSCs retained their osteogenic potential under standard conditions, cells were cultured on tissue culture polystyrene surface in presence of osteogenic induced medium (growth media supplemented with 10 nM β-glycerophosphate, 100 nM dexamethasone, and 155 μM ascorbic acid). Osteogenesis was confirmed by Alizarin red staining and quantitation as previously described [11].

RNA Isolation

Cells were detached from LOG with 0.05% trypsin for approximately 40 min. followed by centrifugation. A cell pellet was combined from two-100 mm LOG coated dishes to ensure the RNA quantity was sufficient for triplicate PCR reactions. Total RNA was isolated using an RNeasy® Mini Kit following the manufacturer's instructions (Qiagen, Germantown, MD, #74104). To measure RNA purity and quantity, samples were loaded onto a Take3 plate, and read on Epoch microplate spectrophotometer (BioTek Instruments, Winooski, VT) with Gen5 version 2.09 software. The 260/280 nm absorbance ratio determined RNA purity and was considered optimal at approximately 2.0. RNA 6000 Nano Kit and the 2100 Bioanalyzer system was used to evaluate the

integrity as per the manufacturer's recommendations (Agilent Technologies, Santa Clara, CA) [21].

Human Osteogenesis PCR Array

RT^2 Profiler PCR Human Osteogenesis Array (Qiagen, Hilden, Germany, #PAHS-026Z) was used to evaluate differentially expressed genes from AD-MSCs and BM-MSCs cultured on LOG. 1 µg of RNA was reversed transcribed to cDNA with a RT^2 First Strand Kit (Qiagen, Hilden, Germany, #330401). The cDNA was added into a RT^2 SYBR Green Mastermix (Qiagen, Hilden, Germany, #330524) before loading 25 µL (~ 10.4 ng) per well. cDNA synthesis and PCR reactions were performed according to the manufacturer's recommendations [22].

Statistical Analysis

Gene expressions from CT values were analyzed using Qiagen Gene Globe software to determine the relative fold change (https://geneglobe.qiagen.com/us/analyze/). In the first analyses, gene expression data obtained from AD-MSCs cultured on tissue culture polystyrene surface in presence of osteogenic induced medium (growth media supplemented with 10 nM β-glycerophosphate, 100 nM dexamethasone, and 155 µM ascorbic acid) for 21 days was set as the control. MSCs cultured on the LOG surface without the differentiation cocktail for 21 days was designated as the test group. Thereafter, all comparisons were carried out between the AD and BM – MSCs cultured solely on the LOG surface.

To evaluate cell signaling on LOG surface, we compared the changes in gene expression for each cell type between days 7 and 21. Expression at day 7 was set as the control and day 21 was designated as the test group. Subsequently, the two cell

types were compared at each time point, with AD-MSCs set as the control group and BM-MSCs as the tested group. All comparisons were normalized using β-2 microglobulin (B2M) and glyceraldehyde-3-Phosphate Dehydrogenase (GAPDH) as the housekeeping genes. Data is shown from triplicate experiments, with fold changes statistically significant at $p < 0.05$.

Cytoscape analyses of potential protein targets

Genes of interest were imported from the appropriate tables into Cytoscape software (https://cytoscape.org/) containing a basal nodal network derived from the updated BioGrid data set for Homo sapiens (https://thebiogrid.org/). The complete network was then filtered based on the target genes resulting in the input gene set nodes with residual connective line elements from the basal map. Genes were then sorted based on associated functional group and graphed onto propellor plot diagrams depicting the up and downregulated candidates for both experimental sample comparisons. Gene sets displayed in propellor plots serve to demonstrate the comparative difference in gene expression and thus, can be translated into protein-protein interactions for these two experimental groups as compared to a common control.

Cytoskeletal organization and expression of ECM proteins

Cytoskeletal organization and morphology of BM-MSCs were assessed by evaluating the pattern of F-actin staining using previously reported methods [11]. The expression patterns of ECM proteins corresponding to the gene targets identified for the BM-MSCs were assessed qualitatively by immunofluorescence detection assays. The assessments were made during cell attachment (i.e within 24 hr of seeding) and

osteogenic differentiation (21 days after seeding) Fibronectin 182, and collagen I, were evaluated as described earlier [11].

RESULTS

Graphene nanomaterials display 6-10% oxygen content

Graphene surfaces have been extensively characterized and reported in previous publications by [6, 7]. The material is distinct from the commercially available forms of pristine graphene and graphene oxide (GO) in oxygen content. It may share similar characteristics with reduced-GO or highly reduced-GO, however, we use the term low-oxygen graphene (LOG) since it is produced directly from commercially obtained pristine graphene powder, and not via the reduction of GO.

LOG preparations were consistent with that reported earlier, and contain 6-10% oxygen content, with trace (<0.5%) amounts of sulfur and nitrogen [9, 10]. The oxygen moieties are distributed within the hydroxyl, carbonyl, ether, and carboxyl groups as reported in functionalized graphene with higher oxygen content, such as GO [6]. In addition to the surface chemistry of LOG, surface roughness, which is an important aspect for cell adhesion/attachment was evaluated [23, 24]. Figure 2.1 displays the root mean squared (R_q) and average (R_a) roughness values as determined from atomic force microscopy (AFM). The images collected from AFM show a rough surface topography providing numerous sites for possible cell attachment. Data is consistent with that reported earlier [6, 11].

Human adipose tissue and bone marrow – derived MSCs display similar osteogenic behavior on LOG surface

We have previously reported that human and goat adipose tissue – derived MSCs undergo spontaneous osteogenesis on LOG without any chemical induction [9-11]. We have also demonstrated that goat adipose tissue and bone marrow - derived MSCs undergo osteogenesis using two distinct signaling pathways [25]. In view of these data, we evaluated and compared the osteogenic differentiation and mineralization of human BM-MSCs to AD-MSCs on LOG surfaces using Alizarin red staining and quantitation (Figure 2.2). The calcium content as judged by Alizarin red staining was significantly greater in human BM-MSCs seeded on LOG surfaces relative to the cells on the tissue culture polystyrene surface ($p < 0.0001$). Interestingly, this upregulation was similar to that reported earlier for human AD-MSCs [11] and was observed in the absence of any osteogenic inducers. Calcium content was enhanced ($p < 0.0025$) when osteogenic inducers were added to the media. Results suggest that irrespective of the source, the LOG surface induces similar accumulation of calcium in both the adipose tissue and bone marrow – derived MSCs *in vitro*.

Surprisingly, in presence of the differentiation media + LOG, there was a decrease in the calcium content relative to the cells on tissue culture polystyrene surface. The reason for this outcome is unknown, and is beyond the scope of this study. Based on published literature, dexamethasone, beta glycerophosphate and ascorbic acid regulate several signal transduction pathways and hence, this effect should be investigated in future studies [26]. Therefore, in the current study, we sought to identify the molecular targets involved in LOG - mediated stem cell signaling without osteogenic inducers. In

the experiments described below, cells were maintained in growth media alone without any supplementation of osteogenic reagents.

High quality RNA was obtained from MSCs

We harvested MSCs from LOG using trypsin, with longer than normal incubation time of about 40 min. As a result, we evaluated the RNA quantity and quality prior to PCR analyses. Electrophoresis of total RNAs from AD-MSCs and BM-MSCs in presence of LOG for both 7 and 21 days showed no degradation and intact ribosomal subunits, 18S and 28S bands (Figure 2.3A, B). RNA quality was measured by RNA integrity number (RIN) ranging from 1 – 10, with RIN < 6 considered as a low quality sample [27]. An electropherogram confirmed high quality RNA with RIN values > 9.0 at both time points for both cell types (Figure 2.3C-F.).

Focused arrays to evaluate graphene - mediated differentiation

Osteogenesis is a complex signaling pathway coordinated by multiple gene and protein targets that mediate osteoblast differentiation of stem cells. Therefore, to understand osteogenic signaling stimulated by graphene, we evaluated gene expression patterns in human AD-MSCs and BM-MSCs using human osteogenesis focused PCR arrays (Qiagen, Hilden, Germany, #PAHS-026Z). These 96 well-arrays are coated with primers that target 84 genes of interest, 5 housekeeping genes for data normalization, and 7 controls to evaluate human genomic DNA contamination, performance of reverse transcription, and positive PCR control reactions. Genes of interest could be classified into the following major categories: transcriptional regulation, osteoblast-related, extracellular matrix markers, cellular adhesion, BMP and SMAD signaling, growth factors, and angiogenic factors. In addition to the above targets, there are other genes

included in these arrays which potentially have minor roles in osteogenesis, and hence, do not fit into the above categories.

As described earlier, expression profiles of ALPL, BGLAP, and RUNX2 during osteogenesis are commonly used as indicators of cell differentiation and hence, are typically evaluated using single gene PCR reactions following Alizarin red staining [17-19]. Therefore, we examined these gene expressions between human AD-MSCs cultured on LOG in absence of osteogenic differentiation reagents to MSCs cultured on tissue culture substrate in presence of differentiation reagents at day 21. Gene expression on tissue culture substrate was set as the control and that on the LOG surface was set as the test group (Figure 2.4). There was a significant ($P<0.05$) increase in the expression of ALPL and BGLAP in cells cultured on LOG, confirming osteogenesis under the media conditions described above. RUNX2 was not statistically different on LOG, thereby suggesting the expression levels are similar across these comparisons. To understand and compare the osteogenic signaling mediated by LOG on human AD-MSCs and BM-MSCs, all further comparisons were performed on cells cultured on the LOG surface only.

Percent of differentially expressed genes suggest early changes in BMMSCs

Gene expressions patterns of AD-MSCs and BM-MSCs cultured on LOG were over time (day 7 set as control to day 21 set as the test group) within each cell type. Subsequently the patterns were compared between the two cell lines at each time point, thus, resulting in a total of 4 comparisons. Differentially expressed and significantly different genes ($p<0.05$) are reported and described in sections below. Over time, the percentage of significantly expressed genes was consistent in both cell types.

Comparisons showed that 61-62% of the genes analyzed changed statistically with 37-43% being upregulated while only 19-24% were downregulated (Figure 2.5A), complementing the osteogenic response of MSCs on LOG. Interestingly, when day 7 results were compared between the two cell types, 60% of genes were upregulated in BM-MSCs while only 13% were downregulated (Figure 2.5B), suggesting upregulation of a higher number of gene targets in BM-MSCs at an earlier time point. Comparatively, at day 21 only 45% of genes were upregulated in BM-MSCs while 23% of genes were downregulated. Across all comparisons, < 10% of genes were unconfirmed, possibly due to low expression or lack of primer annealing, and hence were not detected.

Distinct transcription factors control osteogenesis of MSCs

We examined the expression of four genes, *DLX5, RUNX2, SOX9*, and *SP7* known to control stem cell fate (Table 2.1). As shown, *RUNX2* was significantly upregulated in AD-MSCs, while SOX9 and SP7 were downregulated, suggesting *RUNX2* to be the master regulator in AD-MSCs. Comparatively, in BM-MSCs, all genes were downregulated. Interestingly, when BM-MSCs were compared to AD-MSCs, all transcription factors were upregulated at both time points (Table 2.2). The fold changes at day 7 were comparatively more robust to that observed at day 21, suggesting the involvement of all transcription factors triggering osteogenesis at an early time point in BM-MSCs.

Upregulation of osteoblast-related genes confirm osteogenesis in MSCs

Osteoblast differentiation of MSCs is evidenced by the expression of cell - specific markers. We examined the expression of 4 genes, *ALPL*, *BGLAP*, *PHEX*, and *SPP1*, commonly used as markers of osteogenesis (Table 2.1). As shown, *ALPL*, *BGLAP*

(osteocalcin), and *PHEX* were upregulated in AD-MSCs while *SPP1* was downregulated. Comparatively, in BM-MSCs, in addition to *ALPL* and *PHEX*, *SPP1* was also upregulated, suggesting osteogenesis within 21 days in both cell types. When BM-MSCs were compared to AD-MSCs results were very interesting. Only *BGLAP* was significantly upregulated at day 7, whereas, at day 21 all genes were downregulated with the exception of *SPP1* (Table 2.2), suggesting osteogenesis of BM-MSCs at a time point earlier than day 21.

ECM targets support cell adhesion and differentiation

When cells undergo osteoblast differentiation in both the presence and absence of nanocomposite materials, they express ECM in the form of organic and inorganic molecules. ECM proteins have important roles in cell adhesion and differentiation. ECM proteins trigger signal transduction pathway(s) leading to their differentiation to specific lineages. Once the MSCs are triggered towards differentiation, ECM proteins support the adhesion of the differentiated cells to the substrate, and hence, are required throughout their development. The ECM genes exist as families coding for the various isoforms of the proteins, each form contributing to its function. Here we examined the expression of specific ECM genes including those coding for collagen, fibronectin, and proteoglycan (Tables 2.1, 2.2). In AD-MSCs, predominantly all genes tested including *BGN*, *COL3A1*, *COL14A1*, *COL15A1* and *FN1* were upregulated while only *COL1A2* was downregulated. Comparatively, in BM-MSCs, all genes were upregulated, with the fold changes much higher than that observed in AD-MSCs. Interestingly when AD-MSCs were compared to BM-MSCs at day 7, all genes except *COL3A1* and *COL15A1* were upregulated (Table 2.2). Taken together, these data suggest that the specific

genes encoding ECM proteins support the adherence and osteogenesis of MSCs from both the sources.

Relatively robust upregulation of genes encoding for cell adhesion proteins

MSCs adhere to a given surface and express ECM, and subsequently relay extracellular signals to the nucleus for osteogenic differentiation and communication. MSCs are adherent cells and hence, cell adhesion proteins are required for the attachment and cell development. In this study, 7 cellular adhesion genes were examined (Table 2.1). In AD-MSCs, *ICAM1*, *ITGA1*, and *VCAM1* were all upregulated while only *ITGA2* and *ITGB1* were downregulated. Similar patterns of expression were observed in BM-MSCs with upregulation of *CDH11*, *ICAM1*, *ITGA1*, *ITGA3*, and *VCAM1*, and downregulation of only *ITGA2* and *ITGB1*. Comparatively, when AD-MSCs were compared to BM-MSCs, *CDH11*, *ITGA1*, *ITGA2*, *ITGA3*, *ITGB1* were all upregulated at day 7. Similar expression patterns were observed at day 21, with the exception of *ITGA2*. Noteworthy is the 482.15- and 1376.38-fold upregulation of *VCAM1* at days 7 and 21, respectively (Table 2.2). Results confirm that LOG surface provides an optimal substrate for cells to adhere, communicate, differentiate, and maintain their function.

BMP/SMAD – mediated osteogenesis in MSCs

BMP-SMAD signaling is one of the major pathways that the cells use when they undergo osteoblast differentiation. BMP and the SMAD families of genes consist of multiple isoforms, majority of which were represented in these arrays. We examined 4 BMPs, 4 BMP receptors (BMPRs) and 5 SMAD isoforms (Table 2.1). In AD-MSCs, only *BMP4* and *BMPR2* were upregulated while *BMP6* was downregulated. Similarly, all

SMAD isoforms including, *SMAD2*, *SMAD3*, and *SMAD5* were upregulated suggesting that osteogenesis is potentially mediated by BMP/SMAD signaling. Comparatively, in BM-MSCs, only *BMP4*, *BMPR1A* and *BMPR1B* were upregulated, while *BMP2*, *BMP6* and *BMPR2* were downregulated. Of the SMAD genes tested in BM-MSCs, only *SMAD3* was upregulated while *SMAD1*, *SMAD4*, and *SMAD5* were downregulated. Interestingly when AD-MSCs were compared with BM-MSCs, patterns of expression suggestive of BMP/SMAD signaling in BM-MSCs were observed (Table 2.2). At Day 7, *BMP1*, *BMP2*, and *BMP6* were upregulated while only *BMP4* was downregulated. At Day 21, however, only *BMP2* was upregulated and *BMP4* was downregulated. Additionally, all BMPRs and SMAD genes demonstrated robust upregulation at both time points. Results further support that similar to AD-MSCs, osteogenesis of BM-MSCs is also mediated by BMP/SMAD signaling, and potentially occurs at a time point earlier than day 21.

TGFβ family members are involved in osteogenesis

In addition to the BMPs, growth factors including EGF, FGF, IGF and their corresponding receptors are also involved in bone tissue healing, regeneration, and cell differentiation. In this study we examined 10 growth factors and 6 growth factor receptors (Table 2.1). In AD-MSCs, *IGF1*, *TGFB2*, *TGFB3*, and *TNF* were upregulated while *EGF*, *FGF1*, *FGF2*, and *GDF10* were downregulated. All growth factor receptor genes, including *EGFR*, *IGF1R*, *TGFBR1*, and *TGFBR2* were upregulated. Comparatively, in BM-MSCs, *IGF2*, *TGFB2*, and *TGFB3* were upregulated while *FGF1*, *FGF2*, *IGF1*, *TGFB1* were downregulated. Correspondingly, the growth factor receptors including, *FGFR2*, *TGFBR1*, and *TGFBR2* were upregulated, while only *IGF1R* was

downregulated. Fold expression changes between the two cell types were very striking. At day 7, only *GDF10* was downregulated, while at Day 21 both *GDF10* and *TGFB3* were downregulated (Table 2.2). All other growth factors including *EGF*, *FGF1*, *FGF2*, *IGF1*, *IGF2*, *TGFB1*, and *TGFB2* were upregulated at both time points with significantly higher changes in *TGFB2*. Similarly, all growth factor receptors were upregulated at both time points with the exception of *TGFBR2* and *EGFR* which was downregulated at day 21 only, suggesting the potential involvement of the TGF beta family of genes and their corresponding receptors, mediated osteogenesis of MSCs on LOG.

Significant upregulation of angiogenic factors at all-time points

Angiogenesis is closely entwined with osteoblast differentiation. Formation of new blood vessels along with maintenance of new and old blood vessels are both coupled with osteogenesis [28]. In AD-MSCs, *PDGFA*, *VEGFA*, and *VEGFB* were all upregulated (Table 2.1). Comparatively, in BM-MSCs, only *VEGFB* was upregulated. There was no downregulation of any angiogenic markers at any time point (Table 2.2). Interestingly, when AD-MSCs were compared to BM-MSCs, *PDGFA*, *VEGFA* and *VEGFB*, all displayed significant upregulation at both time points, suggesting the angiogenic potential of MSCs in presence of LOG.

Cytoscape analysis demonstrates potential gene interactions at the protein level

The significant changes described above were translated to potential signaling pathways that the MSCs undergo during osteogenesis on LOG. Using Cytoscape, an open source software platform, we visualized the molecular interaction between the gene targets and their potential proteins (Figure 2.6). The propellor plots shown in this figure demonstrate a significantly high number of gene/protein targets from the ECM

markers and the TGFβ/BMP/SMAD pathways to have a role in osteogenic differentiation of MSCs on LOG. The plots confirm our earlier report that ECM proteins play an important role in the adhesion and subsequent differentiation of MSCs on LOG [11]. Data presented here demonstrates that osteogenesis of both the AD and BM MSCs is potentially mediated by the TGFβ/BMP/SMAD signaling.

Immunofluorescence confirms cytoskeletal organization and distinct ECM protein expression of BM-MSCs

Phalloidin F-actin staining illustrates cytoskeletal organization and cell adhesion and hence, is a powerful tool to show cell attachment onto biomaterials. We have previously demonstrated cytoskeletal health and integrity of AD-MSCs on LOG [11]. In this study, we confirmed the cytoskeletal organization of BM-MSCs on LOG (Figure 2.7A) at 24 hr and 21 days i.e. at the adhesion and differentiation time points. Even though the cytoskeletal integrity appears to be maintained at both time points, subjectively, cells appear discretely localized and clustered at the 24 hr time point, supporting our earlier data that cell attachment to LOG surface is not random. Subsequently, the expression and localization of fibronectin and collagen 1 evaluated at the same time points confirm that the two ECM proteins have roles in cell adhesion and differentiation on LOG surface (Figure 2.7B, C). These data complement our report on the behavior of AD-MSCs [11]. Subjective evaluation of fibronectin and collagen at 24 hr and at day 21 suggests higher expression and a relatively more discrete pattern of expression at 24hr. Even though BM-MSCs express these ECM proteins at day 21, cells are sparse and the expression is weak, suggesting that cells undergo osteogenesis presumably at a time point earlier than day 21. The significant down regulation of genes at day 21 as

described in the above sections complements this observation. A future study that investigates an osteogenic response and the expression of ECM proteins in BM-MSCs, between 24 hr and day 21 is needed to confirm this data.

DISCUSSION

In this study, we present data comparing the osteogenic behavior of human adipose - and bone marrow – derived MSCs in presence of LOG using *in vitro* osteogenesis assays and genetic profiling. To our knowledge, this is the first study to compare changes in gene expressions when MSCs from two distinct tissue sources undergo spontaneous (without any chemical induction) osteogenic differentiation in presence of graphene. Additionally, this is the first study reporting simultaneous genetic profiling of a panel of genes involved in cell adhesion, production of ECM, osteoblast differentiation, and ossification. Changes in gene expression provides a mechanistic overview of the key targets that are potentially involved in graphene – mediated osteogenic signaling of MSCs. This data strengthens the use of MSCs + graphene surfaces as scaffold components for bone tissue engineering.

When placed in an osteogenic environment, MSCs have the potential to differentiate into osteoblasts (bone cells). This commitment is regulated by osteoblast-associated transcription factors (DLX5, RUNX2, SP7, SOX9), adhesion molecules (integrins β1/ITGB1), and extracellular matrix proteins (ECM) (fibronectin, collagen I) [29]. During differentiation, cells generate tissue - specific ECM, express ALPL, BGLAP, and SPP1, and undergo bone cell development. Renowned osteogenic pathways include the WNT/β-catenin and bone morphogenetic protein (BMP)/transforming growth factor beta (TGFβ) pathways. The WNT proteins activate at least three distinct intracellular

signaling cascades important for osteogenic differentiation [30]. Some studies suggest cross talk between WNT, MAPK, and TGFβ signaling when MSCs undergo osteogenesis [31]. On the other hand, BMP/TGFβ signaling has been thoroughly reviewed in bone development which functions through both canonical (SMAD dependent) and non-canonical (SMAD independent) pathways, thereby mediating transcription [32, 33]. Additionally, the Hedgehog (Hh) and Notch pathways are suggested to affect cell osteogenesis, but their exact role is unknown [34-38]. It is thus evident that the osteogenic signaling pathways are complex and involve a coordinated action of multiple genes and their corresponding protein factors.

Bone marrow and adipose tissue are the most common MSC resources [39-44]. Although bone marrow is considered the richest source of MSCs in humans and animals, fat-derived MSCs are preferred in many clinics or in basic research projects, because the tissue harvest is relatively easy, less invasive, and not associated with patient morbidity [45-48]. Although MSCs isolated from the two tissue sources adhere to tissue culture polystyrene surface, show similar expression patterns of cluster-of-differentiation markers, morphology, and trilineage differentiation potential *in vitro* [43], they might exhibit differences in their lineage-specific features and overall functionality. These variations have been reported in presence and absence of biomaterials [49-51]. For instance, we expect the BM-MSCs to exhibit an increased potential towards osteogenesis as studies show that in the absence of any biomaterial, AD and BM-MSCs undergo osteogenesis by different signaling pathways [52]. Therefore, it is possible that their interaction with materials might affect this process, and BM-MSCs may not be the optimal cell type to use. For example, it was found that osteogenic induction of BM-

MSCs was mediated by the p38 MAPK pathway, while AD-MSCS involved the p44/42 MAPK pathway [25]. Contrary to this report, other studies have found that PDGF enhances osteogenesis of AD-MSCs, but not BM-MSCs [53]. Hence, for an efficacious stem cell therapy, it is important to study a specific cell type in context of a given biomaterial *in vitro* and *in vivo*.

The AD and BM-MSCs undergo osteogenesis on tissue culture polystyrene surface within 21-28 days in conditions of chemical induction. Osteogenesis is a programmed process which is accompanied by dynamic changes in the expression profiles of osteoblast-related genes. Early markers of osteogenesis are expressed as early as 7-10 days post induction [43] [54, 55], and completed within 21-28 days concomitant with the expression of late osteogenic markers. As a result, we examined differences in gene expressions at days 7 and 21 when AD and BM-MSCs are cultured on graphene. Since osteoblast development from MSCs is recognized by mineralization, which can be visualized by alizarin red staining and quantitated by elution of the red color, we found that both AD and BM-MSCs were differentiated by 21 days when chemically induced on tissue culture polystyrene and when non-chemically induced on graphene (Figure 2.2). Osteogenic differentiation under these media conditions was confirmed by the increase in ALPL and BGLAP expression in AD-MSCs cultured on graphene relative to the tissue culture polystyrene surface (Figure 2.4). Lower mineralization was observed when AD and BM-MSCs were simultaneously exposed to osteo-chemical inducers and graphene. Although we confirmed the cells were viable (data not shown), it is possible that the combination triggers distinct signal transduction pathway(s) [26], which is beyond the scope of this study.

Graphene-based nanomaterials have been recognized as successful components of bone tissue engineering scaffolds [4, 56-60]. Studies recognize graphene as a delivery vehicle to control the release and dosing of potent BMP2 treatments for endogenous stem cell activation [61-64], or as a nanomaterial which by virtue of its physicochemical properties creates an osteogenic environment triggering both the endogenous and exogenous stem cells to undergo osteogenesis. Graphene studies consistently show osteogenesis of various MSCs sources [17-19, 65-78], which is generally supported by mineralization stains and upregulation of bone – specific markers i.e. RUNX2, ALPL, BMP2, BGLAP, SPP1, and COL I. These studies demonstrate the end result of osteogenic differentiation but lack understanding of how the signaling process occurs. Most recently, it was shown that human dental pulp MSCs in the presence of graphene achieved osteogenesis via the integrin/focal adhesion kinase axis, thereby signaling SMAD phosphorylation, RUNX2 transcription, and production of BGLAP and SPP1 proteins [76]. It is suggested that the carbon arrangement of graphene and its derivatives mimics an organic bone ECM microenvironment, whereby stem cells can attach, proliferate and ultimately differentiate under the appropriate cues [11]. As a result, cell adhesion is the initiating event, since without this attachment, cells have a limited opportunity to produce their ECM and be signaled into differentiation. Subsequently, extracellular ligands can bind to cell surface receptors and relay signals into the nucleus for transcriptional activation that commits osteogenic differentiation. It is possible that by virtue of its planar structure, the low oxygen content form of graphene makes cells accessible to the graphene surface, potentially providing guidance and an appropriate topography to attach, cluster, and thereby differentiate into osteogenic

lineage. Our data supports this theory as both MSC sources on the low oxygen graphene either maintained or positively expressed several adhesion (i.e. CDH11, ICAM1, ITGA1, ITGA3, VCAM1) and ECM (i.e. BGN, COL1A1, COL3A1, COL10A1, COL14A1, COL15A1, FN1) genes over time.

In addition to osteogenesis, there are some reports demonstrating the angiogenic effect of graphene nanomaterials. Park et al. showed that rGO flakes incorporated with MSC spheroids stimulated the expression of angiogenic growth factors, including VEGF, HGF, and FGF2 [79]. Similarly, it was found that graphene-based biomaterials not only differentiated cells into osteoblasts, but simultaneously increased other angiogenic markers, namely von Willibrand factor (vWF) and angiopoietin-1 (ang-1) [74]. Other studies have found that low concentrations of graphene derivatives (up to 100 ng/mL^{-1}) triggers a pro-angiogenic environment via Akt and nitric oxide signaling of endothelial cells [80].

Our data supports a recent study that demonstrated graphene – mediated osteogenesis via BMP/SMAD pathways [81]. However, for the first time, we provide information on the various protein isoforms belonging to these families. We not only show expressions of osteoblast-related genes, but also the coordinated involvement of cellular adhesion molecules, ECM, growth factors, and angiogenic factors which are all necessary for osteogenic signaling, maintenance, and survival. Additionally, no study has completed a head-to-head comparison of different MSC sources on graphene. The current literature primarily studies MSCs associated with mineralized tissues (i.e., bone marrow, dental pulp, and periodontal ligament) [18, 19, 70, 71, 73, 74, 76-78], with only one other research group identifying osteogenesis of AD-MSCs on graphene [69]. Our study

recognizes that AD-MSCs may achieve osteogenesis slower than BM-MSCs but are still a valid and feasible resource for bone healing and repair.

In this study, we demonstrate that both AD and BM-MSCs undergo osteogenesis on graphene surfaces which is mediated by multiple transcription factors in addition to RUNX2, the most commonly reported in all the studies described above. The transcriptional regulation appears to be controlled by RUNX2 and DLX5. This is a novel finding and suggests that the action of RUNX2 and DLX5 may be synergistic in the osteogenic behavior of BM-MSCs in presence of graphene. DLX5 and RUNX2 has been reported to have a significant role in early bone development, by mediating intramembranous and endochondral ossification, respectively [82-84]. Additionally, comparative assessment indicates that the osteogenic commitment of BM-MSCs occurs at a time point earlier than day 21. This is significant and can greatly affect *in vitro* and *in vivo* studies using graphene nanomaterials. Other novel targets identified in this study include *PHEX* (phosphate-regulating gene with homologies to endopeptidase on the X chromosome), an osteoblast-related gene that when inactive, leads to excessive phosphate wasting and consequently causes rickets [85]. In contrast to bone, we also examined chondrocyte-related genes, namely SOX9 and COMP (cartilage oligomeric matrix protein, data not shown) which were downregulated in both cell types over time. Finally, our data supports that culturing MSCs on graphene upregulates angiogenic markers, *VEGF* and *PDGF*. Interestingly, *PDGF* bridges the osteogenic and angiogenic pathways by freeing MSCs from blood vessels and positively regulating *VEGF* signaling [86]. This data suggests that graphene surfaces could simultaneously attract blood vessel ingrowth when implanted *in vivo*.

CONCLUSION

This study investigates the genetic responses when MSCs undergo osteogenesis on graphene. Graphene genetically supports osteogenesis of MSCs by multiple transcription factors, extracellular matrix production, adhesion molecules, growth factor signaling, and angiogenic markers. Additionally, we provide this information from various MSCs sources, which have similar outcomes on graphene, but different mechanisms to osteoblast-development. These results provide optimism that exogenous MSCs implanted with graphene materials could support new bone development in future animal models and human clinical trials.

AUTHORS' CONTRIBUTIONS

AFM, AJB, SDN designed the experiments under the mentorship of MSD. AFM, AJB, SND and LA performed the RNA and immunofluorescence assays; TJM performed the in vitro osteogenesis experiments, and analyzed the results; RDT, CDG and WJK synthesized and characterized the graphene nanoparticles under the mentorship of SEB. SEB's team analyzed the material data and wrote the corresponding portion of the manuscript. MSD's team analyzed the cellular data and wrote the corresponding portion of the manuscript. All authors read and approved the final manuscript.

ACKNOWLEDGEMENTS - FUNDING

This work was supported by a grant from NIH/NIAMS (R15AR070460) to MD. UA-Little Rock acknowledges partial support from FDA (Contract # HSF223201400079C – Arkansas Research Alliance).

AVAILABILITY OF DATA AND MATERIALS

All data generated or analyzed during this study are included in the article.

CONSENT FOR PUBLICATION

Not applicable.

COMPETING INTERESTS

The authors declare that they have no competing interests.

REFERENCES

1. Atala, A., *Tissue engineering and regenerative medicine: concepts for clinical application.* Rejuvenation Res, 2004. **7**(1): p. 15-31.
2. Hong, G., et al., *Carbon Nanomaterials for Biological Imaging and Nanomedicinal Therapy.* Chem Rev, 2015. **115**(19): p. 10816-906.
3. Georgakilas, V., et al., *Functionalization of graphene: covalent and non-covalent approaches, derivatives and applications.* Chem Rev, 2012. **112**(11): p. 6156-214.
4. Mao, H.Y., et al., *Graphene: promises, facts, opportunities, and challenges in nanomedicine.* Chem Rev, 2013. **113**(5): p. 3407-24.
5. Yang, K., et al., *Preparation and functionalization of graphene nanocomposites for biomedical applications.* Nat Protoc, 2013. **8**(12): p. 2392-403.
6. Majeed, W., et al., *The role of surface chemistry in the cytotoxicity profile of graphene.* J Appl Toxicol, 2017. **37**(4): p. 462-470.
7. Bourdo, S.E., et al., *Physicochemical characteristics of pristine and functionalized graphene.* J Appl Toxicol, 2017. **37**(11): p. 1288-1296.
8. Kalbacova, M., et al., *Graphene substrates promote adherence of human osteoblasts and mesenchymal stromal cells.* Carbon, 2010. **48**(15): p. 4323-4329.
9. Elkhenany, H., et al., *Graphene supports in vitro proliferation and osteogenic differentiation of goat adult mesenchymal stem cells: potential for bone tissue engineering.* J Appl Toxicol, 2015. **35**(4): p. 367-74.
10. Elkhenany, H., et al., *Graphene nanoparticles as osteoinductive and osteoconductive platform for stem cell and bone regeneration.* Nanomedicine, 2017. **13**(7): p. 2117-2126.
11. Newby, S.D., et al., *Functionalized Graphene Nanoparticles Induce Human Mesenchymal Stem Cells to Express Distinct Extracellular Matrix Proteins Mediating Osteogenesis.* Int J Nanomedicine, 2020. **15**: p. 2501-2513.
12. Perez, R.A., et al., *Therapeutically relevant aspects in bone repair and regeneration.* Materials Today, 2015. **18**(10): p. 573-589.

13. Prasadh, S., S. Suresh, and R. Wong, *Osteogenic Potential of Graphene in Bone Tissue Engineering Scaffolds.* Materials (Basel), 2018. **11**(8).
14. Phinney, D.G., et al., *Donor variation in the growth properties and osteogenic potential of human marrow stromal cells.* J Cell Biochem, 1999. **75**(3): p. 424-36.
15. Katsara, O., et al., *Effects of donor age, gender, and in vitro cellular aging on the phenotypic, functional, and molecular characteristics of mouse bone marrow-derived mesenchymal stem cells.* Stem Cells Dev, 2011. **20**(9): p. 1549-61.
16. Zaim, M., et al., *Donor age and long-term culture affect differentiation and proliferation of human bone marrow mesenchymal stem cells.* Ann Hematol, 2012. **91**(8): p. 1175-86.
17. Lee, J.H., et al., *Reduced graphene oxide-coated hydroxyapatite composites stimulate spontaneous osteogenic differentiation of human mesenchymal stem cells.* Nanoscale, 2015. **7**(27): p. 11642-51.
18. Xie, H., et al., *Two and three-dimensional graphene substrates to magnify osteogenic differentiation of periodontal ligament stem cells.* Carbon, 2015. **93**.
19. Yang, X., et al., *Effects of graphene oxide and graphene oxide quantum dots on the osteogenic differentiation of stem cells from human exfoliated deciduous teeth.* Artif Cells Nanomed Biotechnol, 2019. **47**(1): p. 822-832.
20. Wofford, A., et al., *Human Fat-Derived Mesenchymal Stem Cells Xenogenically Implanted in a Rat Model Show Enhanced New Bone Formation in Maxillary Alveolar Tooth Defects.* Stem Cells Int, 2020. **2020**: p. 8142938.
21. Mueller, O., S. Lightfoot, and A. Schroeder, *RNA integrity number (RIN)-standardization of RNA quality control.* Agilent Application Note, 2004: p. 1-8.
22. Osteogenesis, H., *Profiler ™ PCR Array.* 2021.
23. Gentile, F., et al., *Cells preferentially grow on rough substrates.* Biomaterials, 2010. **31**(28): p. 7205-12.
24. Tang, L.A., et al., *Highly wrinkled cross-linked graphene oxide membranes for biological and charge-storage applications.* Small, 2012. **8**(3): p. 423-31.
25. Elkhenany, H., et al., *Impact of the source and serial passaging of goat mesenchymal stem cells on osteogenic differentiation potential: implications for*

bone tissue engineering. Journal of animal science and biotechnology, 2016. **7**: p. 16-16.

26. Langenbach, F. and J. Handschel, *Effects of dexamethasone, ascorbic acid and β-glycerophosphate on the osteogenic differentiation of stem cells in vitro.* Stem Cell Res Ther, 2013. **4**(5): p. 117.
27. Kukurba, K.R. and S.B. Montgomery, *RNA Sequencing and Analysis.* Cold Spring Harb Protoc, 2015. **2015**(11): p. 951-69.
28. Grosso, A., et al., *It Takes Two to Tango: Coupling of Angiogenesis and Osteogenesis for Bone Regeneration.* Front Bioeng Biotechnol, 2017. **5**: p. 68.
29. Huang, W., et al., *Signaling and transcriptional regulation in osteoblast commitment and differentiation.* Front Biosci, 2007. **12**: p. 3068-92.
30. Houschyar, K.S., et al., *Wnt Pathway in Bone Repair and Regeneration - What Do We Know So Far.* Front Cell Dev Biol, 2018. **6**: p. 170.
31. Gregory, C.A., et al., *How Wnt signaling affects bone repair by mesenchymal stem cells from the bone marrow.* Ann N Y Acad Sci, 2005. **1049**: p. 97-106.
32. Chen, G., C. Deng, and Y.-P. Li, *TGF-β and BMP signaling in osteoblast differentiation and bone formation.* International journal of biological sciences, 2012. **8**(2): p. 272-288.
33. Guo, X. and X.-F. Wang, *Signaling cross-talk between TGF-beta/BMP and other pathways.* Cell research, 2009. **19**(1): p. 71-88.
34. Long, F., et al., *Ihh signaling is directly required for the osteoblast lineage in the endochondral skeleton.* Development, 2004. **131**(6): p. 1309-18.
35. Huelsken, J. and W. Birchmeier, *New aspects of Wnt signaling pathways in higher vertebrates.* Curr Opin Genet Dev, 2001. **11**(5): p. 547-53.
36. Engin, F., et al., *Dimorphic effects of Notch signaling in bone homeostasis.* Nat Med, 2008. **14**(3): p. 299-305.
37. Wozney, J.M., et al., *Novel regulators of bone formation: molecular clones and activities.* Science, 1988. **242**(4885): p. 1528-34.
38. Gazzerro, E. and E. Canalis, *Bone morphogenetic proteins and their antagonists.* Rev Endocr Metab Disord, 2006. **7**(1-2): p. 51-65.

39. Caplan, A.I., *Review: mesenchymal stem cells: cell-based reconstructive therapy in orthopedics.* Tissue Eng, 2005. **11**(7-8): p. 1198-211.
40. Caplan, A.I., *Adult mesenchymal stem cells for tissue engineering versus regenerative medicine.* J Cell Physiol, 2007. **213**(2): p. 341-7.
41. Caplan, A.I. and J.E. Dennis, *Mesenchymal stem cells as trophic mediators.* J Cell Biochem, 2006. **98**(5): p. 1076-84.
42. De Miguel, M.P., et al., *Immunosuppressive properties of mesenchymal stem cells: advances and applications.* Curr Mol Med, 2012. **12**(5): p. 574-91.
43. Dominici, M., et al., *Minimal criteria for defining multipotent mesenchymal stromal cells. The International Society for Cellular Therapy position statement.* Cytotherapy, 2006. **8**(4): p. 315-7.
44. Pittenger, M.F., *Mesenchymal stem cells from adult bone marrow.* Methods Mol Biol, 2008. **449**: p. 27-44.
45. Al-Nbaheen, M., et al., *Human stromal (mesenchymal) stem cells from bone marrow, adipose tissue and skin exhibit differences in molecular phenotype and differentiation potential.* Stem Cell Rev, 2013. **9**(1): p. 32-43.
46. Barry, F.P. and J.M. Murphy, *Mesenchymal stem cells: clinical applications and biological characterization.* Int J Biochem Cell Biol, 2004. **36**(4): p. 568-84.
47. Bieback, K., et al., *Comparing mesenchymal stromal cells from different human tissues: bone marrow, adipose tissue and umbilical cord blood.* Biomed Mater Eng, 2008. **18**(1 Suppl): p. S71-6.
48. Yoshimura, H., et al., *Comparison of rat mesenchymal stem cells derived from bone marrow, synovium, periosteum, adipose tissue, and muscle.* Cell Tissue Res, 2007. **327**(3): p. 449-62.
49. Im, G.I., Y.W. Shin, and K.B. Lee, *Do adipose tissue-derived mesenchymal stem cells have the same osteogenic and chondrogenic potential as bone marrow-derived cells?* Osteoarthritis Cartilage, 2005. **13**(10): p. 845-53.
50. Kaivosoja, E., et al., *Chemical and physical properties of regenerative medicine materials controlling stem cell fate.* Ann Med, 2012. **44**(7): p. 635-50.

51. Rath, S.N., et al., *Adipose- and bone marrow-derived mesenchymal stem cells display different osteogenic differentiation patterns in 3D bioactive glass-based scaffolds.* J Tissue Eng Regen Med, 2016. **10**(10): p. E497-e509.
52. Alajez, N., et al., *Which stem cells to choose for regenerative medicine application: Bone marrow and adipose tissue stromal stem cells – Similarities and differences.* Journal of Nature and Science of Medicine, 2018. **1**(2): p. 48-54.
53. Hung, B.P., et al., *Platelet-Derived Growth Factor BB Enhances Osteogenesis of Adipose-Derived But Not Bone Marrow-Derived Mesenchymal Stromal/Stem Cells.* Stem Cells, 2015. **33**(9): p. 2773-84.
54. Shui, C., et al., *Changes in Runx2/Cbfa1 expression and activity during osteoblastic differentiation of human bone marrow stromal cells.* J Bone Miner Res, 2003. **18**(2): p. 213-21.
55. Peng, L., et al., *Comparative analysis of mesenchymal stem cells from bone marrow, cartilage, and adipose tissue.* Stem Cells Dev, 2008. **17**(4): p. 761-73.
56. Bressan, E., et al., *Graphene based scaffolds effects on stem cells commitment.* J Transl Med, 2014. **12**: p. 296.
57. Byun, J., *Emerging frontiers of graphene in biomedicine.* J Microbiol Biotechnol, 2015. **25**(2): p. 145-51.
58. Ding, X., Liu, H., and Fan, Y., *Graphene - based materials in regenerative medicine.* Adv. Healthcare Mater., 2015. **4**: p. 1451-1468.
59. Goenka, S., V. Sant, and S. Sant, *Graphene-based nanomaterials for drug delivery and tissue engineering.* J Control Release, 2014. **173**: p. 75-88.
60. Wick, P., Louw-Gaume, A.E., Kucki, M., et al., *Classification framework for graphene-based materials.* Angew. Chem. Int. Ed., 2014. **53**: p. 7714-7718.
61. La, W.-G., et al., *Bone morphogenetic protein-2 for bone regeneration – Dose reduction through graphene oxide-based delivery.* Carbon, 2014. **78**: p. 428–438.
62. Zhong, C., et al., *Continuous release of bone morphogenetic protein-2 through nano-graphene oxide-based delivery influences the activation of the NF-κB signal transduction pathway.* International Journal of Nanomedicine, 2017. **Volume 12**: p. 1215-1226.

63. Fu, C., et al., *Enhancing Cell Proliferation and Osteogenic Differentiation of MC3T3-E1 Pre-osteoblasts by BMP-2 Delivery in Graphene Oxide-Incorporated PLGA/HA Biodegradable Microcarriers.* Sci Rep, 2017. **7**(1): p. 12549.
64. Wang, Q., et al., *Molecular mechanisms of interactions between BMP-2 and graphene: Effects of functional groups and microscopic morphology.* Applied Surface Science, 2020. **525**: p. 146636.
65. Nayak, T.R., et al., *Graphene for controlled and accelerated osteogenic differentiation of human mesenchymal stem cells.* ACS Nano, 2011. **5**(6): p. 4670-8.
66. Crowder, S.W., et al., *Three-dimensional graphene foams promote osteogenic differentiation of human mesenchymal stem cells.* Nanoscale, 2013. **5**(10): p. 4171-6.
67. Kim, J., et al., *Graphene-incorporated chitosan substrata for adhesion and differentiation of human mesenchymal stem cells.* J Mater Chem B, 2013. **1**(7): p. 933-938.
68. Lee, J.H., et al., *Enhanced Osteogenesis by Reduced Graphene Oxide/Hydroxyapatite Nanocomposites.* Sci Rep, 2015. **5**: p. 18833.
69. Lyu, C.Q., et al., *Induction of Osteogenic Differentiation of Human Adipose-Derived Stem Cells by a Novel Self-Supporting Graphene Hydrogel Film and the Possible Underlying Mechanism.* ACS Appl Mater Interfaces, 2015. **7**(36): p. 20245-54.
70. Mo, X., et al., *Enhanced Stem Cell Osteogenic Differentiation by Bioactive Glass Functionalized Graphene Oxide Substrates.* Journal of Nanomaterials, 2016. **2016**: p. 1-11.
71. Zhou, Q., et al., *Bioactivity of periodontal ligament stem cells on sodium titanate coated with graphene oxide.* Sci Rep, 2016. **6**: p. 19343.
72. Hermenean, A., et al., *Chitosan-Graphene Oxide 3D scaffolds as Promising Tools for Bone Regeneration in Critical-Size Mouse Calvarial Defects.* Sci Rep, 2017. **7**(1): p. 16641.

73. Radunovic, M., et al., *Graphene oxide enrichment of collagen membranes improves DPSCs differentiation and controls inflammation occurrence.* J Biomed Mater Res A, 2017. **105**(8): p. 2312-2320.
74. Shie, M.Y., et al., *Synergistic acceleration in the osteogenic and angiogenic differentiation of human mesenchymal stem cells by calcium silicate-graphene composites.* Mater Sci Eng C Mater Biol Appl, 2017. **73**: p. 726-735.
75. Kim, J., et al., *Enhanced osteogenic commitment of murine mesenchymal stem cells on graphene oxide substrate.* Biomater Res, 2018. **22**: p. 1.
76. Xie, H., et al., *Graphene-Induced Osteogenic Differentiation Is Mediated by the Integrin/FAK Axis.* Int J Mol Sci, 2019. **20**(3).
77. Di Carlo, R., et al., *Osteoblastic Differentiation on Graphene Oxide-Functionalized Titanium Surfaces: An In Vitro Study.* Nanomaterials (Basel), 2020. **10**(4).
78. Zhang, J., et al., *3D bioprinting of graphene oxide-incorporated cell-laden bone mimicking scaffolds for promoting scaffold fidelity, osteogenic differentiation and mineralization.* Acta Biomater, 2020.
79. Park, J., et al., *Graphene Potentiates the Myocardial Repair Efficacy of Mesenchymal Stem Cells by Stimulating the Expression of Angiogenic Growth Factors and Gap Junction Protein.* Advanced Functional Materials, 2015. **25**: p. n/a-n/a.
80. Mukherjee, S., et al., *Graphene Oxides Show Angiogenic Properties.* Advanced Healthcare Materials, 2015.
81. Mahmood, M., et al., *Role of carbonaceous nanomaterials in stimulating osteogenesis in mammalian bone cells.* J Mater Chem B, 2013. **1**(25): p. 3220-3230.
82. Tadic, T., et al., *Overexpression of Dlx5 in chicken calvarial cells accelerates osteoblastic differentiation.* J Bone Miner Res, 2002. **17**(6): p. 1008-14.
83. Holleville, N., et al., *BMP signals regulate Dlx5 during early avian skull development.* Developmental Biology, 2003. **257**(1): p. 177-189.

84. McGee-Lawrence, M.E., et al., *Runx2 is required for early stages of endochondral bone formation but delays final stages of bone repair in Axin2-deficient mice.* Bone, 2014. **66**: p. 277-286.
85. Francis, F., et al., *A gene (PEX) with homologies to endopeptidases is mutated in patients with X-linked hypophosphatemic rickets.* Nat Genet, 1995. **11**.
86. Caplan, A. and D. Correa, *PDGF in Bone Formation and Regeneration: New Insights into a Novel Mechanism Involving MSCs.* Journal of orthopaedic research : official publication of the Orthopaedic Research Society, 2011. **29**: p. 1795-803.

APPENDIX

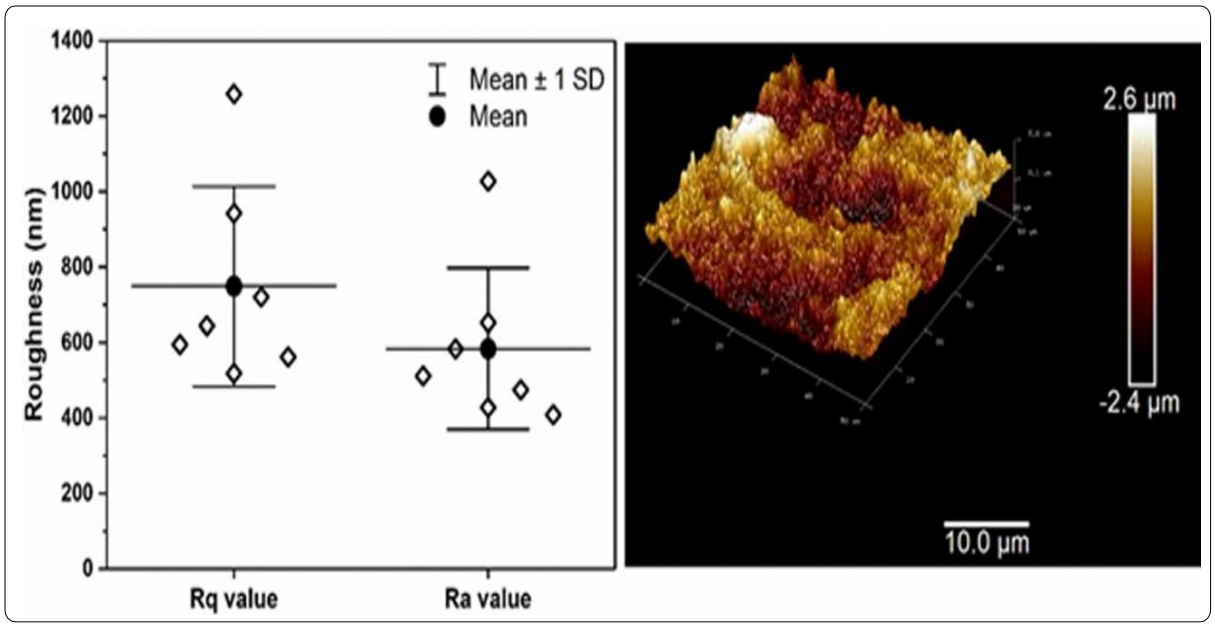

Figure 2.1. Atomic force microscopy. (Left panel) plot of roughness values (Rq and Ra) from 7 AFM imaged: data shown with diamonds, mean value with solid circle + line, and the standard deviation with whiskers. (Right panel) representative AFM image (approximately the average Rq and Ra values from around spot surface on 100 mm plastic petri dish.

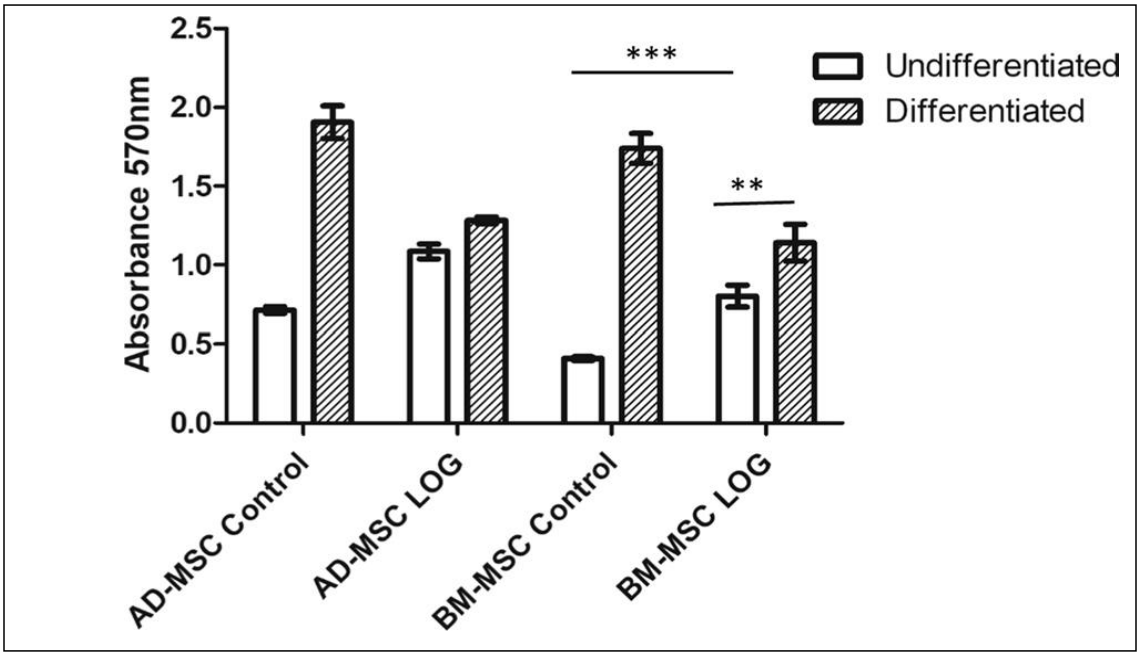

Figure 2.2. Osteogenic differentiation assay. AD-MSCs or BM-MSCs were seeded on tissue culture polystyrene (control) or LOG and cultured in either undifferentiated media (without osteogenic induction) or differentiated media (with osteogenic induction) for 21 days. Cells were then exposed to Alizarin red staining and read at absorbance 570 nm for calcium quantitation. Statistical significance ($p<0.05$) is indicated by asterisks.

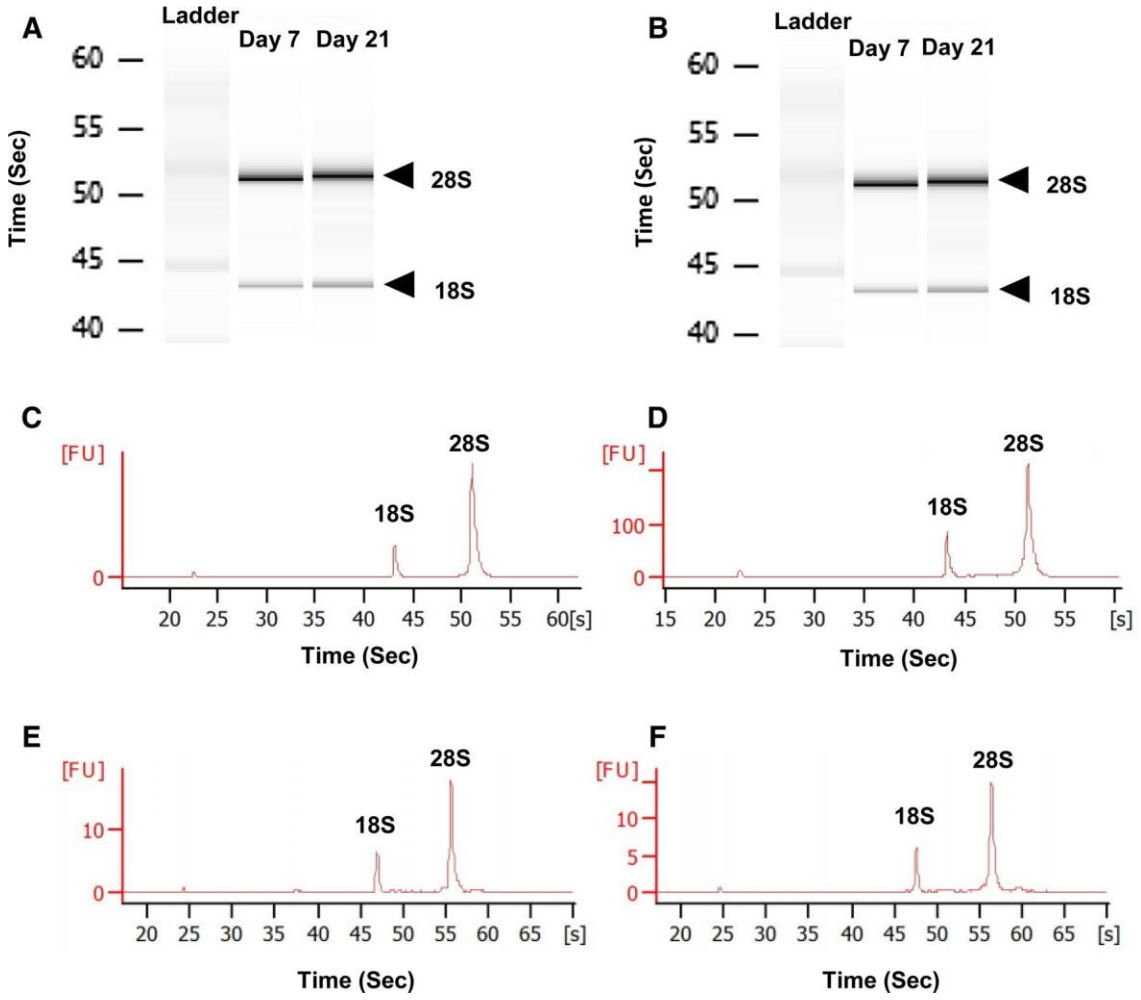

Figure 2.3. Assessment of RNA Quality. (A) Electrophoresis of total RNA from AD-MSCs cultured on LOG for either 7 or 21 days. **(B)** Electrophoresis of total RNA from BM-MSCs cultured on LOG for either 7 or 21 days. Arrows indicate bands of ribosomal subunits. **(C)** Electropherogram of AD-MSCs cultured on LOG for either 7 days (RIN = 9.10) or **(D)** 21 days (RIN = 9.60). **(E)** Electropherogram of BM-MSCs cultured on LOG for either 7 days (RIN = 9.40) or **(F)** 21 days (RIN = 9.50).

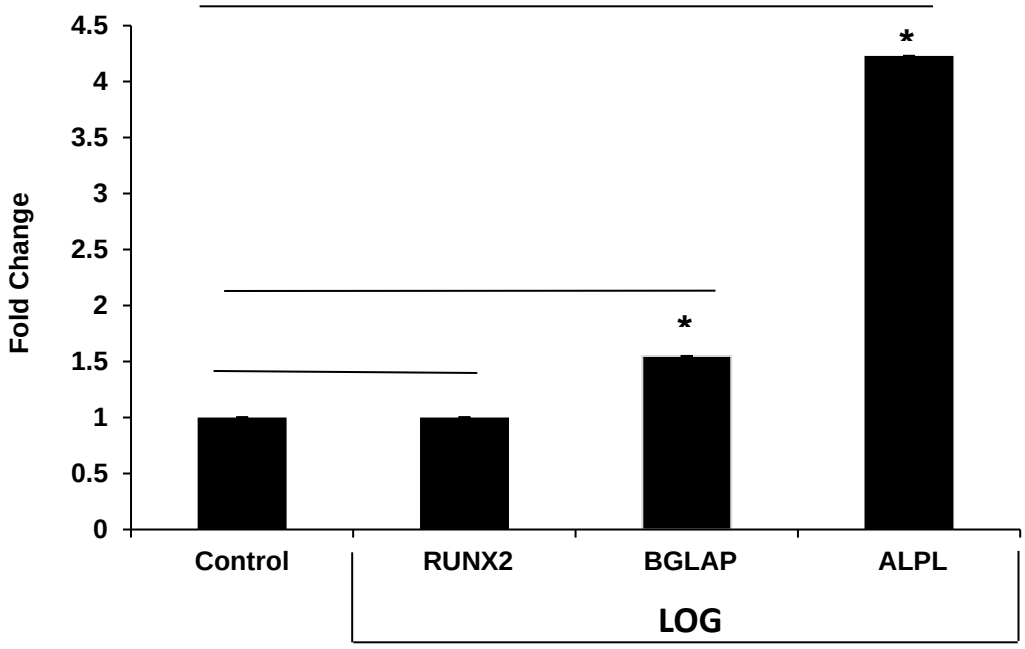

Figure 2.4. The effects of LOG on RUNX2, BGLAP, and ALPL gene expressions. AD-MSCs were cultured for 21 days in either an osteogenic differentiation media on tissue culture polystyrene (control) or in undifferentiated media on low oxygen graphene (LOG). Data was normalized to 1 by B2M. n =3; ***** indicates $p < 0.05$. Error bars presented as standard deviation.

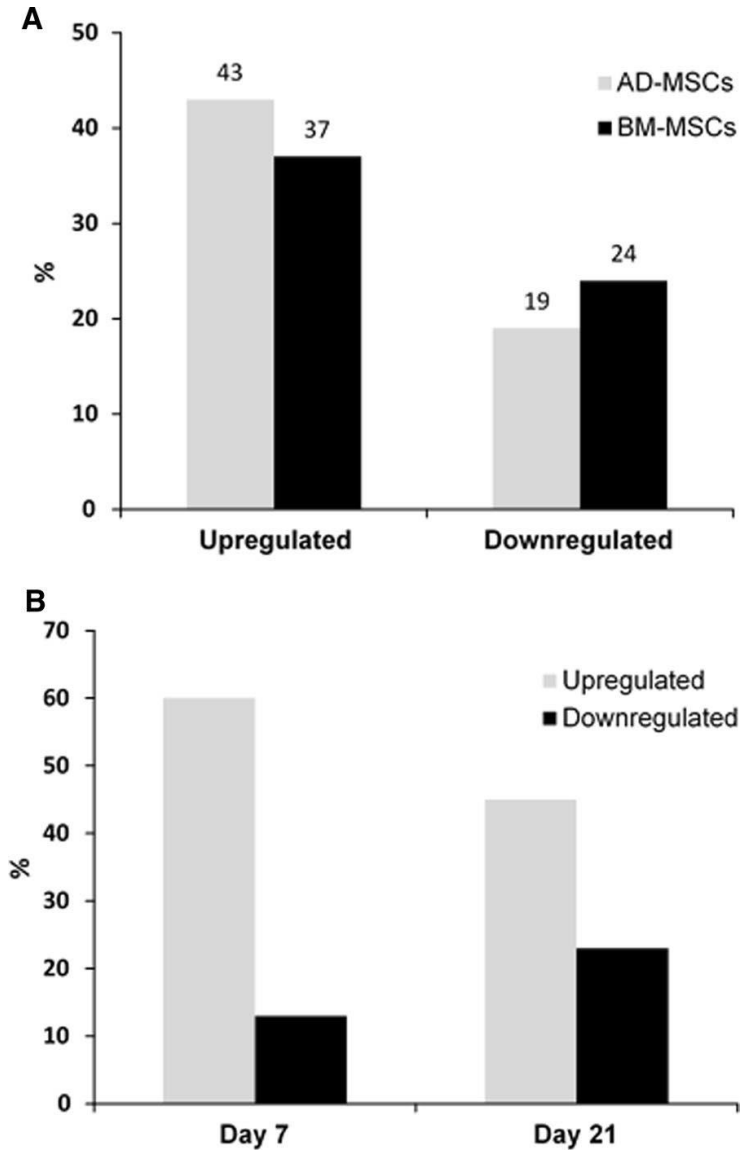

Figure 2.5. Differentially expressed genes when AD-MSCs and BM-MSCs undergo osteogenesis on LOG. (A) Percentage of significantly changed genes at Day 21 in comparison to its control at Day 7. **(B)** Percentage of significantly changed genes in BM-MSCs at each time point in comparison to AD-MSCs set as the control.

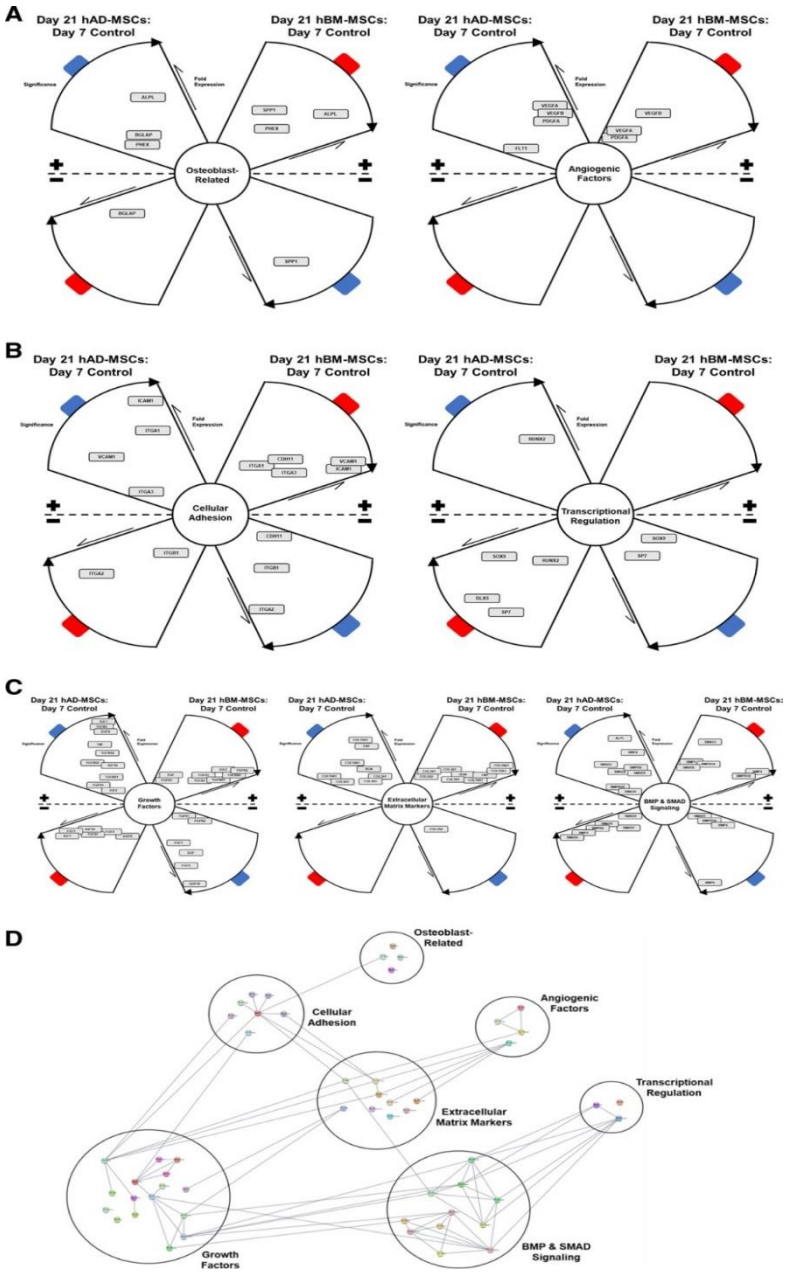

Figure 2.6. Propeller plots depicting potential gene targets and corresponding protein interactions. Cytoscape analyses illustrating differentially expressed genes related to Osteoblast and Angiogenic factors **(A)**, Cellular adhesion and transcriptional regulation **(B)**, and Growth factors, ECM markers and members of BMP/SMAD signaling **(C)** to be the key targets involved in osteogenic differentiation of human AD and BM – derived MSCs. In all analyses, day 7 expression was set as control and day 21 was the treated group. The cell types are color coded, with AD-MSCs (Blue) and BM-MSCs (Red), and the plot arcs with increasing significance moving clockwise and a decrease is represented as anticlockwise. **(D)** Connectively plot for target genes sorted based on established functional groups. Lines linking nodes indicate relationships between associated proteins as annotated by STRING application software within the Cytoscape platform.

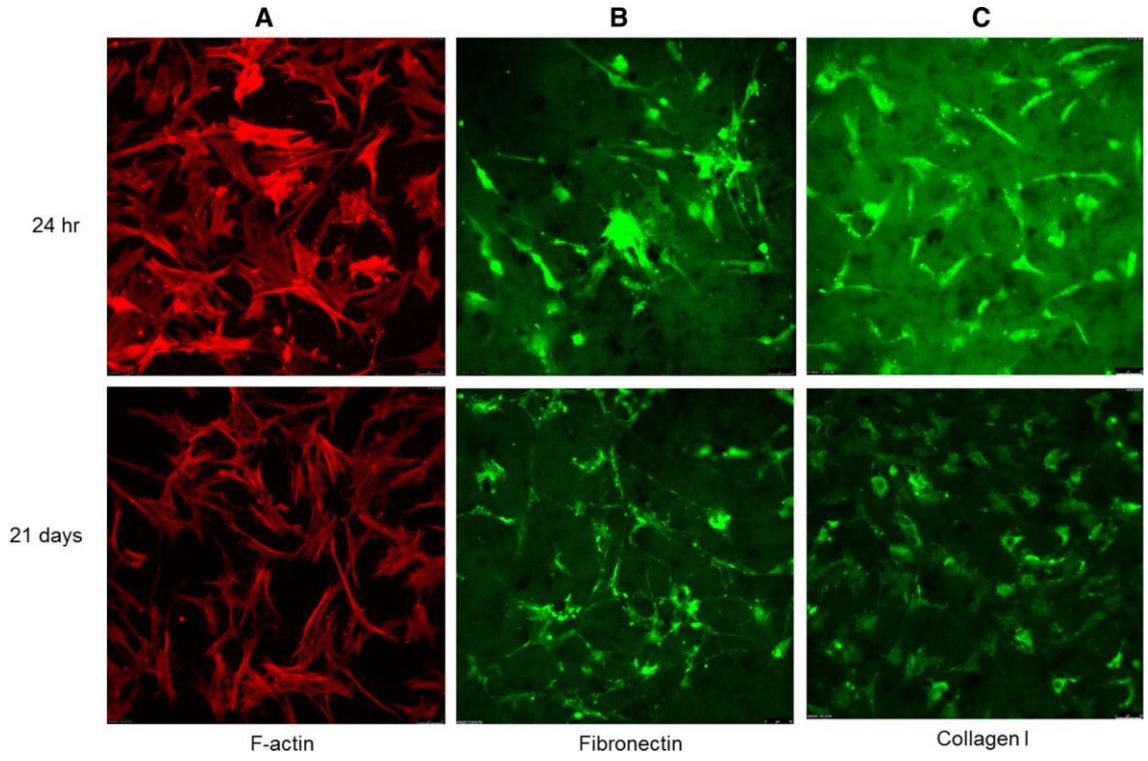

Figure 2.7. Immunofluorescence assays. Assays were performed to assess cytoskeletal organization of BM-MSCs using F-actin **(A)** and expression of specific ECM proteins **(B, C)** during cell adhesion at 24 hr and differentiation at day 21.

Table 2.1. Gene expressions of AD-MSCs and BM-MSCs cultured on LOG between 7 and 21 days. CT values for each gene were normalized using a housekeeping gene and then the fold changes were calculated by using Day 7 expression as the control and Day 21 expression as the tested group. NC = No Change; ND = Non Detectable.

Gene Description	Symbol	Fold Change (AD-MSCs)	Fold Change (BM-MSCs)
Transcriptional Regulation			
Distal-less homeobox 5	*DLX5*	ND	0.26
Runt-related transcription factor 2	*RUNX2*	1.57	0.78
SRY (sex determining region Y)-box 9	*SOX9*	0.70	0.64
Sp7 transcription factor	*SP7*	0.65	0.21
Osteoblast-Related			
Alkaline phosphatase, liver/bone/kidney	*ALPL*	2.09	3.43
Bone gamma-carboxyglutamate (gla) protein/osteocalcin	*BGLAP*	1.30	0.50
Phosphate regulating endopeptidase homolog, X-linked	*PHEX*	1.28	1.49
Secreted phosphoprotein 1/osteopontin	*SPP1*	0.30	1.86
Extracellular Matrix Markers			
Biglycan	*BGN*	1.36	1.46
Collagen, type I, alpha 1	*COL1A1*	NC	1.27
Collagen, type I, alpha 2	*COL1A2*	0.81	NC
Collagen, type III, alpha 1	*COL3A1*	1.22	NC
Collagen, type V, alpha 1	*COL5A1*	NC	NC
Collagen, type X, alpha 1	*COL10A1*	NC	2.11
Collagen, type XIV, alpha 1	*COL14A1*	1.31	13.33
Collagen, type XV, alpha 1	*COL15A1*	2.50	11.63
Fibronectin 1	*FN1*	1.49	2.28
Cellular Adhesion			
Cadherin 11, type 2, OB-cadherin (osteoblast)	*CDH11*	NC	1.62
Intercellular adhesion molecule 1	*ICAM1*	4.69	6.28
Integrin, alpha 1	*ITGA1*	1.62	1.21
Integrin, alpha 2 (CD49B, alpha 2 subunit of VLA-2 receptor)	*ITGA2*	0.49	0.29
Integrin, alpha 3 (antigen CD49C, alpha 3 subunit of VLA-3 receptor)	*ITGA3*	NC	1.66
Integrin, beta 1 (fibronectin receptor, beta polypeptide, antigen CD29 includes MDF2, MSK12)	*ITGB1*	0.66	0.78
Vascular cell adhesion molecular 1	*VCAM1*	2.42	11.13

Table 2.1. Continued.

Gene Description	Symbol	Fold Change (AD-MSCs)	Fold Change (BM-MSCs
BMP and SMAD Signaling			
Bone morphogenetic protein 1	*BMP1*	NC	NC
Bone morphogenetic protein 2	*BMP2*	NC	0.25
Bone morphogenetic protein 4	*BMP4*	1.94	2.61
Bone morphogenetic protein 6	*BMP6*	0.15	0.05
Activin A receptor, type I	*ACVR1*	NC	NC
Bone morphogenetic protein receptor, type IA	*BMPR1A*	NC	1.18
Bone morphogenetic protein receptor, type IB	*BMPR1B*	NC	2.04
Bone morphogenetic protein receptor, type II	*BMPR2*	1.19	0.63
SMAD family member 1	*SMAD1*	NC	0.61
SMAD family member 2	*SMAD2*	1.24	NC
SMAD family member 3	*SMAD3*	2.62	2.13
SMAD family member 4	*SMAD4*	NC	0.93
SMAD family member 5	*SMAD5*	1.14	0.88
Growth Factors			
Epidermal growth factor	*EGF*	0.55	NC
Epidermal growth factor receptor	*EGFR*	1.99	NC
Fibroblast growth factor 1 (acidic)	*FGF1*	0.74	0.69
Fibroblast growth factor 2 (basic)	*FGF2*	0.50	0.78
Fibroblast growth factor receptor 1	*FGFR1*	NC	NC
Fibroblast growth factor receptor 2	*FGFR2*	NC	2.65
Growth differentiation factor 10	*GDF10*	0.18	ND
Insulin-like growth factor 1 (somatomedin C)	*IGF1*	2.53	0.66
Insulin-like growth factor 2 (somatomedin A)	*IGF2*	NC	2.40
Insulin-like growth factor 1 receptor	*IGF1R*	1.44	0.76
Transforming growth factor, beta 1	*TGFB1*	NC	0.76
Transforming growth factor, beta 2	*TGFB2*	1.52	1.53
Transforming growth factor, beta 3	*TGFB3*	2.06	1.80
Transforming growth factor, beta receptor 1	*TGFBR1*	1.32	1.99
Transforming growth factor, beta receptor II (70/80kDa)	*TGFBR2*	1.57	2.60
Tumor necrosis factor	*TNF*	1.76	ND
Angiogenic Factors			
Fms-related tyrosine kinase 1 (vascular endothelial growth factor/vascular permeability factor receptor)	*FLT1*	NC	ND
Platelet-derived growth factor alpha polypeptide	*PDGFA*	1.34	NC
Vascular endothelial growth factor A	*VEGFA*	1.40	NC
Vascular endothelial growth factor B	*VEGFB*	1.38	1.40

Table 2.2. Gene expressions of BM-MSCs in comparison to AD-MSCs cultured on LOG for either 7 or 21 days. CT values for each gene were normalized using a housekeeping gene and then the fold changes were calculated by using AD-MSCs as the control and BM-MSCs as the tested group.NC = No Change; ND = Non Detectable.

		Day 7	Day 21
Gene Description	**Symbol**	**Fold Change**	**Fold Change**
Transcriptional Regulation			
Distal-less homeobox 5	*DLX5*	60.69	11.24
Runt-related transcription factor 2	*RUNX2*	7.24	2.24
SRY (sex determining region Y)-box 9	*SOX9*	6.85	3.89
Sp7 transcription factor	*SP7*	9.56	1.87
Osteoblast-Related			
Alkaline phosphatase, liver/bone/kidney	*ALPL*	0.01	0.01
Bone gamma-carboxyglutamate (gla) protein/osteocalcin	*BGLAP*	3.69	0.88
Phosphate regulating endopeptidase homolog, X-linked	*PHEX*	0.45	0.33
Secreted phosphoprotein 1/osteopontin	*SPP1*	NC	3.06
Extracellular Matrix Markers			
Biglycan	*BGN*	1.93	1.29
Collagen, type I, alpha 1	*COL1A1*	NC	0.59
Collagen, type I, alpha 2	*COL1A2*	NC	NC
Collagen, type III, alpha 1	*COL3A1*	0.45	0.31
Collagen, type V, alpha 1	*COL5A1*	2.08	NC
Collagen, type X, alpha 1	*COL10A1*	13.21	12.50
Collagen, type XIV, alpha 1	*COL14A1*	4.01	25.34
Collagen, type XV, alpha 1	*COL15A1*	0.08	0.22
Fibronectin 1	*FN1*	2.73	2.58
Cellular Adhesion			
Cadherin 11, type 2, OB-cadherin (osteoblast)	*CDH11*	2.11	2.2
Intercellular adhesion molecule 1	*ICAM1*	0.51	0.43
Integrin, alpha 1	*ITGA1*	2.00	NC
Integrin, alpha 2 (CD49B, alpha 2 subunit of VLA-2 receptor)	*ITGA2*	1.95	0.71
Integrin, alpha 3 (antigen CD49C, alpha 3 subunit of VLA-3 receptor)	*ITGA3*	5.00	4.34
Integrin, beta 1 (fibronectin receptor, beta polypeptide, antigen CD29 includes MDF2, MSK12)	*ITGB1*	1.54	1.14
Vascular cell adhesion molecule 1	*VCAM1*	482.15	1376.38

Table 2.2. Continued.

Gene Description	Symbol	Day 7 Fold Change	Day 21 Fold Change
BMP and SMAD Signaling			
Bone morphogenetic protein 1	*BMP1*	1.94	NC
Bone morphogenetic protein 2	*BMP2*	17.92	3.36
Bone morphogenetic protein 4	*BMP4*	0.16	0.13
Bone morphogenetic protein 6	*BMP6*	4.05	NC
Activin A receptor, type I	*ACVR1*	2.26	1.61
Bone morphogenetic protein receptor, type IA	*BMPR1A*	2.23	1.72
Bone morphogenetic protein receptor, type IB	*BMPR1B*	NC	NC
Bone morphogenetic protein receptor, type II	*BMPR2*	4.53	1.50
SMAD family member 1	*SMAD1*	4.14	1.58
SMAD family member 2	*SMAD2*	2.30	1.29
SMAD family member 3	*SMAD3*	NC	NC
SMAD family member 4	*SMAD4*	1.96	1.06
SMAD family member 5	*SMAD5*	3.15	1.50
Growth Factors			
Epidermal growth factor	*EGF*	4.78	7.73
Epidermal growth factor receptor	*EGFR*	2.38	0.61
Fibroblast growth factor 1 (acidic)	*FGF1*	3.44	1.99
Fibroblast growth factor 2 (basic)	*FGF2*	1.53	1.47
Fibroblast growth factor receptor 1 (acidic)	*FGFR1*	2.37	NC
Fibroblast growth factor receptor 2 (basic)	*FGFR2*	7.57	16.8
Growth differentiation factor 10	*GDF10*	0.02	0.10
Insulin-like growth factor 1 (somatomedin C)	*IGF1*	7.34	1.20
Insulin-like growth factor 2 (somatomedin A)	*IGF2*	34.30	43.71
Insulin-like growth factor 1 receptor	*IGF1R*	5.72	1.89
Transforming growth factor, beta 1	*TGFB1*	2.30	NC
Transforming growth factor, beta 2	*TGFB2*	51.51	32.22
Transforming growth factor, beta 3	*TGFB3*	NC	0.71
Transforming growth factor, beta receptor 1	*TGFBR1*	4.07	3.80
Transforming growth factor, beta receptor II (70/80kDa)	*TGFBR2*	0.64	0.66
Tumor necrosis factor	*TNF*	ND	NC
Angiogenic Factors			
Fms-related tyrosine kinase 1 (vascular endothelial growth factor/vascular permeability factor receptor)	*FLT1*	NC	NC
Platelet-derived growth factor alpha polypeptide	*PDGFA*	3.07	1.44
Vascular endothelial growth factor A	*VEGFA*	4.07	1.88
Vascular endothelial growth factor B	*VEGFB*	1.65	NC

CHAPTER III:
COMPARING OSTEOGENIC GENE EXPRESSION OF HUMAN MSCS ON RGO AND GO SUBSTRATES

ABSTRACT

Treatment of traumatic bone injuries is increasingly relying on novel materials that not only supports a defect, but also invokes stem cells into functional bone tissue. Graphene, a carbon-based biomaterial, spontaneously supports new bone differentiation of adult, mesenchymal stem cells (MSCs) without any osteo-chemical inducers. The two most common graphene derivatives for bone differentiation is graphene oxide (GO) and reduced graphene oxide (rGO). However, the question arises if one signals MSC bone differentiation differently than another. To answer this question, we examined the genetic regulation of MSCs cultured on GO and rGO substrates, including genes related to transcriptional regulation, osteoblast-related, the ECM, cell adhesion, growth factors, BMP & SMAD signaling, angiogenic factors, and MMPs. We found that both GO and rGO substrates supported osteogenic gene expression of MSCs. However, a head-to-head comparison showed that genes important to the osteoblast differentiation process were robustly upregulated on rGO than GO. Overall, the information gained from this study could elucidate the optimal graphene derivative for bone differentiation of future *in vivo* and clinical studies.

INTRODUCTION

Treatment of traumatic bone injuries is increasingly relying on novel materials that not only supports a defect, but also invokes stem cells into functional bone tissue. Ideal bone biomaterials are still under investigation, but graphene materials are at the forefront as the next clinical standard. Graphene, a carbon-based monolayer of graphite, is exceedingly strong, light, and yet very flexible, making it an attractive material that provides both skeletal support and endures mechanical stress. Better yet, graphene is a delivery vehicle for stem cell therapies and growth factors at the bone injury site [1-4]. Additionally, graphene substrates supports spontaneous bone differentiation of adult mesenchymal stem cells (MSCs), without any osteo-chemical inducers [5-7]. This means graphene is unlike other bioinert materials (i.e., metals, ceramics, etc.) which are incapable of signaling new bone development [8, 9].

Since graphene's discovery in 2004, various derivatives have been developed to increase its biocompatibility and hydrophilicity. The major graphene derivatives are graphene oxide (GO) and reduced graphene oxide (rGO), both of which are commercially available products, that supports *in vitro* bone differentiation of stem cells [10-14]. In bone tissue engineering, MSCs are the preferred stem cell source as these cells do not demonstrate immunological rejection and are derived from healthy adults, thereby eliminating the ethical concerns of embryonic stem cells [15-17]. Additionally, MSCs are multipotent, meaning they can differentiate into a variety of cell lineages, including osteocytes, chondrocytes, and adipocytes [18]. Therefore, it is important to focus on biological materials, such as graphene, that mimics a bone microenvironment and sustains bone differentiation of MSCs.

Previously, we reported that low oxygen graphene (LOG), an analog of rGO, genetically supported bone differentiation of both human adipose derived MSCs (AD-MSCs) and human bone marrow derived MSCs (BM-MSCs) [5]. However, since GO and rGO are the established graphene derivatives, the question arises if one signals MSC bone differentiation differently than another. To answer this question, we examined the genetic responses of MSCs cultured in the presence of GO and rGO substrates at various time points using focused osteogenic PCR arrays. To our knowledge, there are

no head-to-head comparisons of MSC gene expression exposed to GO and rGO. Overall, the information gained from this study could elucidate the optimal graphene derivative for bone differentiation of future *in vivo* and clinical studies.

METHODS

Preparation of rGO and GO

rGO and GO were commercially purchased from Cheap Tubes Inc. (Grafton, VT) and dispersed in ethanol/water by sonication for 60 min and 20 min, respectively. Non-tissue culture dishes were then coated with either rGO or GO at a final concentration of 0.2 mg/cm^2.

Cell Culture on rGO and GO

We previously isolated and characterized human AD-MSCs [6, 19] which was approved by an IRB protocol at the University of Tennessee Medical Center in Knoxville.

The AD-MSCs were first grown to confluency on standard tissue culture polystyrene in growth media using DMEM-F12, supplemented with 10% FBS, 1% penicillin, and 1% streptomycin. Cells were incubated in an atmosphere of 5% CO^2 at 37°C. For experimental conditions, the media was removed prior to separating cells with 0.05% trypsin for ~40 min. The cells were then reseeded at 1 X 10^6 / 100 mm on rGO or GO coated dishes and harvested after either 3, 7, 14, or 21 days. Throughout the study, cells were maintained in growth media without any osteo-differentiation inducers.

RNA Isolation

At each time point, total RNA was isolated using the Qiagen RNeasy kit as previously described [5]. RNA quantity, purity, and quality were confirmed before proceeding to PCR analysis.

Human Osteogenesis PCR Array

RT2 Profiler PCR Human Osteogenesis Array (Qiagen, Hilden, Germany, #PAHS-026Z) was used to evaluate differentially expressed genes of AD-MSCs on GO or rGO, similar to a recently published report [5]. Briefly, 1 µg of RNA was reversed transcribed for

cDNA synthesis and PCR reactions were completed according to the manufacturer's recommendations [20]. These microplate arrays contain primers that target 84 genes of interest. Following analysis, genes of interest were classified into one of the following categories: transcriptional regulation, osteoblast-related, extracellular matrix markers, cellular adhesion, BMP and SMAD signaling, growth factors, angiogenic factors, and bone remodeling.

Statistical Analysis

Gene expressions from CT values were uploaded into Qiagen Gene Globe software to determine the relative fold change (https://geneglobe.qiagen.com/us/analyze/). We first examined gene expression of AD-MSCs on GO and rGO overtime by designating Day 3 as the control group and subsequent time points as the tested groups. Thereafter, we then compared gene expression between both graphene derivatives at each time point, using GO as the control and rGO as the tested group. All comparisons were normalized using ribosomal protein, large, P0 (RPLP0). Data is shown from triplicate experiments, with fold changes statistically significant at $p<0.05$. A statistically significant gene with a fold change value >1 and <1 indicated upregulation and downregulation, respectively.

RESULTS

Total number of upregulated genes is greater on rGO than GO in MSCs cultured at early time points

We first investigated gene expression of MSCs cultured on GO or rGO overtime (from Day 3 up to Day 21).

When AD-MSCs were cultured on GO, gene expression from day 3 to day 7 showed 8 upregulated and 22 downregulated genes. However, the number of significant genes appeared to increase over extended time periods. Gene expression from day 3 to day 14 showed 24 upregulated and 13 downregulated genes and from day 3 to day 21 there were 53 upregulated and 4 downregulated genes. Overall, these comparisons suggested active bone differentiation of MSCs on GO overtime.

When AD-MSCs were cultured on rGO, gene expression from day 3 to day 7 showed 8 upregulated and 43 downregulated genes, whereas from day 3 to day 14, there were 16 upregulated and 39 downregulated genes.

To further understand the reaction of MSCs between GO and rGO, we investigated gene expression when GO was set as the control and rGO as the tested group at each time point. At day 3, we found 33 upregulated and 8 downregulated genes. Similarly, at day 7, we found 32 upregulated and 13 downregulated genes. By day 14, there were 25 upregulated and 29 downregulated genes. Overall, this data suggested that genetic activity of MSCs is more robust on rGO at early time points.

Osteoblast Transcription is greater on rGO than GO in MSCs cultured at early time points

We next evaluated specific gene clusters important to the bone differentiation process, beginning with genes involved in transcriptional regulation.

When AD-MSCs were cultured on GO, gene expressions from Day 3 to Day 7 showed downregulation of SOX9, whereas from Day 3 to Day 21, RUNX2 and SP7 were both upregulated (Table 3.1).

When AD-MSCs were cultured on rGO, gene expressions from Day 3 to Day 7 showed downregulation of SOX9. Additionally, from Day 3 to Day 14, both SOX9 and SP7 were downregulated (Table 3.2).

When comparing between GO and rGO, RUNX2 and SOX9 were upregulated at all time points (Table 3.3).

Overall, this data shows MSCs on GO express upregulated osteoblast transcription factors, but only after 21 days of culturing. However, when comparing both materials, expression of osteoblast transcription is greatest on rGO than GO at early time points.

MSCs cultured on GO and rGO express specific osteoblast-related markers overtime

When AD-MSCs were cultured on GO, gene expressions from day 3 to day 7 showed downregulation of SPP1. However, upregulation of osteoblast-related genes initiated

from day 3 to day 14. From day 3 to day 21, all osteoblast-related genes (ALPL, BGLAP, PHEX, and SPP1) were upregulated (Table 3.1).

When AD-MSCs were cultured on rGO, gene expressions from day 3 to day 7 showed downregulation of BGLAP, SPP1, but upregulation of ALPL by nearly 5-fold. The expression pattern of these genes was consistent from day 3 to day 14 (Table 3.2).

When comparing between GO and rGO, day 3 expression showed ALPL and BGLAP were downregulated and upregulated, respectively, whereas at day 7, ALPL was upregulated. However, by day 14, ALPL, BGLAP, and SPP1 were all downregulated (Table 3.3).

Overall, this data suggests that specific osteoblast-related genes occurs within 14 days of MSCs cultured on GO, whereas on rGO expression occurs within 7 days.

MSCs cultured on rGO express more upregulated extracellular matrix markers than GO overtime

When AD-MSCs were cultured on GO, most ECM genes from day 3 to day 7 were downregulated (BGN, COL1A1, COL3A1, COL5A1, COL15A1, and FN1); only COL14A1 was upregulated. This pattern was nearly consistent from day 3 to day 14. However, gene expression between day 3 to day 21 showed no downregulated genes and robust upregulation of COL10A1 (~9 fold) and COL14A1 (~10.5 fold) (Table 3.1).

When AD-MSCs were cultured on rGO, gene expressions from day 3 to day 7 showed downregulation of BGN, COL15A1, and FN1, but upregulation of COL1A1, COL1A2, COL3A1, and COL14A1. Similarly, expression of these genes was consistent from day 3 to day 14, with the exception of upregulated BGN and no change of COL15A1 expression (Table 3.2).

When comparing between GO and rGO, day 3 expression showed all significant genes were downregulated (BGN, COL1A1, COL1A2, and COL15A1), whereas at day 7, all significant genes were upregulated (BGN, COL3A1, COL5A1, and FN1). By day 14, COL1A1, COL3A1, COL5A1, and COL15A1 were all upregulated, while BGN and COL14A1 were downregulated (Table 3.3).

Overall, this data shows that MSCs cultured on rGO express several upregulated ECM genes at early and later time points.

Cellular Adhesion is greater on rGO than GO in MSCs cultured at early time points

When AD-MSCs were cultured on GO, gene expressions from day 3 to day 7 showed nearly all genes were downregulated (ITGA1, ITGA2, ITGA3, and ITGB1) except for upregulated ICAM1 expression. From day 3 to day 14, only ITGA2 was downregulated, while ICAM1 and VCAM 1 were upregulated. However, gene expressions from day 3 to day 21 showed all significant genes were upregulated (CDH11, ICAM1, ITGA1, and ITGA3) (Table 3.1).

When AD-MSCs were cultured on rGO, gene expressions from day 3 to day 7 showed all significant genes were downregulated (CDH11, ICAM1, ITGA1, ITGA2, and ITGA3), with the exception of upregulated VCAM1 expression. Similarly, expression of these genes were consistent from day 3 to day 14, with the exception of downregulated ITGB1 (Table 3.2).

When comparing between GO and rGO, day 3 expression showed upregulated ICAM1, ITGA1, and ITGA2, but downregulated VCAM1. At day 7, ITGA1, ITGA2, ITGA3, and ITGB1 were upregulated, but VCAM1 was downregulated. By day 14, ITGA2 and ITGB1 were upregulated, while CDH11, ITGA3, and VCAM1 were downregulated (Table 3.3).

Overall, this data suggests MSCs on GO express upregulated adhesion factors primarily after 21 days of culturing. However, when comparing both materials, expression of adhesion-related genes were greater on rGO than GO at early time points.

BMP & SMAD signaling is greater on rGO than GO in MSCs cultured at early time points

When AD-MSCs were cultured on GO, expressions from day 3 to day 7 showed downregulation of BMP1 and BMP6. From day 3 to day 14, BMP2, BMP4, and

BMPR1B were upregulated. However, expression from day 3 to day 21 showed upregulation of nearly all BMP and SMAD genes (BMP2, BMP4, ACVR1, BMPR1A, BMPR1B, BMPR2, SMAD1, SMAD2, SMAD3, SMAD4, SMAD5); only BMP6 was downregulated (Table 3.1).

When AD-MSCs were cultured on rGO, gene expressions from day 3 to day 7 and day 3 to day 14, showed nearly all BMP and SMAD genes were downregulated (Table 3.2).

When comparing between GO and rGO, day 3 and day 7 expression showed nearly all BMP and SMAD genes were upregulated. Interestingly, BMP2 was robustly expressed at day 3 (~48 fold), compared to day 7 (only ~6 fold). As BMP2 potently stimulates bone differentiation at low concentrations, this suggests that MSC differentiation is rapid on rGO in comparison to GO. We also observed other BMP genes appeared to have greater expression at day 3 than at day 7 such as BMP6 (~10 fold and ~4 fold, respectively) and BMPR1B (~5 fold and ~3 fold, respectively). However, by day 14 there were fewer upregulated genes, and for the first time expressed downregulation of BMP4, SMAD2, and SMAD4 (Table 3.3).

Overall, this data suggests MSCs on GO express upregulation of both BMP and SMAD signaling factors, but mainly after 21 days of culturing. However, when comparing both materials, expression of these genes were greater on rGO than GO at early time points.

Growth factor signaling is greater on rGO than GO in MSCs cultured at early time points

When AD-MSCs were cultured on GO, expressions from day 3 to day 7 showed all significant genes were downregulated (FGF1, FGF2, FGFR2, GDF10, and TGFB1). This pattern was nearly consistent from day 3 to day 14, but additionally showed upregulated EGFR, IGF1, TGFBR2, and TNF. However, expressions from day 3 to day 21 showed only downregulation of GDF10 and several upregulated genes (EGF, EGFR, FGFR1, IGF1, IGF2, IGF1R, TGFB1, TGFB2, TGFB3, TGFBR1, TGFBR2, and TNF) (Table 3.1).

When AD-MSCs were cultured on rGO, expressions from day 3 to day 7 showed only upregulation of EGF, whereas all other significant genes were downregulated (EGFR,

FGF1, FGFR1, GDF10, IGF1, IGF1R, TGFB1, TGFB3, and TGBR1). A similar pattern was observed from day 3 to day 14, however, IGF1 and TGFB2 were upregulated (Table 3.2).

When comparing between GO and rGO, most genes were upregulated at day 3 (EGFR, FGFR1, IGF1, IGF2, IGF1R, TGFB1, TGFB3, TGFBR1, and TGFBR2), with downregulation of FGFR2 and GDF10 (Table 3.3). Similarly, all significant genes were upregulated at day 7, with FGF2 upregulated by ~20 fold. However, expression at day 14 showed the most downregulated genes (EGFR, FGFR2, GDF10, TGFBR2, and TNF), but also maintained upregulation of several other growth factors.

Overall, this data suggests MSCs on GO express upregulation of several growth factors, but mainly after 21 days of culturing. However, when comparing both materials, expression of these genes were greater on rGO than GO at early time points.

rGO and GO supports expression of angiogenic factors in MSCs

When AD-MSCs were cultured on GO, gene expressions from day 3 to day 7 had no change, while from day 3 to day 14 only VEGFB was upregulated. However, gene expressions from day 3 to day 21 showed upregulation of both VEGFA and VEGFB (Table 3.1).

When AD-MSCs were cultured on rGO, genes expressions from day 3 to day 7 showed all genes were downregulated (FLT1, PDGFA, VEGFA, and VEGFB). Similarly, expression of these genes were consistent from day 3 to day 14, except for FLT1 which had no change (Table 3.2).

When comparing between GO and rGO, day 3 expression showed upregulation of PDGFA. However, day 7 expression showed downregulation of FLT1 and VEGFB. By day 14, FLT1 and PDGFA were upregulated, while VEGFA and VEGFB were downregulated (Table 3.3).

Overall, this data suggests that MSCs cultured on GO and rGO can secrete bioactive factors that attracts new blood vessel ingrowth, which is critical to sustaining newly developed bone *in vivo*.

MMP signaling is greater on rGO than GO in MSCs cultured at early time points

When AD-MSCs were cultured on GO, gene expressions from day 3 to day 7 showed upregulation of MMP2 and MMP10 (Table 3.1). Interestingly, from day 3 to day 14 and from day 3 to day 21, all bone remodeling genes tested (MMP2, MMP8, MMP9, and MMP10) were upregulated, with robust expression of MMP8 (~12 and 19-fold, respectively).

When AD-MSCs were cultured on rGO, gene expressions from day 3 to day 7 showed downregulation of MMP2 and MMP10 (Table 3.2). However, day 3 to day 14 showed upregulation of MMP8 and MMP9.

When comparing between GO and rGO, nearly all MMPs tested were upregulated at all time points (Table 3.3). Interestingly, robust expression of MMP10 was observed at day 3 (~33 fold), but only ~2 fold at day 7 and day 14. Similarly, MMP2 and MMP8 were robustly expressed at day 3 than at day 7 or day 14.

Overall, MSCs cultured on GO and rGO express several MMPs, which are important to bone remodeling. Additionally, comparison of GO and rGO reveals MMP expression is notably rapid on rGO.

DISCUSSION

The treatment of traumatic bone injuries is actively investigating biocompatible materials that promotes bone differentiation of stem cells and osteoprogenitors. Graphene, a carbon-based layer of graphite, has very strong and flexible characteristics that mimics natural bone [21]. Simultaneously graphene materials support stem cell bone differentiation, thereby making it an attractive bone substitute [22, 23].

The two most commonly used graphene sources are GO and rGO, with the biggest difference being the amount of oxygen content. Pristine graphene is commonly oxidized with oxygen-containing functional groups (i.e., hydroxyl, epoxy, and carboxyl) to increase biocompatibility and hydrophilicity [24]. The oxidation of pristine graphene produces GO, typically having a C:O ratio of 3:1 (~33% oxygen content) [25]. However, the introduction of functional oxygen groups tampers the natural conductivity of pristine

graphene [26]. As a result, the development of rGO, having a C:O ratio of 13:1 (~13% oxygen content), partially eliminates the functional oxygen groups and restores electrical conductivity potential [27]. In laymen's terms, rGO is thought as the "happy medium" between pristine graphene and GO.

There are few studies that have compared cell activity between GO and rGO. Jaworski et al., 2015 evaluated the toxicity of GO and rGO on human glioblastoma cells and found that both treatments reduced cell viability and proliferation with increasing doses, but yet rGO was more toxic than GO [28]. Other studies indicate that the method of producing rGO strongly influences cell viability and cytotoxicity [29-31]. For example, Jagielllo et al., 2019 found that human umbilical cord MSCs (hUC-MSCs) cultured on GO and a lowly-reduced rGO substrate (via ascorbic acid) had similar cell viability and proliferation rates, which was comparable to control cells cultured on polystyrene [30]. However, hUC-MSCs exposed to a highly reduced rGO substrate (via sodium hypophosphite) demonstrated reduced proliferation and an increase in cell death. It is believed that rGO cytotoxicity is due to greater intracellular reactive oxygen species, thus contributing to DNA damage, cell cycle arrest, and ultimately cell death [29, 32]. Therefore, the method of producing rGO should be seriously considered for an optimal cell environment in tissue engineering.

There are several studies and reviews that have established GO and rGO as bone scaffolds, but most studies have examined these materials individually [12, 33-35]. In this study, we sought to complete a head-to-head comparison of genes important to MSC bone differentiation between GO and rGO over 21 days. These genes were categorized as either transcriptional regulation, osteoblast-related, ECM, cell adhesion, BMP & SMAD signaling, growth factors, angiogenic factors, or bone remodeling. These clusters are well established in the bone differentiation process and have been similarly reported [5, 36-42]. Throughout this study, we observed three main trends: (1) Several genes important to bone development were gradually upregulated when MSCs were cultured on GO after 21 days of culturing (2) gene expression on rGO overtime were mainly downregulated, but (3) upregulated gene expression was greatest on rGO in comparison to GO at early time points. More specifically, the latter comparison

observed that osteoblast transcription, cellular adhesion, BMP & SMAD signaling, several growth factors, and MMP expression were greater on rGO than GO. This suggests that bone differentiation occurs earlier on rGO in comparison to GO. For example, we were surprised to find that BMP2 (the dominant growth factor for bone development), was upregulated by ~48 fold on rGO in comparison to GO, after just 3 days of culturing. This could partially explain why most genes were downregulated on rGO overtime; if cells have completed the bone differentiation process, then they become inactive quiescent bone cells [43]. Interestingly, we could not retrieve cells from rGO at day 21 using 0.05% trypsin (n = 2). We did obtain cells using 0.25% tryspin, however it would not be fair to include this analysis as excessive trypsinization can alter the gene expression profile [44]. Additionally, the current analysis revealed that cell adhesion factors on rGO are stronger than the same cells exposed to GO. Therefore, it is not surprising that cells on rGO imposed challenges for detaching with a lower concentration of trypsin. A few other limitations from this study are that we did not compare mineralization content or surface topography. However, we expect that data will be completed for a future publication.

It is unclear why there are different gene expression profiles between GO and rGO. However, it should be noted that rGO has a much larger surface area (~2400 $m^2 g^{-1}$) than GO (890 $m^2 g^{-1}$) [45]. Possibly, the larger surface area of rGO provides the space for MSCs to signal extracellular cues to neighboring cells. In standard cell culture, cells do not thrive in cramped environments, therefore it is important to design biomaterials with large surface areas for optimal cell communication and functioning.

In the future, GO and rGO scaffolds should be compared in *in vivo* bone defects to determine the optimal bone regenerative outcome. Additionally, this information can be used for ‘priming’ MSCs prior to transplantation. For example, MSCs could be cultured on rGO for 3 days, frozen down, and then implanted into an *in vivo* bone defect. If successful, this could eliminate the extra variable of a scaffold which has its own challenges (i.e., production, toxicity, degradability, etc.). However, before that project can be developed, understanding the gene expression of cells exposed to graphene substrates, such as this study provides, is necessary.

CONCLUSION

In this study, we examined the genetic regulation of MSCs undergoing bone differentiation on GO and rGO substrates, including genes related to transcriptional regulation, osteoblast-related, the ECM, cell adhesion, growth factors, BMP & SMAD signaling, angiogenic factors, and MMPs. We found that both GO and rGO substrates supported osteogenic gene expression of MSCs. However, there were differences in the gene expression profiles between cells cultured on GO and rGO. Most notably, a head-to-head comparison showed that genes important to the osteoblast differentiation process were robust on rGO than GO. In the future, this information can be translated to *in vivo* models that compare GO and rGO scaffolds for optimal bone regeneration.

REFERENCES

1. Wang, Q., et al., *Molecular mechanisms of interactions between BMP-2 and graphene: Effects of functional groups and microscopic morphology.* Applied Surface Science, 2020. **525**: p. 146636.
2. Zhong, C., et al., *Continuous release of bone morphogenetic protein-2 through nano-graphene oxide-based delivery influences the activation of the NF-κB signal transduction pathway.* Int J Nanomedicine, 2017. **12**: p. 1215-1226.
3. Fu, C., et al., *Enhancing Cell Proliferation and Osteogenic Differentiation of MC3T3-E1 Pre-osteoblasts by BMP-2 Delivery in Graphene Oxide-Incorporated PLGA/HA Biodegradable Microcarriers.* Sci Rep, 2017. **7**(1): p. 12549.
4. La, W.-G., et al., *Bone morphogenetic protein-2 for bone regeneration – Dose reduction through graphene oxide-based delivery.* Carbon, 2014. **78**: p. 428-438.
5. MacDonald, A.F., et al., *Genetic profiling of human bone marrow and adipose tissue-derived mesenchymal stem cells reveals differences in osteogenic signaling mediated by graphene.* Journal of Nanobiotechnology, 2021. **19**(1): p. 285.
6. Newby, S.D., et al., *Functionalized Graphene Nanoparticles Induce Human Mesenchymal Stem Cells to Express Distinct Extracellular Matrix Proteins Mediating Osteogenesis.* International journal of nanomedicine, 2020. **15**: p. 2501-2513.
7. Lee, J.H., et al., *Reduced graphene oxide-coated hydroxyapatite composites stimulate spontaneous osteogenic differentiation of human mesenchymal stem cells.* Nanoscale, 2015. **7**(27): p. 11642-11651.
8. Goharian, A. and M.R. Abdullah, *7 - Bioinert Metals (Stainless Steel, Titanium, Cobalt Chromium)*, in *Trauma Plating Systems*, A. Goharian, Editor. 2017, Elsevier. p. 115-142.
9. Anjaneyulu, U., V. Zhang, and P.-G. Ren, *Bioinert Ceramics for Biomedical Applications*. 2019.
10. Raslan, A., et al., *Graphene oxide and reduced graphene oxide-based scaffolds in regenerative medicine.* Int J Pharm, 2020. **580**: p. 119226.
11. Jin, L., et al., *Stimulated Osteogenic Differentiation of Human Mesenchymal Stem Cells by Reduced Graphene Oxide.* J Nanosci Nanotechnol, 2015. **15**(10): p. 7966-70.
12. Kang, M.S., et al., *Reduced graphene oxide coating enhances osteogenic differentiation of human mesenchymal stem cells on Ti surfaces.* Biomaterials Research, 2021. **25**(1): p. 4.
13. Luo, Y., et al., *Enhanced Proliferation and Osteogenic Differentiation of Mesenchymal Stem Cells on Graphene Oxide-Incorporated Electrospun Poly(lactic-co-glycolic acid) Nanofibrous Mats.* ACS Applied Materials & Interfaces, 2015. **7**(11): p. 6331-6339.
14. Puah, P.Y., et al., *Peptide Conjugate on Multilayer Graphene Oxide Film for the Osteogenic Differentiation of Human Wharton's Jelly-Derived Mesenchymal Stem Cells.* Polymers, 2021. **13**(19).
15. De Miguel, M.P., et al., *Immunosuppressive properties of mesenchymal stem cells: advances and applications.* Curr Mol Med, 2012. **12**(5): p. 574-91.
16. Ryan, J.M., et al., *Mesenchymal stem cells avoid allogeneic rejection.* Journal of inflammation (London, England), 2005. **2**: p. 8-8.
17. Volarevic, V., et al., *Ethical and Safety Issues of Stem Cell-Based Therapy.* Int J Med Sci, 2018. **15**(1): p. 36-45.
18. Dominici, M., et al., *Minimal criteria for defining multipotent mesenchymal stromal cells. The International Society for Cellular Therapy position statement.* Cytotherapy, 2006. **8**(4): p. 315-317.
19. Wofford, A., et al., *Human Fat-Derived Mesenchymal Stem Cells Xenogenically Implanted in a Rat Model Show Enhanced New Bone Formation in Maxillary Alveolar Tooth Defects.* Stem Cells International, 2020. **2020**: p. 8142938.
20. Osteogenesis, H., *Profiler ™ PCR Array.* 2022.

21. Cheng, X., Q. Wan, and X. Pei, *Graphene Family Materials in Bone Tissue Regeneration: Perspectives and Challenges.* Nanoscale research letters, 2018. **13**(1): p. 289-289.
22. Xie, H., et al., *CVD-grown monolayer graphene induces osteogenic but not odontoblastic differentiation of dental pulp stem cells.* Dent Mater, 2017. **33**(1): p. e13-e21.
23. Nayak, T.R., et al., *Graphene for controlled and accelerated osteogenic differentiation of human mesenchymal stem cells.* ACS Nano, 2011. **5**(6): p. 4670-8.
24. Rhazouani, A., et al., *Synthesis and Toxicity of Graphene Oxide Nanoparticles: A Literature Review of In Vitro and In Vivo Studies.* BioMed Research International, 2021. **2021**: p. 5518999.
25. Tiginyanu, I., V. Ursaki, and V. Popa, *11 - Ultra-thin membranes for sensor applications*, in *Nanocoatings and Ultra-Thin Films*, A.S.H. Makhlouf and I. Tiginyanu, Editors. 2011, Woodhead Publishing. p. 330-354.
26. Morimoto, N., T. Kubo, and Y. Nishina, *Tailoring the Oxygen Content of Graphite and Reduced Graphene Oxide for Specific Applications.* Scientific Reports, 2016. **6**(1): p. 21715.
27. Wei, X., et al., *3D Printable Graphene Composite.* Scientific Reports, 2015. **5**(1): p. 11181.
28. Jaworski, S., et al., *In vitro and in vivo effects of graphene oxide and reduced graphene oxide on glioblastoma.* Int J Nanomedicine, 2015. **10**: p. 1585-96.
29. Zhang, Q., et al., *Reduction pathway-dependent cytotoxicity of reduced graphene oxide.* Environmental Science: Nano, 2018. **5**(6): p. 1361-1371.
30. Jagiełło, J., et al., *Impact of Graphene-Based Surfaces on the Basic Biological Properties of Human Umbilical Cord Mesenchymal Stem Cells: Implications for Ex Vivo Cell Expansion Aimed at Tissue Repair.* International journal of molecular sciences, 2019. **20**(18): p. 4561.
31. Faniyi, I.O., et al., *The comparative analyses of reduced graphene oxide (RGO) prepared via green, mild and chemical approaches.* SN Applied Sciences, 2019. **1**(10): p. 1181.
32. Tabish, T.A., et al., *In vitro toxic effects of reduced graphene oxide nanosheets on lung cancer cells.* Nanotechnology, 2017. **28**(50): p. 504001.
33. Cheng, J., et al., *Graphene and its Derivatives for Bone Tissue Engineering: In Vitro and In Vivo Evaluation of Graphene-Based Scaffolds, Membranes and Coatings.* Frontiers in Bioengineering and Biotechnology, 2021. **9**.
34. Norahan, M.H., et al., *Reduced graphene oxide: osteogenic potential for bone tissue engineering.* IET nanobiotechnology, 2019. **13**(7): p. 720-725.
35. Sharma, A., et al., *Modified graphene oxide nanoplates reinforced 3D printed multifunctional scaffold for bone tissue engineering.* Materials Science and Engineering: C, 2021: p. 112587.
36. Rutkovskiy, A., K.O. Stensløkken, and I.J. Vaage, *Osteoblast Differentiation at a Glance.* Med Sci Monit Basic Res, 2016. **22**: p. 95-106.
37. Lin, X., et al., *The Bone Extracellular Matrix in Bone Formation and Regeneration.* Front Pharmacol, 2020. **11**: p. 757.
38. Marie, P.J., E. Haÿ, and Z. Saidak, *Integrin and cadherin signaling in bone: role and potential therapeutic targets.* Trends Endocrinol Metab, 2014. **25**(11): p. 567-75.
39. Baylink, D.J., R.D. Finkelman, and S. Mohan, *Growth factors to stimulate bone formation.* J Bone Miner Res, 1993. **8 Suppl 2**: p. S565-72.
40. Prins, H.J., et al., *In vitro induction of alkaline phosphatase levels predicts in vivo bone forming capacity of human bone marrow stromal cells.* Stem Cell Res, 2014. **12**(2): p. 428-40.
41. Paiva, K.B.S. and J.M. Granjeiro, *Matrix Metalloproteinases in Bone Resorption, Remodeling, and Repair.* Prog Mol Biol Transl Sci, 2017. **148**: p. 203-303.
42. Hankenson, K.D., et al., *Angiogenesis in bone regeneration.* Injury, 2011. **42**(6): p. 556-561.

43. Matic, I., et al., *Quiescent Bone Lining Cells Are a Major Source of Osteoblasts During Adulthood.* Stem cells (Dayton, Ohio), 2016. **34**(12): p. 2930-2942.
44. Zeng, J., et al., *A Minimally Invasive Method for Retrieving Single Adherent Cells of Different Types from Cultures.* Scientific Reports, 2014. **4**(1): p. 5424.
45. Dimiev, A. and S. Eigler, *Graphene Oxide: Fundamentals and Applications*. 2016. 1-439.

APPENDIX

Table 3.1. Gene expressions of AD-MSCs cultured on GO over time. CT values for each gene were normalized using a housekeeping gene and then the fold changes were calculated by using Day 3 expression as the control and Day 7 or Day 21 as the tested groups. NC = No Change; ND = Non-Detectable.

Gene Description	Symbol	Fold Change (Day 3 to Day 7)	Fold Change (Day 3 to Day 14)	Fold Change (Day 3 to Day 21)
Transcriptional Regulation				
Distal-less homeobox 5	*DLX5*	ND	ND	ND
Runt-related transcription factor 2	*RUNX2*	NC	NC	**3.41**
SRY (sex determining region Y)-box 9	*SOX9*	**0.57**	NC	NC
Sp7 transcription factor	*SP7*	NC	NC	**3.00**
Osteoblast-Related				
Alkaline phosphatase, liver/bone/kidney	*ALPL*	NC	**3.89**	**3.28**
Bone gamma-carboxyglutamate (gla) protein	*BGLAP*	NC	**1.73**	**2.23**
Phosphate regulating endopeptidase homolog, X-linked	*PHEX*	NC	**1.52**	**3.03**
Secreted phosphoprotein 1	*SPP1*	**0.43**	NC	**1.51**
Extracellular Matrix Markers				
Biglycan	*BGN*	**0.22**	**0.36**	NC
Collagen, type I, alpha 1	*COL1A1*	**0.42**	**0.34**	NC
Collagen, type I, alpha 2	*COL1A2*	NC	NC	NC
Collagen, type III, alpha 1	*COL3A1*	**0.70**	0.67	NC
Collagen, type V, alpha 1	*COL5A1*	**0.22**	**0.32**	NC
Collagen, type X, alpha 1	*COL10A1*	NC	NC	**8.55**
Collagen, type XIV, alpha 1	*COL14A1*	**2.60**	**7.03**	**10.46**
Collagen, type XV, alpha 1	*COL15A1*	**0.21**	**0.30**	NC
Fibronectin 1	*FN1*	**0.31**	NC	NC
Cellular Adhesion				
Cadherin 11, type 2, OB-cadherin (osteoblast)	*CDH11*	NC	NC	**1.73**
Intercellular adhesion molecule 1	*ICAM1*	**1.36**	**3.53**	**6.67**
Integrin, alpha 1	*ITGA1*	**0.48**	NC	**1.82**
Integrin, alpha 2 (CD49B, alpha 2 subunit of VLA-2 receptor)	*ITGA2*	**0.25**	**0.39**	NC
Integrin, alpha 3 (antigen CD49C, alpha 3 subunit of VLA-3 receptor)	*ITGA3*	**0.12**	NC	**3.97**
Integrin, beta 1 (fibronectin receptor, beta polypeptide, antigen CD29 includes MDF2, MSK12)	*ITGB1*	**0.45**	NC	NC
Vascular cell adhesion molecule 1	*VCAM1*	NC	**1.95**	NC

Table 3.1. Continued.

Gene Description	Symbol	Fold Change (Day 3 to Day 7)	Fold Change (Day 3 to Day 14)	Fold Change (Day 3 to Day 21)
BMP and SMAD Signaling				
Bone morphogenetic protein 1	*BMP1*	0.45	NC	NC
Bone morphogenetic protein 2	*BMP2*	NC	4.13	5.34
Bone morphogenetic protein 4	*BMP4*	NC	3.44	5.24
Bone morphogenetic protein 6	*BMP6*	0.36	NC	0.33
Activin A receptor, type I	*ACVR1*	NC	NC	3.26
Bone morphogenetic protein receptor, type IA	*BMPR1A*	NC	NC	2.65
Bone morphogenetic protein receptor, type IB	*BMPR1B*	NC	2.65	8.75
Bone morphogenetic protein receptor, type II	*BMPR2*	NC	NC	1.67
SMAD family member 1	*SMAD1*	NC	NC	3.29
SMAD family member 2	*SMAD2*	NC	NC	2.77
SMAD family member 3	*SMAD3*	NC	NC	3.70
SMAD family member 4	*SMAD4*	NC	NC	2.57
SMAD family member 5	*SMAD5*	NC	NC	2.11
Growth Factors				
Epidermal growth factor	*EGF*	NC	NC	3.08
Epidermal growth factor receptor	*EGFR*	NC	1.82	4.76
Fibroblast growth factor 1 (acidic)	*FGF1*	0.26	0.55	NC
Fibroblast growth factor 2 (basic)	*FGF2*	0.03	0.47	NC
Fibroblast growth factor receptor 1	*FGFR1*	NC	NC	2.79
Fibroblast growth factor receptor 2	*FGFR2*	0.19	0.22	NC
Growth differentiation factor 10	*GDF10*	0.13	0.75	0.40
Insulin-like growth factor 1 (somatomedin C)	*IGF1*	NC	2.24	1.66
Insulin-like growth factor 2 (somatomedin A)	*IGF2*	NC	NC	7.28
Insulin-like growth factor 1 receptor	*IGF1R*	NC	NC	1.88
Transforming growth factor, beta 1	*TGFB1*	0.45	NC	1.78
Transforming growth factor, beta 2	*TGFB2*	NC	NC	3.28
Transforming growth factor, beta 3	*TGFB3*	NC	NC	3.28
Transforming growth factor, beta receptor 1	*TGFBR1*	NC	NC	1.82
Transforming growth factor, beta receptor II (70/80kDa)	*TGFBR2*	NC	2.51	2.66
Tumor necrosis factor	*TNF*	NC	8.17	10.56
Angiogenic Factors				
Fms-related tyrosine kinase 1 (vascular endothelial growth factor/vascular permeability factor receptor)	*FLT1*	NC	NC	NC
Platelet-derived growth factor alpha polypeptide	*PDGFA*	NC	NC	NC
Vascular endothelial growth factor A	*VEGFA*	NC	NC	1.31
Vascular endothelial growth factor B	*VEGFB*	NC	1.53	4.66
Bone Remodeling				
Matrix metallopeptidase 2	*MMP2*	1.67	3.36	6.23
Matrix metallopeptidase 8	*MMP8*	NC	11.96	19.12
Matrix metallopeptidase 9	*MMP9*	NC	2.70	1.15
Matrix metallopeptidase 10	*MMP10*	2.10	6.29	5.15

Table 3.2. Gene expressions of AD-MSCs cultured on rGO over time. CT values for each gene were normalized using a housekeeping gene and then the fold changes were calculated by using Day 3 expression as the control and Day 7 or Day 14 as the tested groups. NC = No Change.

Gene Description	Symbol	Fold Change (Day 3 to Day 7)	Fold Change (Day 3 to Day 14)
Transcriptional Regulation			
Distal-less homeobox 5	*DLX5*	NC	NC
Runt-related transcription factor 2	*RUNX2*	NC	NC
SRY (sex determining region Y)-box 9	*SOX9*	0.52	0.52
Sp7 transcription factor	*SP7*	NC	0.40
Osteoblast-Related			
Alkaline phosphatase, liver/bone/kidney	*ALPL*	4.66	3.43
Bone gamma-carboxyglutamate (gla) protein	*BGLAP*	0.69	0.42
Phosphate regulating endopeptidase homolog, X-linked	*PHEX*	NC	NC
Secreted phosphoprotein 1	*SPP1*	0.34	0.41
Extracellular Matrix Markers			
Biglycan	*BGN*	0.79	1.84
Collagen, type I, alpha 1	*COL1A1*	1.26	1.75
Collagen, type I, alpha 2	*COL1A2*	1.40	1.55
Collagen, type III, alpha 1	*COL3A1*	1.21	1.81
Collagen, type V, alpha 1	*COL5A1*	NC	NC
Collagen, type X, alpha 1	*COL10A1*	NC	NC
Collagen, type XIV, alpha 1	*COL14A1*	2.36	2.90
Collagen, type XV, alpha 1	*COL15A1*	0.54	NC
Fibronectin 1	*FN1*	0.63	0.74
Cellular Adhesion			
Cadherin 11, type 2, OB-cadherin (osteoblast)	*CDH11*	0.61	0.58
Intercellular adhesion molecule 1	*ICAM1*	0.61	NC
Integrin, alpha 1	*ITGA1*	0.40	0.27
Integrin, alpha 2 (CD49B, alpha 2 subunit of VLA-2 receptor)	*ITGA2*	0.14	0.24
Integrin, alpha 3 (antigen CD49C, alpha 3 subunit of VLA-3 receptor)	*ITGA3*	0.35	0.32
Integrin, beta 1 (fibronectin receptor, beta polypeptide, antigen CD29 includes MDF2, MSK12)	*ITGB1*	NC	0.64
Vascular cell adhesion molecule 1	*VCAM1*	4.30	5.13

Table 3.2. Continued.

Gene Description	Symbol	Fold Change (Day 3 to Day 7)	Fold Change (Day 3 to Day 14)
BMP and SMAD Signaling			
Bone morphogenetic protein 1	*BMP1*	0.60	NC
Bone morphogenetic protein 2	*BMP2*	0.14	NC
Bone morphogenetic protein 4	*BMP4*	0.64	0.41
Bone morphogenetic protein 6	*BMP6*	0.16	0.21
Activin A receptor, type I	*ACVR1*	0.64	0.63
Bone morphogenetic protein receptor, type IA	*BMPR1A*	0.70	0.48
Bone morphogenetic protein receptor, type IB	*BMPR1B*	0.54	0.40
Bone morphogenetic protein receptor, type II	*BMPR2*	NC	NC
SMAD family member 1	*SMAD1*	0.76	NC
SMAD family member 2	*SMAD2*	0.65	0.58
SMAD family member 3	*SMAD3*	NC	NC
SMAD family member 4	*SMAD4*	0.61	0.46
SMAD family member 5	*SMAD5*	0.58	0.63
Growth Factors			
Epidermal growth factor	*EGF*	2.29	NC
Epidermal growth factor receptor	*EGFR*	0.53	0.50
Fibroblast growth factor 1 (acidic)	*FGF1*	0.49	0.62
Fibroblast growth factor 2 (basic)	*FGF2*	NC	0.75
Fibroblast growth factor receptor 1	*FGFR1*	0.62	NC
Fibroblast growth factor receptor 2	*FGFR2*	NC	NC
Growth differentiation factor 10	*GDF10*	0.56	0.60
Insulin-like growth factor 1 (somatomedin C)	*IGF1*	0.73	1.89
Insulin-like growth factor 2 (somatomedin A)	*IGF2*	NC	NC
Insulin-like growth factor 1 receptor	*IGF1R*	0.41	0.43
Transforming growth factor, beta 1	*TGFB1*	0.53	0.60
Transforming growth factor, beta 2	*TGFB2*	NC	2.36
Transforming growth factor, beta 3	*TGFB3*	0.43	0.43
Transforming growth factor, beta receptor 1	*TGFBR1*	0.69	NC
Transforming growth factor, beta receptor II (70/80kDa)	*TGFBR2*	NC	0.54
Tumor necrosis factor	*TNF*	NC	NC
Angiogenic Factors			
Fms-related tyrosine kinase 1 (vascular endothelial growth factor/vascular permeability factor receptor)	*FLT1*	0.23	NC
Platelet-derived growth factor alpha polypeptide	*PDGFA*	0.48	0.62
Vascular endothelial growth factor A	*VEGFA*	0.52	0.48
Vascular endothelial growth factor B	*VEGFB*	0.57	0.50
Bone Remodeling			
Matrix metallopeptidase 2	*MMP2*	0.65	0.86
Matrix metallopeptidase 8	*MMP8*	NC	4.42
Matrix metallopeptidase 9	*MMP9*	NC	3.14
Matrix metallopeptidase 10	*MMP10*	0.11	0.35

Table 3.3. Gene expressions of AD-MSCs cultured on rGO in comparison to AD-MSCs cultured on GO for either 3, 7, or 14 days. CT values for each gene were normalized using a housekeeping gene and then the fold changes were calculated by using GO as the control and rGO as the tested group. NC = No Change; ND = Non-Detectable.

Gene Description	Symbol	Fold Change (Day 3)	Fold Change (Day 7)	Fold Change (Day 14)
Transcriptional Regulation				
Distal-less homeobox 5	*DLX5*	NC	ND	ND
Runt-related transcription factor 2	*RUNX2*	3.94	2.58	1.64
SRY (sex determining region Y)-box 9	*SOX9*	2.79	2.51	1.49
Sp7 transcription factor	*SP7*	NC	NC	0.48
Osteoblast-Related				
Alkaline phosphatase, liver/bone/kidney	*ALPL*	0.35	2.07	0.31
Bone gamma-carboxyglutamate (gla) protein	*BGLAP*	1.43	NC	0.34
Phosphate regulating endopeptidase homolog, X-linked	*PHEX*	NC	NC	NC
Secreted phosphoprotein 1	*SPP1*	NC	NC	0.68
Extracellular Matrix Markers				
Biglycan	*BGN*	0.43	1.54	2.17
Collagen, type I, alpha 1	*COL1A1*	0.34	NC	1.76
Collagen, type I, alpha 2	*COL1A2*	0.55	NC	NC
Collagen, type III, alpha 1	*COL3A1*	NC	1.32	2.06
Collagen, type V, alpha 1	*COL5A1*	NC	2.64	2.12
Collagen, type X, alpha 1	*COL10A1*	NC	NC	NC
Collagen, type XIV, alpha 1	*COL14A1*	NC	NC	0.46
Collagen, type XV, alpha 1	*COL15A1*	0.43	NC	1.84
Fibronectin 1	*FN1*	NC	1.71	NC
Cellular Adhesion				
Cadherin 11, type 2, OB-cadherin (osteoblast)	*CDH11*	NC	NC	0.61
Intercellular adhesion molecule 1	*ICAM1*	2.23	NC	NC
Integrin, alpha 1	*ITGA1*	2.08	1.75	NC
Integrin, alpha 2 (CD49B, alpha 2 subunit of VLA-2 receptor)	*ITGA2*	6.42	3.71	3.94
Integrin, alpha 3 (antigen CD49C, alpha 3 subunit of VLA-3 receptor)	*ITGA3*	NC	2.27	0.78
Integrin, beta 1 (fibronectin receptor, beta polypeptide, antigen CD29 includes MDF2, MSK12)	*ITGB1*	NC	2.57	1.37
Vascular cell adhesion molecule 1	*VCAM1*	0.10	0.53	0.25

Table 3.3. Continued.

Gene Description	Symbol	Fold Chang (Day 3)	Fold Change (Day 7)	Fold Change (Day 14)
BMP and SMAD Signaling				
Bone morphogenetic protein 1	*BMP1*	NC	1.87	1.57
Bone morphogenetic protein 2	*BMP2*	**48.06**	5.68	7.24
Bone morphogenetic protein 4	*BMP4*	1.90	NC	0.23
Bone morphogenetic protein 6	*BMP6*	9.56	4.38	2.27
Activin A receptor, type I	*ACVR1*	1.93	1.18	NC
Bone morphogenetic protein receptor, type IA	*BMPR1A*	1.76	1.41	NC
Bone morphogenetic protein receptor, type IB	*BMPR1B*	5.21	2.61	NC
Bone morphogenetic protein receptor, type II	*BMPR2*	NC	1.52	NC
SMAD family member 1	*SMAD1*	NC	NC	NC
SMAD family member 2	*SMAD2*	1.69	1.45	0.77
SMAD family member 3	*SMAD3*	1.39	NC	NC
SMAD family member 4	*SMAD4*	1.84	1.41	0.67
SMAD family member 5	*SMAD5*	1.69	NC	NC
Growth Factors				
Epidermal growth factor	*EGF*	NC	NC	NC
Epidermal growth factor receptor	*EGFR*	2.19	NC	0.61
Fibroblast growth factor 1 (acidic)	*FGF1*	NC	2.12	NC
Fibroblast growth factor 2 (basic)	*FGF2*	NC	**19.56**	1.28
Fibroblast growth factor receptor 1	*FGFR1*	2.49	1.79	1.57
Fibroblast growth factor receptor 2	*FGFR2*	0.13	NC	0.44
Growth differentiation factor 10	*GDF10*	0.52	NC	0.42
Insulin-like growth factor 1 (somatomedin C)	*IGF1*	2.18	1.32	1.84
Insulin-like growth factor 2 (somatomedin A)	*IGF2*	4.69	NC	NC
Insulin-like growth factor 1 receptor	*IGF1R*	2.54	1.89	1.38
Transforming growth factor, beta 1	*TGFB1*	1.78	2.09	NC
Transforming growth factor, beta 2	*TGFB2*	NC	NC	1.73
Transforming growth factor, beta 3	*TGFB3*	10.39	5.88	2.95
Transforming growth factor, beta receptor 1	*TGFBR1*	1.66	NC	1.41
Transforming growth factor, beta receptor II (70/80kDa)	*TGFBR2*	2.69	2.85	0.58
Tumor necrosis factor	*TNF*	NC	NC	0.11
Angiogenic Factors				
Fms-related tyrosine kinase 1 (vascular endothelial growth factor/vascular permeability factor receptor)	*FLT1*	NC	0.26	1.51
Platelet-derived growth factor alpha polypeptide	*PDGFA*	1.80	NC	1.75
Vascular endothelial growth factor A	*VEGFA*	NC	NC	0.77
Vascular endothelial growth factor B	*VEGFB*	NC	0.83	0.40
Bone Remodeling				
Matrix metallopeptidase 2	*MMP2*	3.45	1.34	NC
Matrix metallopeptidase 8	*MMP8*	11.21	4.18	4.14
Matrix metallopeptidase 9	*MMP9*	3.38	4.72	3.93
Matrix metallopeptidase 10	*MMP10*	**33.21**	1.71	1.84

CHAPTER IV:
NEXT GENERATION RNA SEQUENING REVEALS GENETIC ALTERATIONS DURING CHEMICALLY INDUCED BONE DIFFERENTIATION OF MESENCHYMAL STEM CELLS FROM A POST-MENOPAUSE ANIMAL MODEL

This chapter is under review to the *International Journal of Molecular Sciences* by Amber F. MacDonald:

[a] Amber MacDonald, [a] Lisa Amelse, [a] Steven Newby, [a] Austin Bow, [a] Thomas Masi, [a] Madhu Dhar

Affiliations:
[a] College of Veterinary Medicine, University of Tennessee, Knoxville, Tennessee 37996, USA

Corresponding author:
Madhu Dhar, Ph.D., College of Veterinary Medicine, University of Tennessee, 2407 River Dr. Knoxville, Tennessee 37996, USA; email: mdhar@utk.edu; phone: 865-974-5703; Fax: 865-974-5773

Key words
MSCs, bone differentiation, RNA sequencing, gene expression, ovariectomized rats

ABSTRACT

The lack of mesenchymal stem cell (MSC) differentiation contributes to challenges in bone repair of age-related bone degenerative diseases. However, the genes involved in this process are not clearly defined. We therefore obtained MSCs from the post-menopause ovariectomized rat model, which parallels human bone degeneration. MSCs from both control (con-MSCs) and ovariectomized (ovx-MSCs) animals were exposed to an osteogenic differentiation cocktail for 7 and 21 days. Results confirmed ovx-MSCs failed to respond to osteogenic differentiation in comparison to con-MSCs. We then examined a genome-wide expression profile of both MSC groups via RNA sequencing. Genes important to bone differentiation were clustered as either cell adhesion (integrins and cadherins), ECM (collagens, glycoproteins, and proteoglycans), growth factors (estrogens, androgens, BMPs, TGFs, FGFs, PDGFs, VEGFs, IGFs, and EGFs), Wnt-Catenin signaling (Wnts, Catenins, Frizzelds, SMADs), cell signaling factors (MAPKs, PI3Ks, Akts), mineralization (calcium and phosphatase-regulated genes), or bone remodeling (MMPs). For each cluster, gene expressions were examined using day 7 as the control and day 21 as the tested group. Analysis showed the percentage of upregulated clusters were consistently highest within con-MSCs. Additionally, we specify the genes that did not share commonality between con-MSCs and ovx-MSCs. Overall, this data suggests that following menopause, multiple genes affect MSC bone differentiation, thereby contributing to the onset of bone degeneration. This information is necessary for future drug targets and gene editing strategies that could treat or prevent bone degeneration.

INTRODUCTION

Cell-based therapies are under thorough investigation for treating bone degenerative diseases. The preferred cell source in stimulating new bone are mesenchymal stem cells (MSCs) as they have the potential to undergo differentiation into various lineages and do not demonstrate immunological rejection or abnormal growth patterns [1, 2]. Traditionally, MSCs are either derived autologously (from the patient in need) or as allogenic cells (from an appropriate donor) and then implanted with the expectation of undergoing differentiation and/or triggering pathways to heal the bone defect [3]. However, both autologous and allogenic MSCs require months of strategic testing and planning, thereby delaying those needing immediate treatment. Additionally, autologous MSCs from patients with bone degenerative diseases are invalid due to cellular senescence and other non-modifiable risk factors (i.e. age, sex, history, etc.) [4, 5]. Therefore, the focus should be on targeting endogenous MSCs that restores activity within chronic bone conditions such as osteoarthritis, osteopenia, and osteoporosis. However, this strategy will not be pharmaceutically effective until there is thorough characterization of MSCs from diseased bone. In other words, examining the behavior of MSCs derived from diseased bone will allow new developments of effective treatment strategies.

The ovariectomized (OVX) rat is an FDA approved model that mimics bone degeneration associated with osteoporosis in humans [6, 7]. The model is characterized by low bone mass and structural deterioration of bone tissue leading to bone fragility and thus, an increased susceptibility to fractures. It has been demonstrated that ovariectomy (or estrogen deficiency), prevents the synthesis of mineralized matrix and expression of osteocyte – specific genes in MSCs isolated from OVX rats [8, 9]. Ren et al., 2020 showed that bone marrow-derived MSCs (BM-MSCs) from OVX rats display down regulation of osteogenic differentiation supported by changes in ALP, OCN and OPN [8]. Interestingly, Boelloni et al., 2014 found that adipose tissue – derived MSCs (AD-MSCs) from OVX rats have higher osteogenic potential than BM-MSCs [10], thereby suggesting that AD-MSCs are more appropriate for autologous cell therapy of bone diseases post-menopause. In all these studies, standard protocols of alizarin red staining and single gene traditional PCRs were used to demonstrate *in vitro*

osteogenesis/bone mineralization and changes in osteogenic gene expression patterns, respectively.

Next – generation high throughput RNA sequencing introduced roughly a decade ago, provides insight into the transcriptome of a cell in a given physiological condition [11, 12]. RNA-sequencing provides higher coverage and greater resolution of the dynamic nature of the transcriptome. This technique thus, presents significant advantages over traditional Sanger sequencing or microarray-based transcriptomic approaches and hence, could yield valuable information about the MSCs isolated from an OVX rat relative to MSCs isolated from matched sham controls (con-MSCs). Therefore, our primary goal was to isolate MSCs from the OVX rat model and understand the genetic behavior following exposure to a chemically induced bone differentiation cocktail. We hypothesized that osteoblast differentiation of MSCs derived from OVX animals (ovx-MSCs) would be affected, and that RNA sequencing would reveal the genetic alterations during this process. This information identifies specific molecular gene transcripts and protein isoforms important for osteoblast development in the OVX condition and thus, will help develop new pharmaceutical drugs and bone tissue engineering strategies.

METHODS

Animal Model

All procedures were approved by the University of Tennessee Institutional Animal Care and Use Committee. 12 female Sprague-Dawley rats were purchased from Charles River (Wilmington, MA) and either sham operated (n=6) or ovariectomized (OVX) (n=6). The animals were housed in pairs and acclimatized for one week at the University of Tennessee Medical Center, Animal Facility. Following acclimatization, animals were housed individually to control for diet consumption.

All rats were fed a commercially available low calcium diet (Envigo,Indianapolis, ID). The formula consisted of casein (200 g/Kg), L-cystine (3.0 g/Kg), sucrose (342.188 g/Kg), corn starch (320.0 g/Kg), soybean oil (60 g/Kg), cellulose (40 g/Kg), mineral mix (Ca-P deficient) (13.37 g/Kg), potassium phosphate (monobasic) (11.43 g/Kg), vitamin mix (10.0 g/Kg), and ethoxyquin, an antioxidant (0.012 g/Kg). The casein contributed ~0.01% calcium or less. The diet also contained ~0.4% phosphorus and 2200 IU

vitamin D/Kg diet. Food was stored at 4°C and used within 6 months of purchasing. Each rat was fed 210 g (+/- 5 g) of diet every 7 days according to manufacturer recommendations. The rats consumed this diet for 8 weeks, with food intake and body weights recorded weekly.

Serum CTX-1/TRAP5b Ratio

On the day of sacrifice, whole blood was extracted from the apex of the left ventricle and aliquoted into EDTA tubes for serum collection. Samples were placed on ice for approximately one hour, and then centrifuged at 300 X G for 10 min and supernatant was stored at -80°C before analysis.

The ratio of C-telopeptide of type I collagen (CTX-1) to tartrate-resistant acid phosphate isoform 5b (TRAP5B) was analyzed using enzyme-linked immunosorbent assays (ELISA). CTX-1 is a serum biomarker of osteoclast activity while TRAP5b is an enzyme that reflects osteoclast number [13-15]. The average activity of a single osteoclast is defined as the ratio of CTX-1:TRAP5b, both of which are expressed in blood and provides stronger evidence of bone resorption rather than examining either marker alone [16, 17]. Rat CTX-1 and TRAP5b ELISA kits were purchased from Cusabio Biotechnology (Wuhan, China) and Immunodiagnostic Systems (East Boldon, United Kingdom), respectively. CTX-1 and TRAP5b were analyzed and quantitated from serum samples according to the manufacturer's instructions. A resorption index was created by dividing CTX-1 (pg/mL) by TRAP5b (U/L) and was compared between sham and OVX serum.

Isolation of Rat MSCs

Animals were sacrificed using a CO^2 chamber and the femur bones were immediately harvested for MSC isolation of the bone marrow as described in similar reports [18, 19]. The femurs were first rinsed with PBS before clipping the ends of the bone. An 18-gauge needle was used to extrude the bone marrow and rinsed into a collection tube using a syringe filled with media. A cell pellet was collected from centrifugation at 1000 rpm for 5 min and then re-suspended with 5.5 mL media. Cells were filtered with a 70 μm strainer, then 2 mL of media was added and the filter process was repeated to ensure full collection. In general, cells from 2 animals were combined to obtain sufficient numbers prior to *in vitro* experiments. Cells were grown to 80—90% confluency and

then harvested with 0.05% trypsin for cryopreservation (80% FBS, 10% DMEM-F12, and 10% DMSO) or re-seeded for expansion in growth media (DMEM/F12, 10% FBS, 1% penicillin-streptomycin and 1% amphotericin B). All experiments were performed using cells from passage 2–6.

Characterization of Rat MSCs

Rat MSC characterizations were performed as previously reported for rat and human MSCs [20]. MSCs are identified by the expression of specific cluster-of-differentiation (CD) markers, found at the cell surface [21]. Specific markers tested were CD11b/c, CD29, CD44, CD45, CD73, CD90.All markers tested are recognized by the Mesenchymal and Tissue Stem Cell Committee of the International Society for Cellular Therapy [21]. All antibodies were used at concentrations as per the manufacturer's recommendations (Biolegend, San Diego, CA). Stained cells were assayed on BD FACS Calibur and expression was measured and analyzed by FlowJo software.

Differentiation of Rat MSCs into Osteoblasts

Osteogenic differentiation was carried out according to standard method as reported earlier [22, 23]. For experimental conditions, cells were collected using 0.05% trypsin and seeded onto tissue culture dishes in growth media. The cells were incubated at 37°C, 5% CO_2 and induced towards osteogenesis with media that was supplemented with 10 mM β-glycerol phosphate, 50 µM ascorbic acid, and 100 nm dexamethasone. The osteogenic media was replaced every other day up to 21 days.

To determine mineralization and visualize any morphological changes, cells were stained with alizarin red after 21 days of osteogenic induction. Mineralization was evaluated by quantitation of Alizarin red staining as described earlier [24-26]. Cells were imaged on the Leica DMi1 Inverted Microscope with LAS V4.12 software. All pictures were taken on the same day under the same parameters for brightness, contrast, saturation, resolution, and magnification.

RNA Extraction

To evaluate changes in gene expression during osteogenesis, cells were harvested after 7 and 21 days of osteogenic induction. Total RNA was extracted using the RNeasy® Mini Kit (Qiagen, Germantown, MD) and RNA integrity was evaluated using

the RNA 6000 Nano Kit and 2100 Bioanalyzer system (Agilent Techologies, Santa Clara, CA) as previously reported [26, 27].

RNA Sequencing

Library Construction and Sequencing

The total RNA preparation and deep sequencing of the whole transcriptome library were performed by Novogene Corporation Inc. (Sacramento, CA). A total amount of 1 μg RNA per sample was used as input material for the RNA sample preparations. Sequencing libraries were generated using NEBNext® Ultra™ RNA Library Prep Kit for Illumina® (NEB, USA) and index codes were added to attribute sequences to each sample. The clustering of the index-coded samples was performed on a cBot Cluster Generation System using PE Cluster Kit cBot-HS (Illumina). After cluster generation, the library preparations were sequenced on an Illumina platform and paired-end reads were generated.

Quality Control

Following sequencing, raw reads were processed through fastp whereby clean reads were obtained by removing any read containing adapter and poly-N sequences. After filtering, sequencing error rate check (Q20 and Q30) and GC content of the clean data were calculated. The paired-end clean reads were then mapped to the reference genome using HISAT2 software. The reference genome and gene model annotation files were directly downloaded from genome website browser (NCBI/UCSE/Ensembl).

Data Analysis

All gene expressions were reported in a Microsoft Excel spreadsheet. Genes of interest were searched with a key phrase (i.e. bone morphogenetic protein) and all isoforms were clustered within a group. We evaluated gene clusters well established in the bone differentiation process and thereby categorized these clusters as either cell adhesion (integrins and cadherins); ECM (collagens, glycoproteins, and proteoglycans); growth factors (estrogens, androgens, BMPs, TGFs, FGFs, PDGFs, VEGFs, IGFs, EGFs); Wnt / Catenin signaling (Wnts, Frizzleds, Catenins, SMADs); cell signaling factors (MAPKs, PI3Ks, Akts); mineralization (calcium and phosphatase-regulated genes); and bone remodeling genes (MMPs). All genes within each cluster were then sorted between significant and non-significant expression. Because these clusters are suggested to

have increased activity during bone differentiation [28-34], we focused on upregulated gene expression using day 7 as the control and day 21 as the tested group within both con-MSCs and ovx-MSCs.

Statistical Analysis

The average body weight, osteoclast activity, and mineralization quantification were tested with the 2-Tailed Student's T-test; data is presented as standard error of the mean. For RNA sequencing, 2 biological replicates per condition were analyzed. Featurecounts was used to count the number of reads mapped to each gene. The RPKM (Reads Per Kilobase of exon model per Million mapped reads) was used to normalize the sequencing depth and gene length for the reads count. Differential expression analysis between groups (with biological replications) was performed using DESeq2 R package, which provides statistical information using a model based on the negative binomial distribution. The resulting *P* values were adjusted using the Benjamini and Hochberg's approach for controlling the False Discovery Rate (FDR). Genes with an adjusted *P* value < 0.05 were assigned as differentially expressed and the $\log_2^{(\text{foldchange})}$ of 1 were set as the threshold, whereby expression >1 and <1 indicated positive and negative upregulation, respectively. All sample values were related to the control at Day 7 and presented as the percentage of upregulated genes within each cluster.

RESULTS

OVX animals have higher body weights and osteoclast activity than control animals

All animals demonstrated healthy eating patterns and showed no signs of stress. On the day of sacrifice, final body weights of OVX rats were significantly higher than the control group (Figure 4.1A), which is consistent with previous reports [8, 35]. Supportively, ELISA analysis of serum samples showed a greater CTX-1:TRAP5b ratio in OVX animals (117.12) in comparison to the control (52.61) (Figure 4.1B). These results confirmed that OVX animals had greater bone resorption activity than that of control animals.

Rat bone marrow – derived cells express specific MSC markers

Following cell isolation and expansion, both the con - and ovx – MSCs showed >90% expression of CD29 and CD90 and >70% expression of CD73 (Figure 4.2). In contrast, there was no expression (<5%) of CD11b/c and CD45. These data confirmed that the cells isolated and expanded from both the control and OVX rats were indeed MSCs.

Higher Bone Mineralization in con - MSCs

To evaluate the osteogenic potential, both con-MSCs and ovx-MSCs were exposed to osteogenic differentiation media up to 21 days. Cell morphology and *in vitro* differentiation/mineralization was assessed by standard Alizarin red staining and quantitated as reported earlier [26, 36]. Both con – and OVX – MSCs showed cell clustering and formation of nodules indicating *in vitro* mineralization (Figure 4.3A). However, discrete nodules and larger clusters of cells were observed in con-MSCs only, indicating greater osteogenic differentiation. Additionally, ovx-MSCs morphologically resembled control cells that were not exposed to differentiation media (inset Figure 4.3A). Quantitation of the alizarin red stain confirmed that ovx-MSCs had a significant decrease in calcium content in comparison to con-MSCs (Figure 4.3B). These results confirmed that even though ovx-MSCs express specific CD markers, and contain progenitors with osteogenic potential, the osteoblast differentiation process is inferior to con-MSCs.

High quality RNA was isolated from MSCs

Prior to sequencing, RNA integrity was evaluated as described earlier [26]. Intact RNA is recognized by specific ribosomal subunits: 18S and 28S; therefore, any degradation of RNA would lack these subunits, and provide uneven gene coverage thus, making the RNA less efficient and unsuitable for RNA sequencing. The RNA integrity number (RIN) measured on a scale from 1 – 10 is used as an index for RNA quality and suitability for RNA sequencing. RIN values < 6 represent low quality RNA [12]. In this study, RIN values were > 8.5 for all RNA samples isolated at both time points from both cell sources.

Control MSCs express more significantly changed genes

After comparing from day 7 to day 21, RNA sequencing results showed the expression of 13,855 genes in con-MSCs compared to 17,409 genes in ovx-MSCs. Of these, 41%

genes in con-MSCs were significantly altered compared to only 28% in ovx-MSCs, suggesting more genetic changes in con-MSCs.

Table 4.2 describes specific genes from each cluster that were upregulated in con-MSCs, but not in ovx-MSCs.

OVX derived MSCs express downregulation of ALPL

MSCs typically undergo osteogenesis *in vitro* over a period of 21-28 days when exposed to a dexamethasone/beta glycerophosphate and ascorbic acid cocktail [26]. Hence, genetic expression of osteogenic markers such as transcription factors (DLX5, RUNX2, and SOX9) and osteoblast/osteocyte markers (ALPL and SPP1) were examined over time (day 7 to day 21) within con-MSCs and ovx-MSCs. RUNX2 and SPP1 were upregulated confirming that the con-MSCs undergo *in vitro* osteogenesis and mineralization as expected (Table 4.1). Similarly, ovx-MSCs expressed upregulation in RUNX2 and SPP1, but downregulation of ALPL, the prominent gene of bone mineralization. Overall, this suggests that ovx-MSCs contain osteoprogenitors, but lack the ability to undergo mineralization, further supporting the decreased mineralization content demonstrated above.

Control and OVX derived MSCs reveal differences in cell adhesion, ECM, and growth factor genes

As single gene reactions are not representative of a genome that expresses thousands of genes, we next examined gene clusters well established in the bone differentiation process. Here we first examined genes related to cell adhesion and the ECM, which are the early foundation of bone differentiation. For the ECM, con-MSCs expressed more upregulated collagens (44%), glycoproteins (34%), and proteoglycans (20%), compared to ovx-MSCs (Figure 4.4B).

Additionally, the integrin and cadherin genes are important cell adhesion molecules for early cell communication. More specifically, the integrins are receptors that bind to the ECM and regulate both intracellular and extracellular signals, while cadherins bind cells and promote cell-to-cell communication [28, 37, 38]. Con-MSCs expressed upregulated integrin genes by 52%, compared to only 41% in ovx-MSCs (Figure 4.4A). Additionally, con-MSCs expressed upregulated cadherin genes by 43%, compared to only 26% in

ovx-MSCs. Overall, these data suggest that ovx-MSCs express fewer initiators of the bone differentiation process.

With establishment of cell adhesion and ECM, growth factor signaling stimulates a chain-of-command beginning at the membrane, through the cytosol, and into the nucleus for genetic transcription and ultimately protein synthesis. We therefore investigated several growth factor clusters including sex hormones (estrogens and androgens), BMPs, TGFs, FGFs, PDGFs, VEGFs, IGFs, and EGFs. Consistent patterns were found within most growth factor clusters (Figure 4.4C). For example, con-MSCs and ovx-MSCs expressed upregulated BMPs by 44% and 38%, TGFs by 53% and 47%, FGFs by 40% and 14%, and PDGFs by 75% and 25%, respectively. Other growth factors investigated were VEGFs, IGFs, and EGFs, which showed similar expression patterns between both cell groups.

Interestingly and as expected, we confirmed that the con-MSCs upregulated 33% of estrogens and androgens compared to 0% for both clusters in ovx-MSCs (Figure 4.4D). The lack of estrogen production within ovx-MSCs was expected as these cells were derived from ovariectomized animals, further confirming the OVX state of the animals.

Control and OVX derived MSCs reveal differences in Wnt-Catenin Signaling

A prominent signaling pathway in bone development is the Wnt/Catenin pathway which includes several Wnt, frizzled, catenin, and SMAD isoforms. Con-MSCs and ovx-MSCs expressed upregulated Wnts by 17% and 9%, frizzleds by 36% and 25%, catenins by 71% and 50%, and SMADs by 45% and 33%, respectively (Figure 4.5). Overall, these clusters were consistently lower in ovx-MSCs, suggestive of altered Wnt/Catenin signaling following bone differentiation cues.

Control and OVX derived MSCs reveal differences in cell differentiation genes

There are several other intracellular signaling molecules involved in cell survival, proliferation, and bone differentiation. These molecules communicate signals into the nucleus for transcriptional activity, which are often regulated by MAPK, PI3K, and Akt. In our analysis, we find differences in upregulated MAPK genes which was 26% in con-MSCs, but 19% in ovx-MSCs (Figure 4.6). Additionally, upregulated PI3K genes was expressed by 36% in con-MSCs and 31% in ovx-MSCs. In contrast, a similar expression pattern was observed for Akts within these cell groups. Overall, this data

suggests that con-MSCs have more intracellular signaling mechanisms occurring compared to the ovx-MSCs.

Control and OVX derived MSCs reveal differences in calcium and phosphatase regulated genes

MSC differentiation and subsequent mineralization does not occur without the presence of calcium and phosphate, which together forms hydroxyapatite, the inorganic portion of bone. Because some genes are regulated by the presence of calcium and phosphate groups, it would be presumed that mineralized cells would express more genes controlled by calcium and phosphatases. In our analysis, con-MSCs expressed upregulated calcium-regulated genes by 21%, compared to only 11% in ovx-MSCs (Figure 4.7). Additionally, we found that con-MSCs expressed upregulated phosphatases by 31%, compared to 22% in ovx-MSCs. This data supports that ovx-MSCs lack mineralization, despite being in the presence of osteo-inducers.

Table 4.2 describes the specific calcium and phosphatase-regulated genes that were upregulated in con-MSCs, but not in ovx-MSCs.

Control and OVX derived MSCs reveal differences in bone remodeling genes

Following bone mineralization, matrix metallopeptidases (MMPs) are enzymes critical to bone maintenance and remodeling [34, 39]. As expected, we found that con-MSCs expressed upregulated MMPs by 77%, compared to only 38% in ovx-MSCs (Figure 4.8). Overall, this data supports that MMP expression is less active in cells derived from the OVX model and may be an important target for future therapies.

DISCUSSION

The progression of age-related bone degenerative diseases is largely contributed by lack of adult, mesenchymal stem cell differentiation [4, 5, 40]. There are many theories for this inadequate bone differentiation (i.e., hormonal changes, decreased calcium absorption), but the overall issue is a bone remodeling imbalance whereby bone resorption activity outpaces new bone formation led by MSCs [41]. As cell behavior is controlled by genes, it is necessary to compare the response of MSCs during bone differentiation from a compromised model.

In this study, we obtained an OVX rat model, which is considered the gold standard for studying bone degenerative diseases [9]. This model shares many clinical similarities with estrogen deficient, postmenopausal bone loss including: (1) increased rate of bone turnover (2) initial phase of rapid bone loss followed by a much slower decline in bone loss and (3) greater loss of cancellous than cortical bone [9, 42]. Additionally, the reduction of bone density post ovariectomy is accelerated by consumption of a low calcium diet [9, 43, 44]. Using this OVX model, serum biomarkers confirmed greater bone resorption activity within OVX animals versus control animals (Figure 5.1). This result was similar to other tested markers previously reported [9, 35, 45]. We then proceeded to isolate, expand, and characterize MSCs from the bone marrow of both animal groups. A major criterion of MSCs identity is the positive and negative expression of specific CD markers. Both con-MSCs and ovx-MSCs demonstrated positive expression of CD29, CD73, and CD90 and negative expression of CD11b/c and CD45, the latter associated with the hematopoietic lineage (Figure 5.2).

To examine the osteogenic potential, con-MSCs and ovx-MSCs were exposed to osteo-chemical inducers using a well-established cocktail of dexamethasone, beta glycerol phosphate, and ascorbic acid. Under these *in vitro* conditions, rat and human MSCs undergo osteogenic differentiation in ~3 weeks [22, 23, 46]. After 21 days, our analysis confirmed that con-MSCs responded to the bone differentiation cocktail, whereas ovx-MSCs did not.

To investigate the genetic differences between these cells, we performed a genome-wide expression analyses using RNA sequencing. For the first time, our study investigates specific gene clusters well established in the bone differentiation process, including cell adhesion, ECM, growth factors, Wnt-Catenin signaling, MAPK signaling, mineralization, and bone remodeling [28-33, 47]. Similar gene clusters have been investigated in other bone differentiation studies [26]. Overall, we observed a consistent pattern whereby con-MSCs expressed more upregulated genes within most clusters. However, there were some clusters with no obvious differences between con-MSCs and ovx-MSCs (i.e. VEGFs, EGFs, AKTs, etc.). This is also important as these targets may

not be necessary during new drug developments or gene editing strategies. In other clusters, (i.e. proteoglycans, Wnts, Frizzleds, PI3K, etc.), the total number of upregulated genes are the same between con-MSCs and ovx-MSCs, but yet the overall ratio is greater in con-MSCs. For example, the total number of proteoglycans in con-MSCs and ovx-MSCs overtime was 10 and 12, respectively, yet both groups had the same upregulated proteoglycans. Hence, the ratio of upregulated proteoglycans appears greater in con-MSCs (Figure 5.4B), but specific genes different between these two groups were not found. It is also possible that since con-MSCs completed differentiation by Day 21, these cells subsequently advanced to a bone remodeling cycle, which is evident by several changes in MMPs, the bone remodeling genes (Figure 5.9) [39, 47]. In other words, once cells have entered bone remodeling, the proactive goal is bone maintenance rather than bone differentiation.

Hereafter, we named several gene isoforms that did not share commonality between both MSC sources (Table 4.2). Identifying these genes opens more strategies in targeting the endogenous MSCs following menopause. For example, current pharmaceutical strategies commonly target one gene, protein, or pathway to treat bone degenerative diseases [48, 49]. However, osteogenic differentiation is a complex system that requires coordination from hundreds to thousands of genes [50]. Many studies draw conclusions of osteogenesis (or lack thereof) based on single markers (i.e. RUNX2, ALPL, etc.) via PCR reactions [51-53]. Although these genes are important, the genome as a whole is necessary to keep the cell functionally active, healthy, and responsive to differentiation signals. Therefore, PCR is not suitable when studying cell behavior during a diseased process. As such, examining genome wide expression via RNA sequencing is a valuable tool to dissect out exactly what genes are affected by this bone degenerative model.

Several studies have implemented RNA sequencing strategies within the OVX rodent model to identify novel targets during osteoporosis, sarcopenia, and menopausal syndrome [54-59]. Chai et al., 2019 identified many long non-coding RNA (lncRNA) transcripts from the bone and skeletal muscle of OVX rats [54]. Similarly, Gu et al., 2021

also identified several lncRNAs in the pathogenesis of ovx-MSCs [55]. Supportively, Teng et.al., 2020 identified lncRNAs from serum exosomes of osteoporotic, human samples [60]. Finally, mechanistic studies of anti-osteoporotic drugs on ovx-MSCs have been reported [57]. However, until now no study had established that MSCs from the OVX model are genetically dysfunctional during new bone development.

It should also be noted that because RNA sequencing produces expression on thousands of genes, there are challenges on how this data is reported. Traditionally, RNA sequencing studies report results from bioinformatics databases [61-63]. These databases interpret results by pooling information from other literature sources which arbitrarily maps possibly involved pathways, thereby drawing indefinite conclusions. In other words, without specifically targeting those pathways with chemical inhibitors or knockdown/knockout experiments, then it is difficult to elucidate the exact mechanisms. Overall, our data shows that the pathophysiology of MSCs during bone degeneration is a complex process that is not attributed to one single factor, but rather a combination of multiple factors which conjunctively delays new bone differentiation. For example, normal bone development begins with activated MSCs that advances through a series of stages: proliferation and commitment (osteoprogenitors), differentiation (pre-osteoblasts), and mineralization (osteoblasts), before finally becoming mature osteocytes [64]. Each of these stages are governed by various molecules, such as RUNX2 which commits the MSC into osteoprogenitors and pre-osteoblasts [31, 64]. Similarly, we found RUNX2 upregulation in both con-MSCs and ovx-MSCs, but yet mineralization content was different between these two groups. Supportively, ALPL, being a major phosphatase for bone mineralization, was downregulated in ovx-MSCs. This indicates the ovx-MSCs were functioning as osteoprogenitors, but could not reach the end goal of mineralization due to lack of other signaling molecules, as presented in this study (i.e. cadherins, growth factors, MAPKs, MMPs, etc.). The question arises then, could the genome of geriatric MSCs be engineered to behave “normally” and ultimately reverse bone degeneration? To answer that question, this study lays the foundation for identifying genes of MSCs that do not behave normally when cued by bone differentiation signals. Future experiments to confirm these genetic changes in animal models are under development.

CONCLUSIONS

Understanding the pathophysiology of MSCs during bone degeneration is critical to developing effective strategies that both improves the human quality of life and relieves economic healthcare burdens. Since bone degeneration is in part attributed to MSC senescence, we studied the genetic expressions of MSCs derived from an *in vivo* bone degenerative model. Our data found that con-MSCs do have the ability to respond to bone differentiation, whereas ovx-MSCs do not. Further analysis showed clear genetic alterations that likely causes MSC senescence, and hence reduced bone formation. This information is necessary for future medical interventions that could prevent or even reverse the onset of age-related bone degeneration.

REFERENCES

1. Ryan, J.M., et al., *Mesenchymal stem cells avoid allogeneic rejection.* J Inflamm (Lond), 2005. **2**: p. 8.
2. Kariminekoo, S., et al., *Implications of mesenchymal stem cells in regenerative medicine.* Artificial cells, nanomedicine, and biotechnology, 2016. **44**: p. 1-9.
3. Pan, Q., et al., *Local administration of allogeneic or autologous bone marrow-derived mesenchymal stromal cells enhances bone formation similarly in distraction osteogenesis.* Cytotherapy, 2021. **23**(7): p. 590-598.
4. Wang, Q., et al., *Decreased proliferation ability and differentiation potential of mesenchymal stem cells of osteoporosis rat.* Asian Pac J Trop Med, 2014. **7**(5): p. 358-63.
5. Chen, H., et al., *Aging and Mesenchymal Stem Cells: Therapeutic Opportunities and Challenges in the Older Group.* Gerontology, 2021.
6. Thompson, D.D., et al., *FDA Guidelines and animal models for osteoporosis.* Bone, 1995. **17**(4 Suppl): p. 125s-133s.
7. Johnston, B.D. and W.E. Ward, *The ovariectomized rat as a model for studying alveolar bone loss in postmenopausal women.* BioMed research international, 2015. **2015**: p. 635023-635023.
8. Ren, W., et al., *CHANGES OF WNT/B-CATENIN SIGNALING AND DIFFERENTIATION POTENTIAL OF BONE MARROW MESENCHYMAL STEM CELLS IN PROCESS OF BONE LOSS IN OVARIECTOMIZED RATS.* Acta Endocrinol (Buchar), 2020. **16**(2): p. 156-164.
9. Gao, X., et al., *Establishing a rapid animal model of osteoporosis with ovariectomy plus low calcium diet in rats.* Int J Clin Exp Pathol, 2014. **7**(8): p. 5123-8.
10. Boeloni, J.N., et al., *Comparative study of osteogenic differentiation potential of mesenchymal stem cells derived from bone marrow and adipose tissue of osteoporotic female rats.* Connect Tissue Res, 2014. **55**(2): p. 103-14.
11. Wang, Z., M. Gerstein, and M. Snyder, *RNA-Seq: a revolutionary tool for transcriptomics.* Nature reviews. Genetics, 2009. **10**(1): p. 57-63.
12. Kukurba, K.R. and S.B. Montgomery, *RNA Sequencing and Analysis.* Cold Spring Harb Protoc, 2015. **2015**(11): p. 951-69.
13. Eastell, R. and R.A. Hannon, *CHAPTER 27 - Biochemical Markers of Bone Turnover*, in *Treatment of the Postmenopausal Woman (Third Edition)*, R.A. Lobo, Editor. 2007, Academic Press: St. Louis. p. 337-349.
14. Lv, Y., et al., *Tartrate-resistant acid phosphatase 5b is a marker of osteoclast number and volume in RAW 264.7 cells treated with receptor-activated nuclear κB ligand.* Experimental and therapeutic medicine, 2015. **9**(1): p. 143-146.
15. Kuo, T.-R. and C.-H. Chen, *Bone biomarker for the clinical assessment of osteoporosis: recent developments and future perspectives.* Biomarker Research, 2017. **5**(1): p. 18.
16. Zou, W., et al., *Congenital lipodystrophy induces severe osteosclerosis.* PLoS Genet, 2019. **15**(6): p. e1008244.
17. Abdelmagid, S.M., et al., *Mutation in Osteoactivin Promotes Receptor Activator of NFkappaB Ligand (RANKL)-mediated Osteoclast Differentiation and Survival but Inhibits Osteoclast Function.* J Biol Chem, 2015. **290**(33): p. 20128-46.

18. Raghuvanshi, P.D., *Mesenchymal Stem Cells Derived from Rat Bone Marrow (rBM MSC): Techniques for Isolation, Expansion and Differentiation.* 2018.
19. Fafián-Labora, J., et al., *Influence of age on rat bone-marrow mesenchymal stem cells potential.* Scientific Reports, 2015. **5**(1): p. 16765.
20. Alghazali, K., et al., *Functionalized gold nanorod nanocomposite system to modulate differentiation of human mesenchymal stem cells into neural-like progenitors.* Scientific Reports, 2017. **7**.
21. Dominici, M., et al., *Minimal criteria for defining multipotent mesenchymal stromal cells. The International Society for Cellular Therapy position statement.* Cytotherapy, 2006. **8**(4): p. 315-7.
22. Lee, D.J., et al., *Osteogenic potential of mesenchymal stem cells from rat mandible to regenerate critical sized calvarial defect.* Journal of tissue engineering, 2019. **10**: p. 2041731419830427-2041731419830427.
23. Kaur, G., et al., *Regulation of osteogenic differentiation of rat bone marrow stromal cells on 2D nanorod substrates.* Biomaterials, 2010. **31**(7): p. 1732-1741.
24. Elkhenany, H., et al., *Impact of the source and serial passaging of goat mesenchymal stem cells on osteogenic differentiation potential: implications for bone tissue engineering.* Journal of Animal Science and Biotechnology, 2016. **7**(1): p. 16.
25. Newby, S.D., et al., *Functionalized Graphene Nanoparticles Induce Human Mesenchymal Stem Cells to Express Distinct Extracellular Matrix Proteins Mediating Osteogenesis.* International journal of nanomedicine, 2020. **15**: p. 2501-2513.
26. MacDonald, A., et al., *Genetic profiling of human bone marrow and adipose tissue-derived mesenchymal stem cells reveals differences in osteogenic signaling mediated by graphene.* Journal of Nanobiotechnology, 2021. **19**.
27. Mueller, O., S. Lightfoot, and A. Schroeder, *RNA integrity number (RIN)-standardization of RNA quality control.* Agilent Application Note, 2004: p. 1-8.
28. Marie, P.J., E. Haÿ, and Z. Saidak, *Integrin and cadherin signaling in bone: role and potential therapeutic targets.* Trends Endocrinol Metab, 2014. **25**(11): p. 567-75.
29. Lin, X., et al., *The Bone Extracellular Matrix in Bone Formation and Regeneration.* Frontiers in Pharmacology, 2020. **11**.
30. Zhang, L. and H. Ai, *Concentrated growth factor promotes proliferation, osteogenic differentiation, and angiogenic potential of rabbit periosteum-derived cells in vitro.* Journal of Orthopaedic Surgery and Research, 2019. **14**(1): p. 146.
31. Rutkovskiy, A., K.-O. Stensløkken, and I.J. Vaage, *Osteoblast Differentiation at a Glance.* Medical science monitor basic research, 2016. **22**: p. 95-106.
32. Zayzafoon, M., *Calcium/calmodulin signaling controls osteoblast growth and differentiation.* J Cell Biochem, 2006. **97**(1): p. 56-70.
33. Prins, H.-J., et al., *In vitro induction of alkaline phosphatase levels predicts in vivo bone forming capacity of human bone marrow stromal cells.* Stem Cell Research, 2014. **12**(2): p. 428-440.
34. Paiva, K. and J. Granjeiro, *Matrix Metalloproteinases in Bone Resorption, Remodeling, and Repair*. 2017. p. 203-303.

35. Tsai, Y.-F., et al., *Long-Term Oral Toxicity and Anti-osteoporotic Effect of Sintered Dicalcium Pyrophosphate in Rat Model of Postmenopausal Osteoporosis.* Journal of medical and biological engineering, 2017. **37**(2): p. 181-190.
36. Newby, S.D., et al., *Functionalized Graphene Nanoparticles Induce Human Mesenchymal Stem Cells to Express Distinct Extracellular Matrix Proteins Mediating Osteogenesis.* Int J Nanomedicine, 2020. **15**: p. 2501-2513.
37. Di Benedetto, A., et al., *Osteogenic differentiation of mesenchymal stem cells from dental bud: Role of integrins and cadherins.* Stem Cell Research, 2015. **15**(3): p. 618-628.
38. Klezovitch, O. and V. Vasioukhin, *Cadherin signaling: keeping cells in touch.* F1000Research, 2015. **4**(F1000 Faculty Rev): p. 550-550.
39. Liang, H., et al., *Matrix metalloproteinases in bone development and pathology: current knowledge and potential clinical utility.* Metalloproteinases In Medicine, 2016. **Volume 3**: p. 93-102.
40. Zupan, J., et al., *Age-related alterations and senescence of mesenchymal stromal cells: Implications for regenerative treatments of bones and joints.* Mechanisms of Ageing and Development, 2021. **198**: p. 111539.
41. Feng, X. and J.M. McDonald, *Disorders of bone remodeling.* Annual review of pathology, 2011. **6**: p. 121-145.
42. Kalu, D.N., *The ovariectomized rat model of postmenopausal bone loss.* Bone Miner, 1991. **15**(3): p. 175-91.
43. Mao, H., et al., *Metabolomics and physiological analysis of the effect of calcium supplements on reducing bone loss in ovariectomized rats by increasing estradiol levels.* Nutrition & Metabolism, 2021. **18**(1): p. 76.
44. Lee, M.-R., et al., *Effects of a Low Calcium Diet and Oxalate Intake on Calcium Deposits in Soft Tissues and Bone Metabolism in Ovariectomized Rats.* kjn, 2011. **44**(2): p. 101-111.
45. Hsiao, C.-Y., et al., *Calcitonin Induces Bone Formation by Increasing Expression of Wnt10b in Osteoclasts in Ovariectomy-Induced Osteoporotic Rats.* Frontiers in Endocrinology, 2020. **11**.
46. Hu, H., et al., *An Inhibitory Role of Osthole in Rat MSCs Osteogenic Differentiation and Proliferation via Wnt/β-Catenin and Erk1/2-MAPK Pathways.* Cellular Physiology and Biochemistry, 2016. **38**(6): p. 2375-2388.
47. Paiva, K.B.S. and J.M. Granjeiro, *Matrix Metalloproteinases in Bone Resorption, Remodeling, and Repair.* Prog Mol Biol Transl Sci, 2017. **148**: p. 203-303.
48. Drake, M.T., B.L. Clarke, and S. Khosla, *Bisphosphonates: mechanism of action and role in clinical practice.* Mayo Clinic proceedings, 2008. **83**(9): p. 1032-1045.
49. Casas, A.I., et al., *From single drug targets to synergistic network pharmacology in ischemic stroke.* Proceedings of the National Academy of Sciences, 2019. **116**(14): p. 7129.
50. Cohen-Zinder, M., D. Karasik, and I. Onn, *Structural maintenance of chromosome complexes and bone development: the beginning of a wonderful relationship?* BoneKEy reports, 2013. **2**: p. 388-388.

51. Frank, O., et al., *Real-time quantitative RT-PCR analysis of human bone marrow stromal cells during osteogenic differentiation in vitro.* J Cell Biochem, 2002. **85**(4): p. 737-46.
52. Okamura, K., et al., *RT-qPCR analyses on the osteogenic differentiation from human iPS cells: an investigation of reference genes.* Scientific Reports, 2020. **10**(1): p. 11748.
53. Pettersson, L.F., et al., *In Vitro Osteogenic Differentiation of Human Mesenchymal Stem Cells from Jawbone Compared with Dental Tissue.* Tissue Engineering and Regenerative Medicine, 2017. **14**(6): p. 763-774.
54. Chai, S., et al., *Systematic analysis of long non-coding RNA and mRNA profiling using RNA sequencing in the femur and muscle of ovariectomized rats.* Journal of musculoskeletal & neuronal interactions, 2019. **19**(4): p. 422-434.
55. Gu, H., et al., *Expression Profile Analysis of Long Non-coding RNA in OVX Models-Derived BMSCs for Postmenopausal Osteoporosis by RNA Sequencing and Bioinformatics.* Frontiers in Cell and Developmental Biology, 2021. **9**.
56. Wang, W., et al., *Transcriptomic changes in the hypothalamus of ovariectomized mice: Data from RNA-seq analysis.* Annals of Anatomy - Anatomischer Anzeiger, 2022: p. 151886.
57. Guo, X., et al., *RNA-Seq investigation and in vivo study the effect of strontium ranelate on ovariectomized rat via the involvement of ROCK1.* Artificial Cells, Nanomedicine, and Biotechnology, 2018. **46**(sup1): p. 629-641.
58. Kanaya, N., et al., *Single-cell RNA-sequencing analysis of estrogen- and endocrine-disrupting chemical-induced reorganization of mouse mammary gland.* Communications Biology, 2019. **2**(1): p. 406.
59. Iqbal, J., et al., *Estradiol Alters Hippocampal Gene Expression during the Estrous Cycle.* Endocr Res, 2020. **45**(2): p. 84-101.
60. Teng, Z., et al., *Osteoporosis Is Characterized by Altered Expression of Exosomal Long Non-coding RNAs.* Frontiers in genetics, 2020. **11**: p. 566959-566959.
61. Kang, W., et al., *Transcriptome analysis reveals the mechanism of stromal cell-derived factor-1 and exendin-4 synergistically promoted periodontal ligament stem cells osteogenic differentiation.* PeerJ, 2021. **9**: p. e12091.
62. Zhao, Z., et al., *Radial extracorporeal shockwave promotes subchondral bone stem/progenitor cell self-renewal by activating YAP/TAZ and facilitates cartilage repair in vivo.* Stem Cell Research & Therapy, 2021. **12**(1): p. 19.
63. Shaik, S., et al., *Transcriptomic Profiling of Adipose Derived Stem Cells Undergoing Osteogenesis by RNA-Seq.* Scientific Reports, 2019. **9**(1): p. 11800.
64. Javed, A., H. Chen, and F.Y. Ghori, *Genetic and transcriptional control of bone formation.* Oral and maxillofacial surgery clinics of North America, 2010. **22**(3): p. 283-v.

APPENDIX

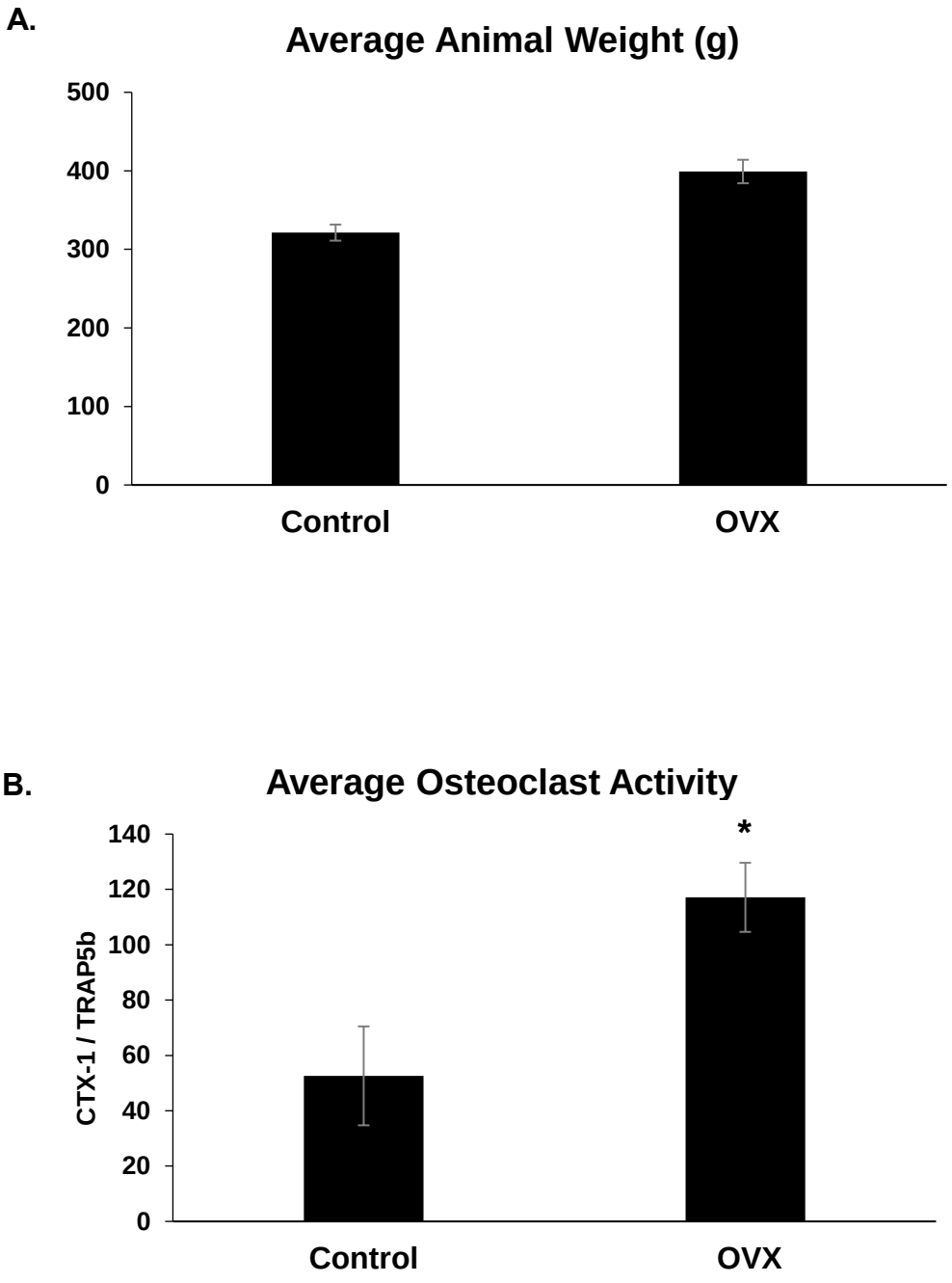

Figure 4.1. (A) Final weight of control and ovariectomized animals on the day of sacrifice. **(B)** The ratio of C-telopeptide of type I collagen (CTX-1) to tartrate-resistant acid phosphate isoform 5b (TRAP5B) in serum protein collected from animals on the day of sacrifice; n = 6; asterisk indicates statistical significance; error bars presented as SEM.

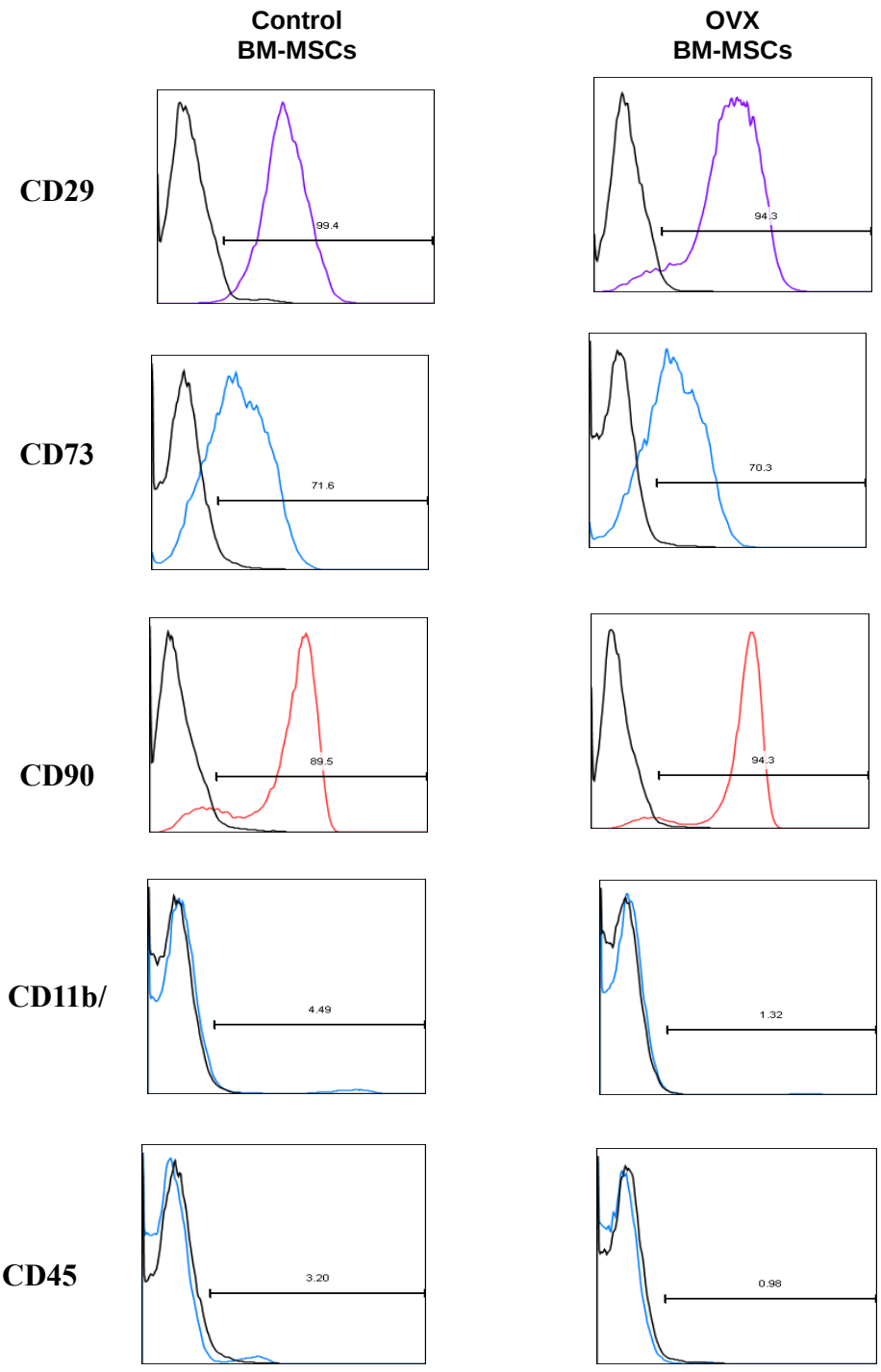

Figure 4.2. Expression of MSC Markers. Flow cytometry analysis showed that all MSC sources positively expressed positive markers (CD29, CD73, CD90) and negatively expressed negative markers (CD11b/c and CD45).

A.

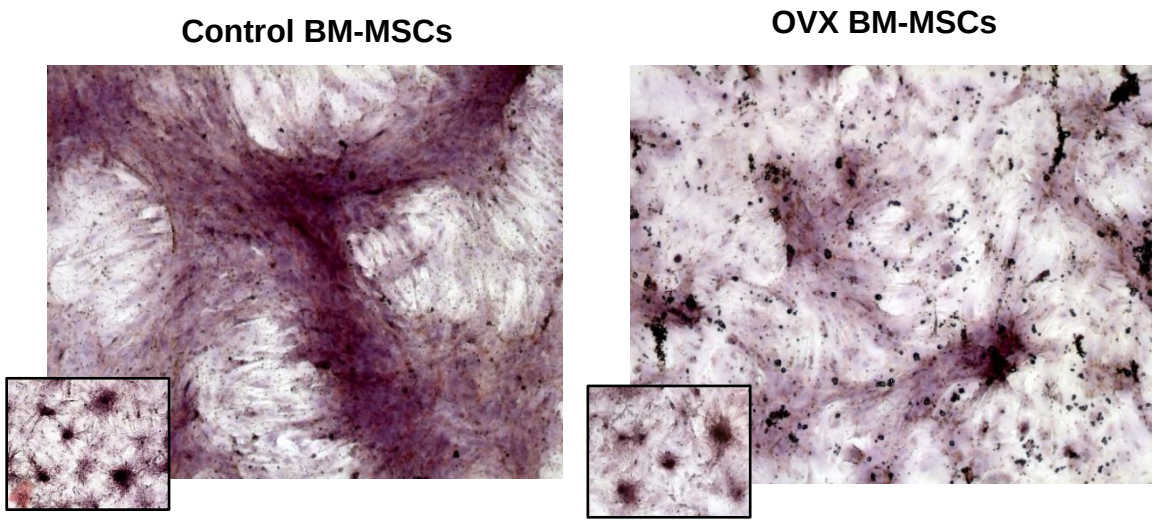

B.

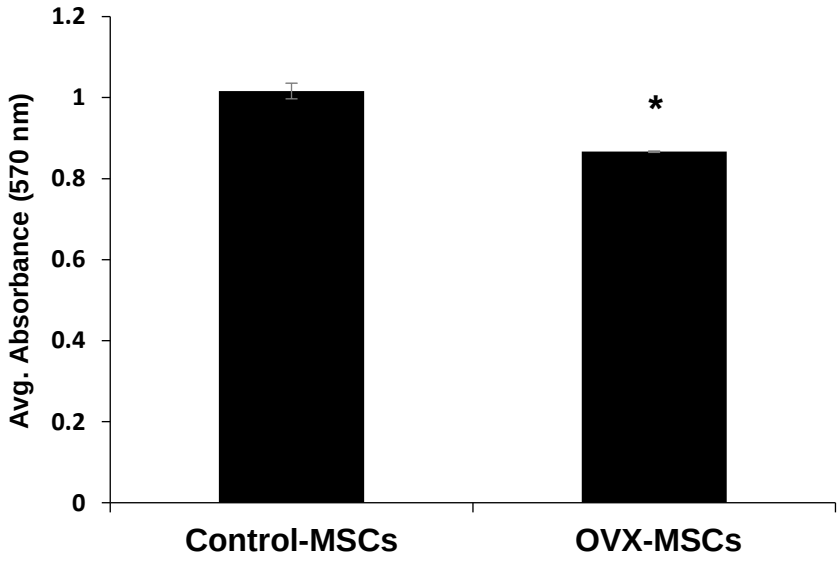

Figure 4.3. Osteogenic Differentiation Assay. (A) Calcium content of control and OVX derived MSCs cultured in either undifferentiated (inset) or osteogenic differentiation media for 21 days. Images were taken at 10X magnification. **(B)** Quantification of alizarin red staining of cells exposed to osteogenic induction media for 21 days; n=3, error bars presented as SEM.

Table 4.1. RNA sequencing analysis of common bone differentiation markers. For each group, MSCs cultured in osteo-differentiation media for 7 days was set as the control, while cells cultured for 21 days was set as the tested group. The p-adjusted value was set to 0.05 with a log2 fold change of a positive (+) or negative (-) value indicating upregulation and downregulation, respectively. NC = No Change.

	CON-MSCs	**OVX-MSCs**
Gene Name	**log2FoldChange**	**log2FoldChange**
Dlx5	NC	NC
Runx2	**+**	**+**
Sox9	NC	NC
Sp7	NC	NC
Alpl	NC	**-**
Spp1	**+**	**+**

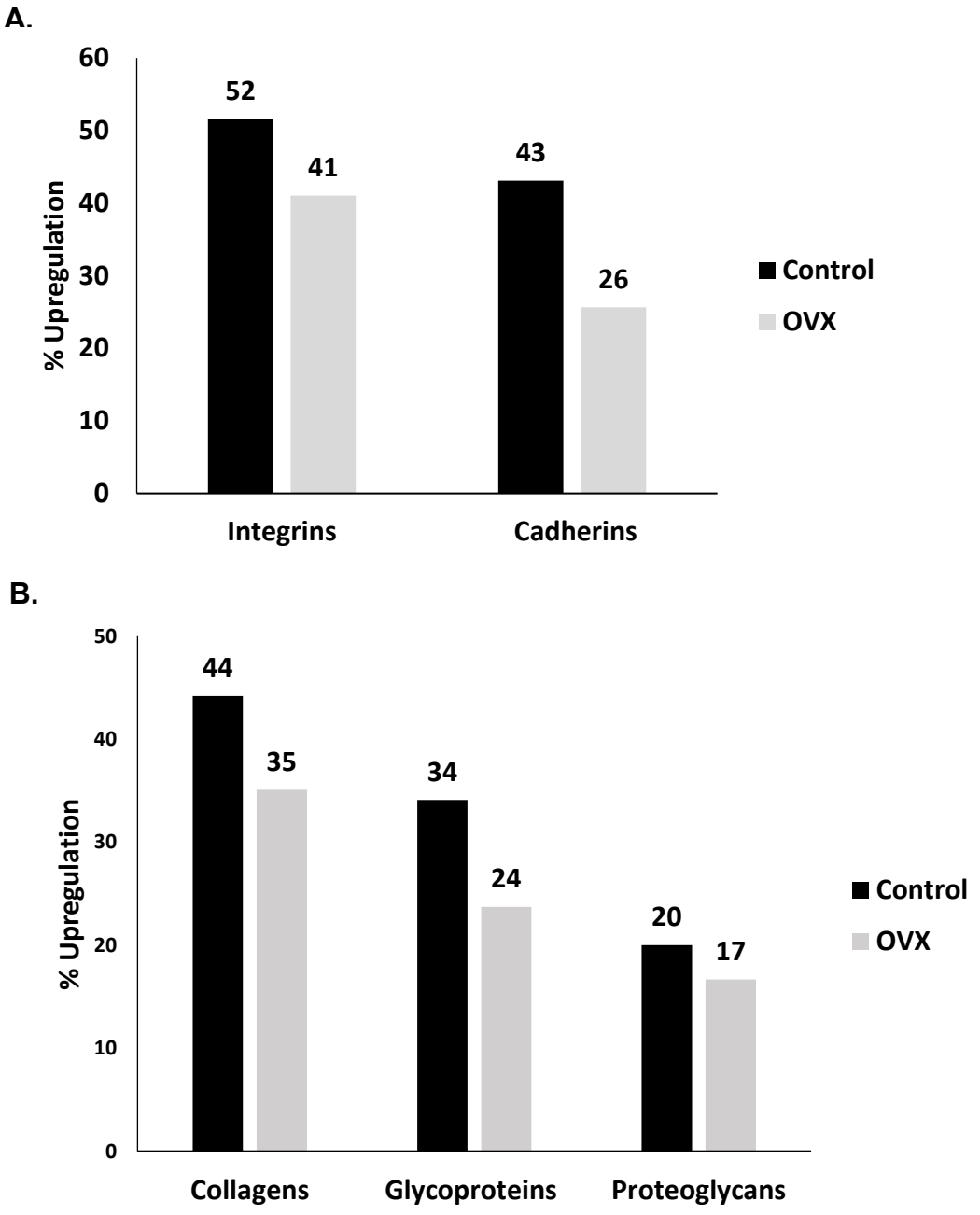

Figure 4.4. The percentage of upregulated genes related to adhesion, extracellular matrix, and growth factors. For each group, MSCs cultured in osteo-differentiation media for 7 days were set as the control, while cells cultured for 21 days was set as the tested group. **(A)** The percentage of upregulated integrin and cadherin genes within MSCs derived from both control and OVX animals. **(B)** The percentage of upregulated ECM genes within MSCs derived from both control and OVX animals. **(C)** The percentage of upregulated growth factors and **(D)** sex hormones

C.

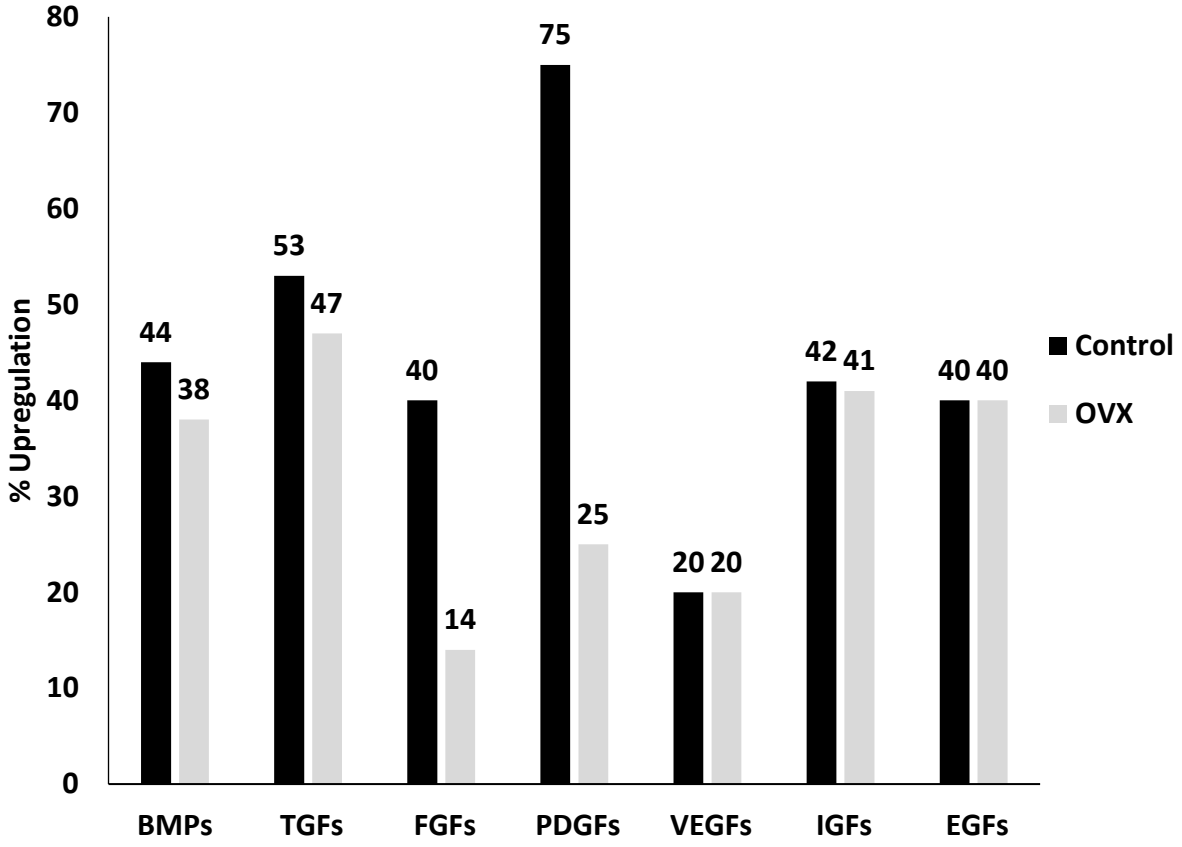

D.

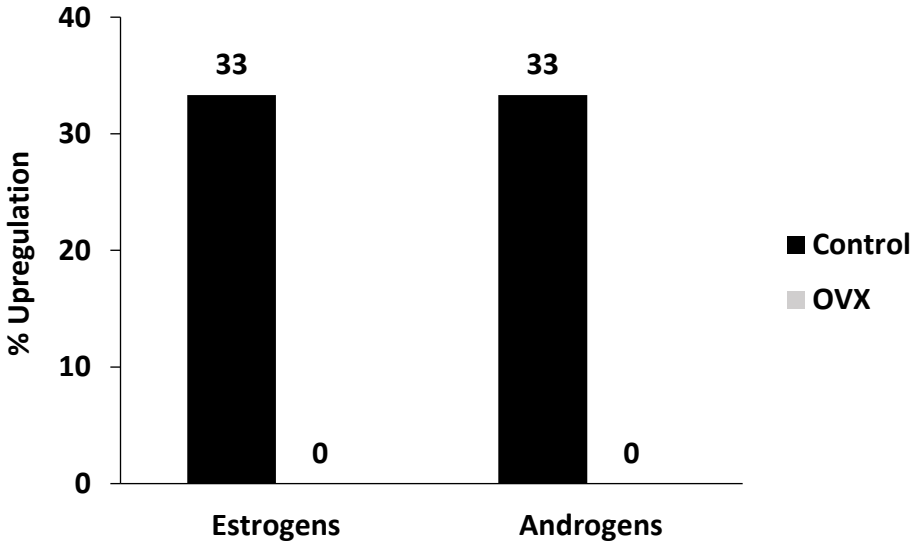

Figure 4.4. Continued.

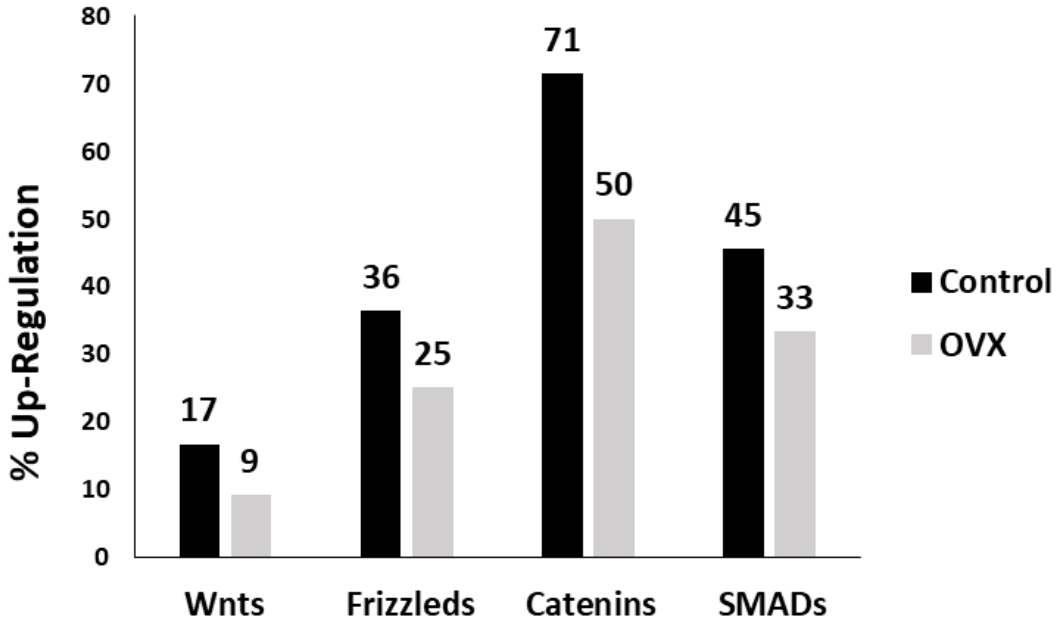

Figure 4.5. The percentage of upregulated genes related to Wnt/β-Catenin signaling. For each group, MSCs cultured in osteo-differentiation media for 7 days were set as the control, while cells cultured for 21 days was set as the tested group.

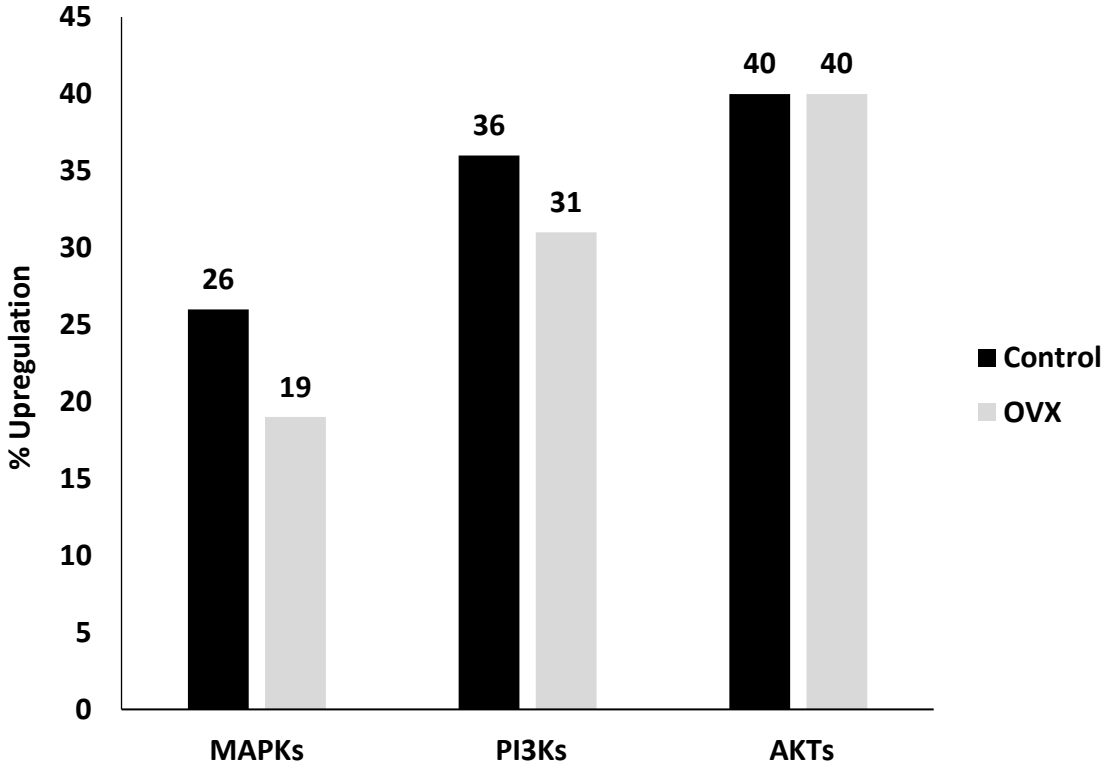

Figure 4.6. The percentage of upregulated genes related to cell signaling/differentiation. For each group, MSCs cultured in osteo-differentiation media for 7 days were set as the control, while cells cultured for 21 days was set as the tested group.

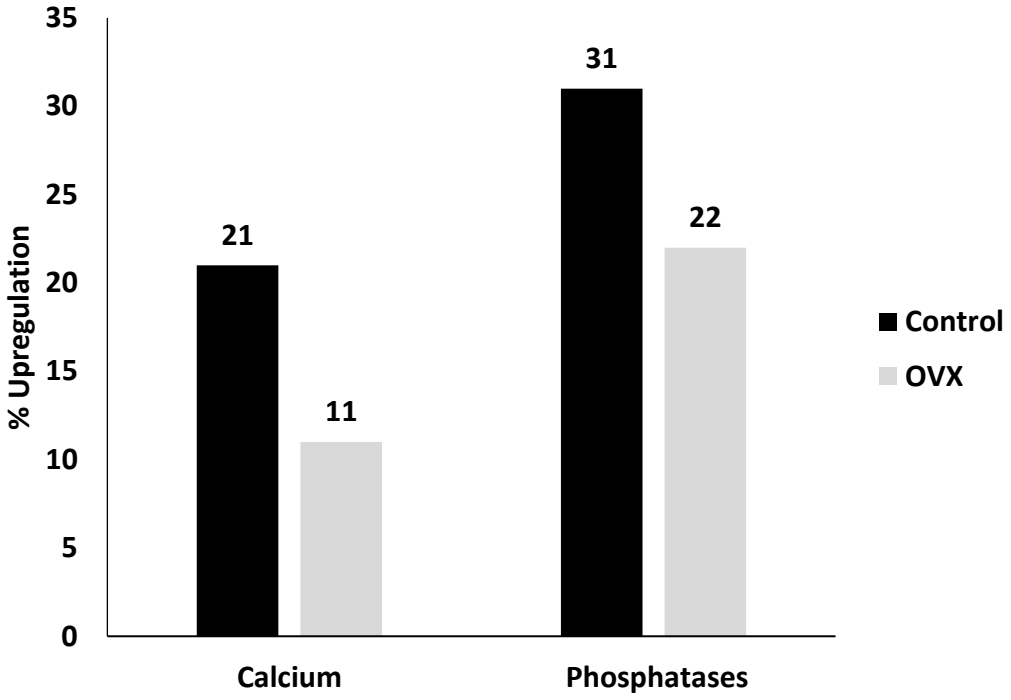

Figure 4.7. The percentage of upregulated genes related to mineralization. For each group, MSCs cultured in osteo-differentiation media for 7 days were set as the control, while cells cultured for 21 days was set as the tested group. The percentage of upregulated genes involving calcium or phosphatases within MSCs derived from both control and OVX animals.

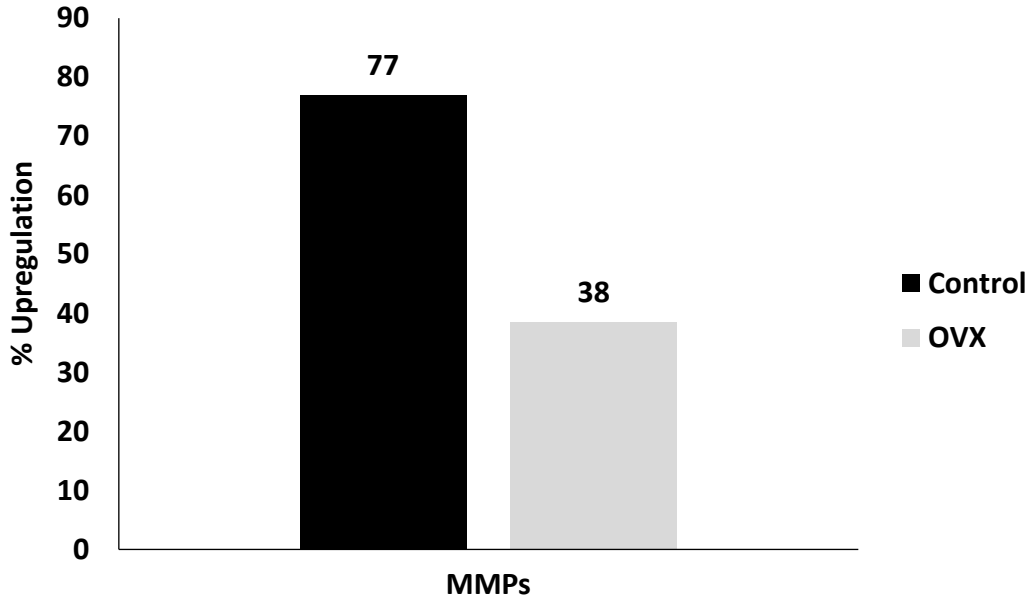

Figure 4.8. The percentage of upregulated metallopeptidase (bone remodeling) genes. For each group, MSCs cultured in osteo-differentiation media for 7 days were set as the control, while cells cultured for 21 days was set as the tested group.

Table 4.2. List of specific genes upregulated in con-MSCs, but not in ovx-MSCs. For each group, MSCs cultured in osteo-differentiation media for 7 days were set as the control, while cells cultured for 21 days was set as the tested group. + indicates upregulation; NC = No Change.

Gene Description	Symbol	log2 Fold Change (Con-MSCs)	log2 Fold Change (OVX-MSCs)
Adhesion			
Integrins			
integrin alpha FG-GAP repeat containing 1	Itfg1	+	NC
Cadherins			
Protocadherin alpha-4	AC103179.2	+	NC
cadherin 6, type 2, K-cadherin	Cdh6	+	NC
catenin (cadherin-associated protein), delta 2	Ctnnd2	+	NC
protocadherin 18	Pcdh18	+	NC
protocadherin 7	Pcdh7	+	NC
protocadherin alpha subfamily C, 1	Pcdhac1	+	NC
protocadherin gamma subfamily A, 10	Pcdhga10	+	NC
protocadherin gamma subfamily A, 2	Pcdhga2	+	NC
protocadherin gamma subfamily A, 7	Pcdhga7	+	NC
ECM			
Collagens			
collagen, type IV, alpha 3 (Goodpasture antigen) binding protein	Col4a3bp	+	NC
collagen, type IV, alpha 6	Col4a6	+	NC
Glycoproteins			
synaptic vesicle glycoprotein 2b	Sv2b	+	NC
Estrogens			
RAS-like, estrogen-regulated, growth-inhibitor	Rerg	+	NC
G protein-coupled estrogen receptor 1	Gper1	+	NC
breast cancer anti-estrogen resistance 3	Bcar3	+	NC
Androgens			
prostate androgen-regulated mucin-like protein 1	Parm1	+	-

Table 4.2. Continued.

Gene Description	Symbol	Log2 Fold Change (Con-MSCs)	Log2 Fold Change (OVX-MSCs)
Growth Factors			
BMPs			
bone morphogenetic protein receptor, type IB	Bmpr1b	+	NC
TGFs			
latent transforming growth factor beta binding protein 4	Ltbp4	+	NC
FGFs			
Fibroblast growth factor receptor 1	Fgfr1	+	NC
FGFR1 oncogene partner 2	Fgfr1op2	+	NC
fibroblast growth factor receptor 3	Fgfr3	+	NC
PDGFs			
platelet derived growth factor C	Pdgfc	+	NC
platelet derived growth factor D	Pdgfd	+	NC
IGFs			
insulin-like growth factor binding protein 5	Igfbp5	+	NC
insulin induced gene 2	Insig2	+	NC
Wnt / Catenin Signaling			
Catenins			
catenin (cadherin-associated protein), delta 2	Ctnnd2	+	NC
SMADs			
SMAD family member 1	Smad1	+	NC
Cell Signaling			
MAPK			
mitogen-activated protein kinase 1 interacting protein 1-like	Mapk1ip1l	+	NC
mitogen-activated protein kinase 8	Mapk8	+	NC
mitogen-activated protein kinase 9	Mapk9	+	NC

Table 4.2. Continued.

Gene Description	Symbol	Log2 Fold Change (Con-MSCs)	Log2 Fold Change (OVX-MSCs)
Mineralization			
Calcium			
C2 calcium-dependent domain containing 2	C2cd2	+	NC
C2 calcium-dependent domain containing 3	C2cd3	+	NC
calcium/calmodulin-dependent protein kinase ID	Camk1d	+	NC
mitochondrial calcium uniporter	Mcu	+	NC
mitochondrial calcium uniporter regulator 1	Mcur1	+	NC
mitochondrial calcium uptake 1	Micu1	+	NC
protein phosphatase, EF-hand calcium binding domain 1	Ppef1	+	NC
SPARC related modular calcium binding 1	Smoc1	+	NC
Phosphatases			
dual specificity phosphatase 16	Dusp16	+	NC
dual specificity phosphatase 18	Dusp18	+	NC
dual specificity phosphatase 8	Dusp8	+	NC
ectonucleotide pyrophosphatase/phosphodiesterase 2	Enpp2	+	NC
EYA transcriptional coactivator and phosphatase 1	Eya1	+	NC
inositol polyphosphate-4-phosphatase, type II	Inpp4b	+	NC
protein phosphatase, EF-hand calcium binding domain 1	Ppef1	+	NC
protein phosphatase, Mg2+/Mn2+ dependent, 1B	Ppm1b	+	NC
protein phosphatase, Mg2+/Mn2+ dependent, 1F	Ppm1f	+	NC
protein phosphatase, Mg2+/Mn2+ dependent, 1K	Ppm1k	+	NC
protein phosphatase, Mg2+/Mn2+ dependent, 1L	Ppm1l	+	NC
Protein Ppp1r12b; Protein phosphatase 1, regulatory (Inhibitor) subunit 12B (Predicted)	Ppp1r12b	+	NC
protein phosphatase 1, regulatory subunit 13B	Ppp1r13b	+	NC
protein phosphatase 1, regulatory (inhibitor) subunit 2	Ppp1r2	+	NC
protein phosphatase 1, regulatory subunit 3C	Ppp1r3c	+	NC
protein phosphatase 1, regulatory subunit 3D	Ppp1r3d	+	NC
protein phosphatase 3, catalytic subunit, alpha isozyme	Ppp3ca	+	NC
protein phosphatase 3, regulatory subunit B, alpha	Ppp3r1	+	NC
PTC7 protein phosphatase homolog (S. cerevisiae)	Pptc7	+	NC
protein tyrosine phosphatase, non-receptor type 4	Ptpn4	+	NC
protein tyrosine phosphatase, receptor type, A	Ptpra	+	NC
protein tyrosine phosphatase, receptor type, M	Ptprm	+	NC
Bone Remodeling			
MMPs			
matrix metallopeptidase 12	Mmp12	+	NC
matrix metallopeptidase 13	Mmp13	+	NC
matrix metallopeptidase 16	Mmp16	+	NC
matrix metallopeptidase 2	Mmp2	+	NC
matrix metallopeptidase 9	Mmp9	+	NC

CHAPTER V:
3D-PRINTED RGO CONSTRUCTS SUPPORT MANDIBULAR DEFECTS IN AN OSTEOPOROTIC RODENT MODEL

ABSTRACT

Mandibular bone degeneration is a rising concern for post-menopause osteoporotic women, thereby increasing the risk of traumatic jaw injuries. The current standard for repairing mandible defects are autologous bone grafts, but this strategy creates a second morbidity site and increases the risk of infection. Alternatively, the field of tissue engineering is actively investigating the use of stem cells and 3D biomaterials to stimulate new bone for mandible injuries. Reduced graphene oxide (rGO), is a carbon-based material that spontaneously supports bone differentiation of adult mesenchymal stem cells (MSCs). However, rGO-MSC constructs have not been tested in *in vivo* mandible defects. To mimic post-menopause osteoporosis, we began this study with the ovariectomized (OVX) rodent model and created critical-sized mandible defects. These defects were filled with 3D-printed rGO-MSC constructs and treated for 60 days. Micro-CT and histology analysis demonstrated that the rGO-MSC constructs supported new bone regeneration of mandibular defects in both normal adult rats and osteoporotic rats, and hence is a potential strategy for reconstructing traumatic jaw injuries. To our knowledge, this is one of the first studies to (1) examine a bone regenerative treatment of osteoporotic mandibles and (2) to test rGO scaffolds in maxillofacial bones. In the future, long-term studies are needed to determine the maximum bone differentiation potential of rGO scaffolds, and whether this process should be enhanced with other biological components.

INTRODUCTION

Mandibular bone degeneration is a rising concern for post-menopause osteoporotic women, thereby increasing susceptibility of traumatic jaw fractures [1, 2]. Currently, jaw reconstruction is treated with autologous bone grafts, but this strategy is infeasible for patients with bone degenerative diseases [3]. Additionally, anti-osteoporotic medications such as bisphosphonates have harmful side effects, are too expensive, and are linked to osteonecrosis of the jaw [4-6].

The alternative strategy for treating mandibular defects is regenerative medicine, whereby the primary goal is to rebuild functional tissues with stem cells and three-dimensional (3D) biomaterials. Graphene, an allotrope of carbon, is a proposed bone biomaterial, due to its very strong, yet lightweight and flexible properties. Additionally, graphene supports traumatic bone defects, demonstrates cell compatibility, and spontaneously stimulates bone differentiation of adult mesenchymal stem cells (MSCs) [7, 8]. However, it is unclear if graphene materials can similarly regenerate new tissue within a diseased, bone degenerative model. Therefore, we overall investigated if graphene scaffolds would be an ideal candidate for (1) supporting mandible defects and (2) supporting new bone development within an osteoporotic model.

In this study, we successfully 3D printed reduced graphene oxide (rGO) scaffolds, specifically tailored for mandibular deformities. Subsequently, these scaffolds were implanted into mandible defects of the ovariectomized (OVX) rodent model, which mimics post-menopause osteoporosis [9, 10]. We hypothesized that rGO scaffolds would support mandibular bone development in both normal and osteoporotic rats.

METHODS

Cell Isolation and Culture

Patient consent for collecting adipose tissue following a panniculectomy was obtained and approved by an IRB protocol at the University of Tennessee Medical Center in Knoxville. Human adipose-derived mesenchymal stem cells (AD-MSCs) were isolated and characterized as previously described [7, 11]. AD-MSCs were cultured in DMEM-

F12 media, supplemented with 10% FBS, 1% penicillin, and 1% streptomycin and maintained in an atmosphere of 5% CO^2 at 37°C.

Scaffold Design and Preparation

The scaffold design (as previously described by Newby et al., unpublished) was constructed in computer-aided design (CAD) software (Autodesk Fusion 360), whereby the scaffold pattern was a 5 mm diameter circle, composed of 15 layers. Additionally, the scaffold was designed to achieve ~80% porosity, whereby the gap size between printed lines was 100-300 µm to support osteogenic potential [12]. The final design was then digitally formatted into a Standard Tessellation Language (STL) file format and loaded into the Element slicing software. The slicing software 'slices' the design into values that denote how each layer is to be printed, overall developing a control language known as a G-code file. These files were then exported to the Cellink-BIO X6™ printer.

Prior to printing, rGO (Cheap Tubes Inc., Grafton, VT), was mixed into poly(lactic-co-glycolic) acid (PLGA), being 65% lactic acid and 35% glycolic acid (Sigma-Aldrich, St. Louis, MO) and 0.5 mL DMSO, for a final concentration of 0.5% rGO. The mixture was then melted at 85°C for ~2 hr. or until homogeneous, followed by overnight storage in -20°C. The rGO-PLGA material was then loaded into a syringe connected to the Cellink-BIO X6™ printer. Each scaffold was printed at 5 (L) X 5 (W) X 2 (H) mm. Printing parameters (i.e. extruder temperature, print bed temperature, speed, and pressure) were manually set and adjusted as necessary.

DiI Staining

To identify cell attachment to the rGO scaffold, we stained AD-MSCs with CellTracker™-DiI Dye (Invitrogen molecular probes, #C7001). DiI Dye is a fluorescent stain with a red excitation/emission spectra of 553/570 nm maxima. It freely passes through the cell membrane and subsequently transforms into cell-impermeant reaction products. Briefly, AD-MSCs were split in 0.5% trypsin, then centrifuged before washing with 1X HBSS. The DiI Dye solution was added to the cell pellet at a total volume of 1 mL and incubated at 37°C for 15 min before washing and resuspending in media. To direct cell attachment, scaffolds were placed inside a collection tube and AD-MSCs

were seeded at 1 X 10^6. The rGO-cell construct was incubated for 48 hr and then fixed in 4% paraformaldehyde prior to imaging (Leica SP8 confocal microscope).

Animal Model

All procedures were approved by the University of Tennessee Institutional Animal Care and Use Committee. 12 female Sprague Dawley rats were purchased from Charles River (Wilmington, MA) that underwent either a bilateral ovariectomy (n=6) or were sham-operated (n=6) to mimic surgical stress between both groups. The animals (at 9 weeks old) arrived to the University of Tennessee Veterinary Medical Center, were housed in pairs, and acclimatized for one week. Following acclimatization, animals were housed individually to control for diet consumption.

Rats were fed a commercially available low calcium diet (Envigo,Indianapolis, ID), as previously described (MacDonald et al., in review). The formula consisted of casein (200 g/Kg), L-cystine (3.0 g/Kg), sucrose (342.188 g/Kg), corn starch (320.0 g/Kg), soybean oil (60 g/Kg), cellulose (40 g/Kg), mineral mix (Ca-P deficient) (13.37 g/Kg), potassium phosphate (monobasic) (11.43 g/Kg), vitamin mix (10.0 g/Kg), and ethoxyquin, an antioxidant (0.012 g/Kg). The casein contributed ~0.01% calcium or less. The diet also contained ~0.4% phosphorus and 2200 IU vitamin D/Kg diet. Food was stored at 4°C and used within 6 months of purchasing. Each rat was fed 210 g (+/- 5 g) of diet every 7 days according to manufacturer recommendations. The rats consumed this diet for 10 weeks, with food intake and body weights recorded weekly. A separate group of sham-operated animals (n = 5) were not fed a low calcium diet, but rather a standard chow diet for 10 weeks.

Surgical Procedure

Prior to surgery, rGO scaffolds were UV sterilized at least 2 hours before seeding AD-MSCs at 5 X 10^5 and incubating overnight at 37°C, 5% CO_2.

Animals were anesthetized under isoflurane, the fur was removed, and skin was cleaned with ethanol and chlorhexidine prior to incision. A linear incision was made through the skin, subcutaneous tissues, and masseter muscle paralleling the inferior border of the mandible. The buccal and lingual surfaces of the mandible were exposed with an elevator, and a 5-mm full-thickness circular defect was drilled in the mandibular angle (right-side), posterior to the root of the incisor. This ostectomy was performed

using a high-speed Dremel with a trephine bur and did not interrupt mandibular continuity at the alveolus. The defect was immediately filled with a rGO-cell construct and the muscle/skin incisions were sutured (4-0). Buprenorphine was administered pre-surgery and twice daily for 3 days post-surgery at 0.05 mg/kg. All animals received water supplemented with Gatorade and Baytril® for one week. A cube of soft-food (Bio-Serve, Flemington, NJ, #S5769) was refreshed daily for 6 weeks before switching to a standard chow diet. All mandibular defects were treated with the rGO-cell construct for 60 days before sacrificing for further analysis.

Micro-CT

Bilateral mandibles were imaged using a micro-CT specimen scanner (μCT 35, Scanco Medical; Bassersdorf, Switzerland). Scan parameters were 55 kVp, 145 μA, 400 msec exposure time, average of 3 exposures per projection, 0.5 mm aluminum filter, 1000 projections per 180 degrees and a 15-micron voxel size. A circle ROI of 6 mm diameter and 3 mm length was selected for both the defected area and the contralateral (non-defected) side. A region of trabecular bone (ROI = 1.2 mm in length) was taken rostral-to-caudal in the mandible, ventral to the incisor's root, on the contralateral (non-defected) side only. The raw images were calibrated using a hydroxyapatite (HA) phantom of varying HA concentrations. Noise in the images was reduced by use of a low-pass Gaussian filter. A threshold of 380 to 3000 mgHA/mm was used to partition mineralized tissue from other less-dense tissues (low threshold is to exclude soft-tissue and void space, high threshold is the highest value in the scan). The bone volume fraction (BV/TV) was determined by dividing the number of voxels (denser than the threshold) representing mineralized tissue (BV: bone volume) by the total number of voxels in the region (TV: total volume). The mean density of all material in the volume is apparent bone mineral density (aBMD). The mean density of only the mineralized material is the tissue bone mineral density (tBMD). Trabecular number, mean trabecular thickness, and mean trabecular separation were calculated using a direct morphometric analysis [13, 14]. Connectivity density was calculated by dividing the connectivity measure by TV, where connectivity is the maximum number of trabeculae that can be broken before the specimen is separated into two parts [15].

Histology

Mandible samples were sent to Ratliff Histology Consultants, LLC and embedded in undecalcified methylmethacrylate (MMA). Samples were stained and counterstained with Von kossa and MacNeal's tetrachrome, respectively. The Von kossa stain was used to visualize any new mineralized tissue, while MacNeal's tetrachrome distinguished the unmineralized tissue. These stains were completed on the defected mandibles of both sham and OVX rats.

STATISTICS

The average food consumption, body weight, and micro-CT results were analyzed by the 2-Tailed Student's T-test and presented as standard error of the mean. Data with an adjusted *P* value < 0.05 was considered statistically significant. To determine new bone regeneration, the BV/TV of the defect relative to the BV/TV of the contralateral side was quantitated and reported as a percentage.

RESULTS

rGO scaffolds support AD-MSC attachment

rGO scaffolds were successfully constructed via the Cellink Biox6 3D printer (Figure 5.1A-D). Each scaffold was produced in ~7 minutes, with dimensions of 5 (L) X 5 (W) X 2 (H) mm, and a highly porous structure (Figure 5.1E/F). To determine cell attachment, we stained AD-MSCs with DiI before seeding onto the rGO scaffold. Confocal imaging revealed the scaffold was confluent with AD-MSCs (Figure 5.1G/H). Overall, this data shows that rGO can (1) be 3D printed for scaffold construction and (2) support cell attachment.

OVX animals have higher body weights than control animals

Pre-surgery, both sham and OVX animals were placed on a low calcium diet for 10 weeks. Within the first four weeks, OVX animals consumed more food than sham animals (Figure 5.3A). However, there were no differences in diet consumption from weeks 5 – 10.

Post-surgery, both sham and OVX animals were placed on a soft food diet. However, we noticed that both animal groups stopped consuming the soft food after 6 weeks. We therefore supplemented a standard chow diet, and weight was either gained or maintained in the subsequent weeks.

On the day of surgery and sacrifice, the average body weight of OVX rats was significantly higher (403 g and 414 g, respectively) than the sham group (313 g and 318 g, respectively) (Figure 5.3B), which is consistent with previous reports [16, 17](MacDonald et al., in review). We also previously established that the average osteoclast activity (CTX-1:TRAP5b) was greater in OVX animals, thereby confirming bone resorption activity within OVX animals (MacDonald et al., in review).

Low calcium diet has no effect on mandibular bone density or structure of sham-operated animals

We first examined if there were any differences in mandibular bone density or trabecular bone architecture of sham animals that were placed on either a standard chow diet (n=5) or a low calcium diet (n=6). Micro-CT data revealed there were no changes in any of the parameters tested (BV/TV, aBMD, tBMD, Tb.N, Tb.Th, Tb.Sp, and connective density) (Table 5.1). Overall, this data is consistent with previous reports that the low calcium diet does not affect bone density or microarchitecture of sham-operated animals [18].

Micro-CT reveals changes in mandibular bone density and structure of OVX animals

We next tested if sham and OVX animals had any changes in mandibular bone density or structure of the control (non-defect) side only. Micro-CT analysis revealed that the control mandibles of OVX animals had less BV/TV, aBMD, TB.N, TB.Th, and more Tb.Sp (Table 5.2). Overall, this data shows that post-menopause bone degeneration does occur in the mandible and is not limited to common weight-bearing regions such as the hip or spine.

rGO-cell constructs support new bone material in both sham and OVX animals

Bone regenerated in all mandible defects, with mean percentages of 32% and 39% for respectively sham and OVX animals, as measured by micro-CT after 60 days (Figure 5.4). Additionally, there was no statistical difference in the BV/TV or aBMD after comparing the average defect-side: nondefect-side between sham and OVX animals (Table 5.3). Finally, no osteonecrosis was observed around the ring of the defect. This suggests that the rGO-cell construct (1) supports new bone regeneration of mandibular

injuries and (2) is not limited by disease status. However, we were unable to conclude if the new mineralization was due to the addition of rGO, AD-MSCs, or both.

To further validate the micro-CT analysis, in vivo results of histological von Kossa and MacNeal's tetrachrome staining highlighted calcium deposits and collagen formation, respectively (Figure 5.5). There was noticeably a cartilage outline within the defect site, suggesting that cells were supported by a porous scaffold structure. Additionally, the area between existing bone and the defect showed cell integration, suggesting cell migration to the construct. However, it should be noted that some rGO particles are mixed within mineralization sites, and therefore it is difficult to accurately quantitate new bone formation. We therefore examined Masson's Trichrome staining and did observe faint green areas within the defect site of both sham and OVX animals (Figure 5.6). This suggested the presence of osteoprogenitors, but are not yet mature osteocytes. Overall, these data suggests that the rGO-cell construct supported mandibular bone regeneration of a critical-sized defect in both sham and OVX animals.

DISCUSSION

The mandible is one of the most proactive bones of the body, vital for eating, talking, and swallowing. Therefore, any traumatic injury of the mandible could be debilitating. The current standard for mandible reconstruction is autologous bone grafts, commonly derived from the fibula [19, 20]. However, this strategy imposes a donor site morbidity, increases the risk of infection, and further yet is infeasible for individuals already undergoing chronic bone degeneration. The alternative, yet undeveloped strategy is regenerative medicine, which focuses on engineering new tissues with 3D-biological materials and stem cell therapies. But alarmingly, in vivo studies of mandibular bone regeneration are limited, leaving few treatment strategies for maxillofacial surgeons.

To study mandibular bone regeneration, we obtained the OVX rat model, which is well established in mimicking post-menopause osteoporosis [9]. However, there are questions surrounding the effects of estrogen deficiency on mandibular bone density. In other words, does post-menopause osteoporosis systematically effect all bones, or does it only effect common weight-bearing regions (i.e., femur, spine, etc.). Miyake et al., 1995 reported that a patient diagnosed with a severe case of post-menopause osteoporosis had defects of both mandibular condyles [21]. Other studies indicate that

osteoporosis of the mandible represents an advanced stage, whereby the disease is preceded in the femur [22]. Further yet, specific anatomical regions of the mandible are more sensitive to osteolytic changes than others [22, 23]. For example, alveolar bone deteriorates more quickly than the mandibular body or condyle [22]. Overall, different laboratories have identified that post-menopause bone degeneration is not limited to weight bearing regions and does affect maxillofacial bones [24-27].

In this study, we established that mandibles of OVX rats had reduced bone density and microarchitectural changes, confirming mandibular bone degeneration (Table 5.2). This is novel as most studies have used the OVX model to focus on osteoporosis of weight bearing regions [28-34]. Additionally, few studies have attempted treating mandible defects with novel regenerative strategies. Leeuwen et al., 2012 created a 5 mm circular defect in the mandibular angle and studied bone regeneration upon implanting membranes composed of collagen, e-PTFE, or a novel, degradable membrane based on poly-(trimethylene carbonate) (PTMC) [35]. It was found that all membrane-treated defects progressively showed new bone formation over 12 weeks. Most recently, Cooke et al., 2020 found that mandible defects treated with 3D-printed LayFomm scaffolds had increased bone mass, greater trabecular thickness, and less trabecular separation in comparison to mandibles that were treated with Norian CRS putty (a calcium phosphate bone cement) [36]. In the OVX model, Jiang et al., 2017 found significant mandibular condyle bone loss, which was in part inhibited by bisphosphonate treatment [37]. Similarly, we created a critical sized mandible defect in both normal adult rats and osteoporotic rats. These defects were immediately filled with a 3D-printed rGO scaffold to both support the defect and deliver stem cells, with the goal of stimulating new bone differentiation. We chose a carbon-based, graphene material as it spontaneously stimulates human MSCs into bone differentiation without any osteo-inductive reagents [7, 8, 38]. This is important as a major goal is to develop bone regenerative treatments that are both cost-effective and with limited side effects. Supportively, graphene materials demonstrate ectopic osteogenesis in vivo, thereby confirming its osteoinductivity at non-bony sites [39]. Finally, graphene materials are under study to not only deliver exogenous stem cells, but also to attract endogenous stem cell migration and differentiation at the injury site. If effective, this strategy would eliminate

the regulatory concerns of stem cell therapies, thereby making graphene scaffolds more clinically feasible.

To design a mandible scaffold, we successfully 3D-printed rGO constructs with consistent morphology and porosity. In tissue engineering, 3D-printing technology is revolutionizing personalized treatment, whereby scaffolds can be immediately produced to match the dimensions of an injury site. Yet, many studies have opted to produce graphene scaffolds by conventional foam techniques which limits consistent control of morphology and porosity [40-45](MacDonald et al., in review). Creating highly porous structures not only facilitates stem cell migration and attachment, but also allows blood vessels to pass through the scaffold and support newly differentiating cells [46-48]. Following 3D-printing construction, we confirmed the rGO scaffold supported cell attachment of human AD-MSCs. The rGO content was 0.5% which has the best mechanical performance (i.e., compressive strength and stiffness) in comparison to higher rGO concentrations at 1% and 3% [49]. Additionally, 0.5% rGO scaffolds demonstrate good cytocompatibility, whereby human AD-MSCs proliferate and remain viable over time [49]. These results are also encouraging as AD-MSCs are a preferred clinical source of stem cells, being much easier to obtain than MSCs derived from bone marrow.

On the day of surgery, rGO-cell constructs were implanted in mandible defects of both sham and OVX rats. During treatment, all animals exhibited healthy behavior and no signs of stress or infection. However, it should be noted that after 6 weeks, our Sprague Dawley animals preferred standard chow over a soft-food diet. Nonetheless, this indicates that animals could comfortably consume a hard-food diet, despite having a mandible injury, which could reduce expenses in future studies.

After 60 days of treatment, the mandibles were harvested for further micro-CT and histological evaluation. Micro-CT analysis showed that all defects had partial bone regeneration when compared to the contralateral, non-defect side. Additionally, the amount of new bone formation between normal adult rats and OVX rats was similar, thereby suggesting rGO-cell constructs are useful in diseased, osteoporotic bone. However, all rats received the same rGO-cell construct, therefore we cannot determine if the new bone regeneration was due to the addition of rGO, AD-MSCs, or both.

Additionally, the AD-MSCs were not tracked, so we could not distinguish between exogenous and endogenous stem cell activity. However, we previously established that MSCs derived from OVX animals lack normal osteogenic potential in comparison to MSCs derived from healthy adult rats (MacDonald et al., in review). Therefore, it is reasonable that implanting exogenous MSCs enhanced a signaling environment for stem cell proliferation and differentiation [50, 51]. In the future, long-term studies are needed to determine the maximum bone differentiation potential of rGO scaffolds, and whether this process should be enhanced with other biological components.

CONCLUSIONS

Post-menopause osteoporotic women are at risk of experiencing traumatic fractures of the mandible. In this study, we developed an osteoporotic rodent model with critical-sized mandible defects and investigated rGO-cell constructs as a candidate for mandibular bone regeneration. We found that rGO-cell constructs supported new bone regeneration of mandibular defects in both normal adult rats and osteoporotic rats, and hence is a potential strategy for reconstructing traumatic jaw injuries. To our knowledge, this is one of the first studies to (1) examine a bone regenerative treatment of osteoporotic mandibles and (2) to test rGO scaffolds in maxillofacial bones. Materials consisting of rGO should be further explored for bone regeneration of mandibular fractures.

ACKNOWLEDGEMENTS

We acknowledge the J.D. Wheat Veterinary Orthopedic Research Laboratory, University of California, Davis, CA and the Ratliff Histology Consultants, LLC, Franklin, TN.

REFERENCES

1. Gulsahi, A., *Osteoporosis and jawbones in women.* Journal of International Society of Preventive & Community Dentistry, 2015. **5**(4): p. 263-267.
2. Ikeo, T., A. Kamada, and S. Goda, *[Osteoporosis and oral biology].* Clin Calcium, 2007. **17**(2): p. 150-6.
3. Sajid, M.A., et al., *Reconstruction of mandibular defects with autogenous bone grafts: a review of 30 cases.* J Ayub Med Coll Abbottabad, 2011. **23**(3): p. 82-5.
4. Alt, V., et al., *An economic analysis of using rhBMP-2 for lumbar fusion in Germany, France and UK from a societal perspective.* Eur Spine J, 2009. **18**(6): p. 800-6.
5. Ferreira Jr, L.H., Jr., et al., *Bisphosphonate-associated osteonecrosis of the jaw.* Minerva Dent Oral Sci, 2021. **70**(1): p. 49-57.
6. Guarneri, V., et al., *Bevacizumab and osteonecrosis of the jaw: incidence and association with bisphosphonate therapy in three large prospective trials in advanced breast cancer.* Breast Cancer Res Treat, 2010. **122**(1): p. 181-8.
7. Newby, S.D., et al., *Functionalized Graphene Nanoparticles Induce Human Mesenchymal Stem Cells to Express Distinct Extracellular Matrix Proteins Mediating Osteogenesis.* International journal of nanomedicine, 2020. **15**: p. 2501-2513.
8. MacDonald, A.F., et al., *Genetic profiling of human bone marrow and adipose tissue-derived mesenchymal stem cells reveals differences in osteogenic signaling mediated by graphene.* Journal of nanobiotechnology, 2021. **19**(1): p. 285-285.
9. Thompson, D.D., et al., *FDA Guidelines and animal models for osteoporosis.* Bone, 1995. **17**(4 Suppl): p. 125s-133s.
10. Yousefzadeh, N., et al., *Ovariectomized rat model of osteoporosis: a practical guide.* EXCLI journal, 2020. **19**: p. 89-107.
11. Wofford, A., et al., *Human Fat-Derived Mesenchymal Stem Cells Xenogenically Implanted in a Rat Model Show Enhanced New Bone Formation in Maxillary Alveolar Tooth Defects.* Stem Cells Int, 2020. **2020**: p. 8142938.
12. Ishaug-Riley, S.L., et al., *Ectopic bone formation by marrow stromal osteoblast transplantation using poly(DL-lactic-co-glycolic acid) foams implanted into the rat mesentery.* J Biomed Mater Res, 1997. **36**(1): p. 1-8.
13. Hildebrand, T., et al., *Direct three-dimensional morphometric analysis of human cancellous bone: microstructural data from spine, femur, iliac crest, and calcaneus.* J Bone Miner Res, 1999. **14**(7): p. 1167-74.
14. Tr, H. and P. Rüegsegger, *A New Method for the Model-Independent Assessment of Thickness in Three-Dimensional Images.* Journal of Microscopy, 2003. **185**: p. 67-75.
15. Odgaard, A. and H.J. Gundersen, *Quantification of connectivity in cancellous bone, with special emphasis on 3-D reconstructions.* Bone, 1993. **14**(2): p. 173-82.
16. Ren, W., et al., *CHANGES OF WNT/B-CATENIN SIGNALING AND DIFFERENTIATION POTENTIAL OF BONE MARROW MESENCHYMAL STEM CELLS IN PROCESS OF BONE LOSS IN OVARIECTOMIZED RATS.* Acta Endocrinol (Buchar), 2020. **16**(2): p. 156-164.
17. Tsai, Y.F., et al., *Long-Term Oral Toxicity and Anti-osteoporotic Effect of Sintered Dicalcium Pyrophosphate in Rat Model of Postmenopausal Osteoporosis.* J Med Biol Eng, 2017. **37**(2): p. 181-190.
18. Gao, X., et al., *Establishing a rapid animal model of osteoporosis with ovariectomy plus low calcium diet in rats.* Int J Clin Exp Pathol, 2014. **7**(8): p. 5123-8.
19. González-García, R., et al., *Vascularized free fibular flap for the reconstruction of mandibular defects: clinical experience in 42 cases.* Oral Surg Oral Med Oral Pathol Oral Radiol Endod, 2008. **106**(2): p. 191-202.

20. Rana, M., et al., *Reconstruction of mandibular defects - clinical retrospective research over a 10-year period.* Head Neck Oncol, 2011. **3**: p. 23.
21. Miyake, M., et al., *A case of osteoporosis with bilateral defects in the mandibular processes.* J Nihon Univ Sch Dent, 1995. **37**(2): p. 108-14.
22. Lee, C., et al., *Site-specific and time-course changes of postmenopausal osteoporosis in rat mandible: comparative study with femur.* Sci Rep, 2019. **9**(1): p. 14155.
23. Tanaka, M., et al., *Effects of ovariectomy on trabecular structures of rat alveolar bone.* J Periodontal Res, 2002. **37**(2): p. 161-5.
24. Du, Z., et al., *Estrogen Deficiency-Associated Bone Loss in the Maxilla: A Methodology to Quantify the Changes in the Maxillary Intra-radicular Alveolar Bone in an Ovariectomized Rat Osteoporosis Model.* Tissue Eng Part C Methods, 2015. **21**(5): p. 458-66.
25. Dai, Q.G., et al., *Ovariectomy induces osteoporosis in the maxillary alveolar bone: an in vivo micro-CT and histomorphometric analysis in rats.* Oral Dis, 2014. **20**(5): p. 514-20.
26. Dai, Q.G., et al., *[Changes of the microarchitecture of alveolar bone due to different duration of ovariectomy: a Micro-CT study in rats].* Shanghai Kou Qiang Yi Xue, 2014. **23**(6): p. 641-5.
27. Johnston, B.D. and W.E. Ward, *The Ovariectomized Rat as a Model for Studying Alveolar Bone Loss in Postmenopausal Women.* BioMed Research International, 2015. **2015**: p. 635023.
28. Zhang, R., et al., *Effect of alendronate on the femoral metaphyseal defect under carbamazepine in ovariectomized rats.* Journal of Orthopaedic Surgery and Research, 2021. **16**(1): p. 14.
29. Zheng, S., et al., *Melatonin Accelerates Osteoporotic Bone Defect Repair by Promoting Osteogenesis–Angiogenesis Coupling.* 2022. **13**.
30. Sakata, M., et al., *Osteoporotic effect on bone repair in lumbar vertebral body defects in a rat model.* J Orthop Surg (Hong Kong), 2018. **26**(2): p. 2309499018770349.
31. Shen, G.-Y., et al., *Effect of osteoporosis induced by ovariectomy on vertebral bone defect/fracture in rat.* Oncotarget, 2017. **8**(43): p. 73559-73567.
32. Tao, Z.-S., et al., *Hydrogel contained valproic acid accelerates bone-defect repair via activating Notch signaling pathway in ovariectomized rats.* Journal of Materials Science: Materials in Medicine, 2021. **33**(1): p. 4.
33. Tao, Z.-S., et al., *Single-dose local administration of parathyroid hormone (1–34, PTH) with β-tricalcium phosphate/collagen (β-TCP/COL) enhances bone defect healing in ovariectomized rats.* Journal of Bone and Mineral Metabolism, 2019. **37**(1): p. 28-35.
34. Wang, J., et al., *CD31hiEmcnhi Vessels Support New Trabecular Bone Formation at the Frontier Growth Area in the Bone Defect Repair Process.* Scientific Reports, 2017. **7**.
35. van Leeuwen, A.C., et al., *Guided bone regeneration in rat mandibular defects using resorbable poly(trimethylene carbonate) barrier membranes.* Acta Biomater, 2012. **8**(4): p. 1422-9.
36. Cooke, M.E., et al., *3D Printed Polyurethane Scaffolds for the Repair of Bone Defects.* 2020. **8**.
37. Jiang, L., et al., *Effects of bisphosphonates on mandibular condyle of ovariectomized osteoporotic rats using micro-ct and histomorphometric analysis.* J Oral Pathol Med, 2017. **46**(5): p. 398-404.
38. Lee, J.H., et al., *Reduced graphene oxide-coated hydroxyapatite composites stimulate spontaneous osteogenic differentiation of human mesenchymal stem cells.* Nanoscale, 2015. **7**(27): p. 11642-51.
39. Șelaru, A., et al., *Graphene-Oxide Porous Biopolymer Hybrids Enhance In Vitro Osteogenic Differentiation and Promote Ectopic Osteogenesis In Vivo.* Int J Mol Sci, 2022. **23**(1).

40. Li, N., et al., *Three-dimensional graphene foam as a biocompatible and conductive scaffold for neural stem cells.* Scientific Reports, 2013. **3**(1): p. 1604.
41. Crowder, S.W., et al., *Three-dimensional graphene foams promote osteogenic differentiation of human mesenchymal stem cells.* Nanoscale, 2013. **5**(10): p. 4171-6.
42. Amani, H., et al., *Three-Dimensional Graphene Foams: Synthesis, Properties, Biocompatibility, Biodegradability, and Applications in Tissue Engineering.* ACS Biomater Sci Eng, 2019. **5**(1): p. 193-214.
43. Tasnim, N., et al., *The Efficacy of Graphene Foams for Culturing Mesenchymal Stem Cells and Their Differentiation into Dopaminergic Neurons.* Stem Cells Int, 2018. **2018**: p. 3410168.
44. Shin, Y.C., et al., *Three-dimensional graphene oxide-coated polyurethane foams beneficial to myogenesis.* J Biomater Sci Polym Ed, 2018. **29**(7-9): p. 762-774.
45. Bahremandi Tolou, N., et al., *A three-dimensional nerve guide conduit based on graphene foam/polycaprolactone.* Mater Sci Eng C Mater Biol Appl, 2021. **126**: p. 112110.
46. Loh, Q.L. and C. Choong, *Three-dimensional scaffolds for tissue engineering applications: role of porosity and pore size.* Tissue Eng Part B Rev, 2013. **19**(6): p. 485-502.
47. Bružauskaitė, I., et al., *Scaffolds and cells for tissue regeneration: different scaffold pore sizes-different cell effects.* Cytotechnology, 2016. **68**(3): p. 355-369.
48. Chiu, Y.C., et al., *The role of pore size on vascularization and tissue remodeling in PEG hydrogels.* Biomaterials, 2011. **32**(26): p. 6045-51.
49. Seyedsalehi, A., et al., *Fabrication and characterization of mechanically competent 3D printed polycaprolactone-reduced graphene oxide scaffolds.* Scientific Reports, 2020. **10**(1): p. 22210.
50. Caplan, A.I., *Mesenchymal Stem Cells: Time to Change the Name!* Stem Cells Transl Med, 2017. **6**(6): p. 1445-1451.
51. Caplan, A.I. and J.E. Dennis, *Mesenchymal stem cells as trophic mediators.* J Cell Biochem, 2006. **98**(5): p. 1076-84.

APPENDIX

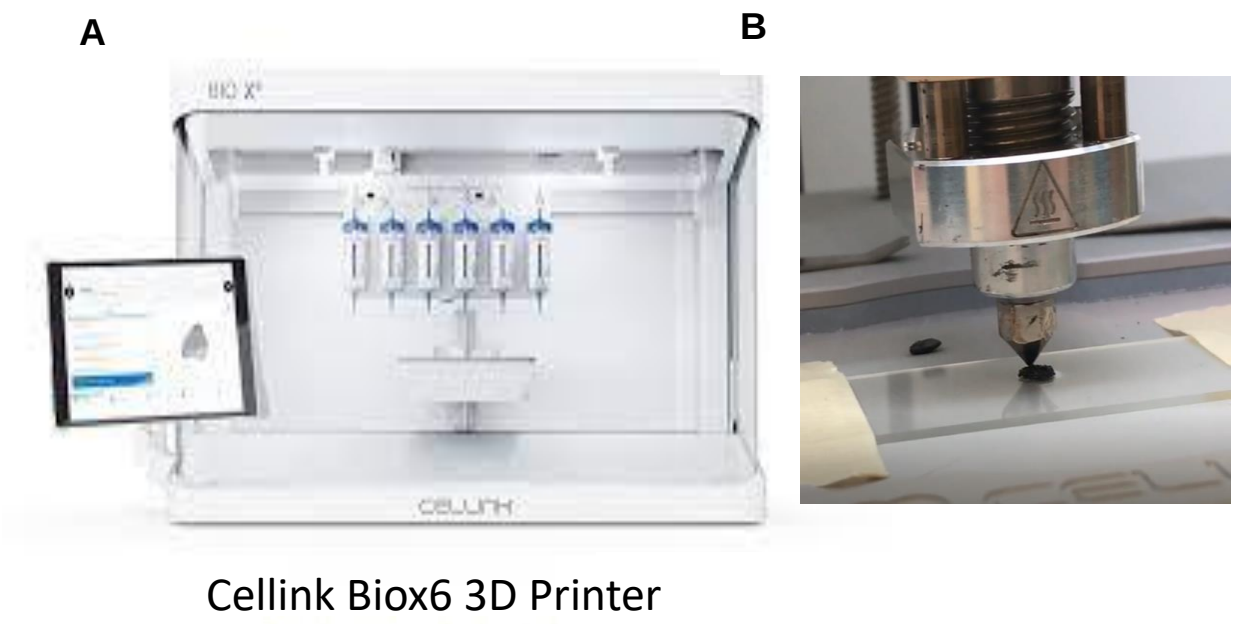

Figure 5.1. 3D Printing of Scaffolds and Cell Attachment. (A) Image of Cellink Biox6 3D Printer. **(B)** Image of printing 3D rGO scaffold. **(C)** Final rGO printed scaffold (top view) and **(D)** side view; white artifacts are due to reflection of camera during photography. **(E)** Confocal Image of AD-MSCs attached to rGO scaffold after 48 hr. Red fluorescence indicates cells stained with DiI.

A

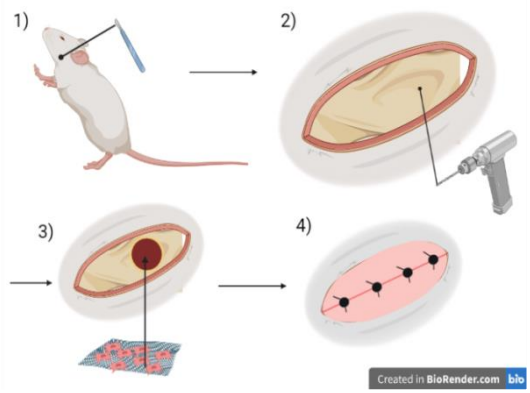

B

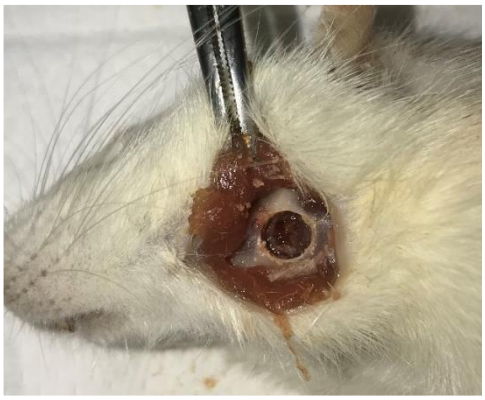

Figure 5.2. Diagram of Surgical Procedure. (A) An incision was made at the mandible area, followed by a circular defect at the mandibular angle. The defect was then filled with AD-MSCs attached to an rGO scaffold, followed by suturing. **(B)** Image of rat cadaver with a mandible defect.

A

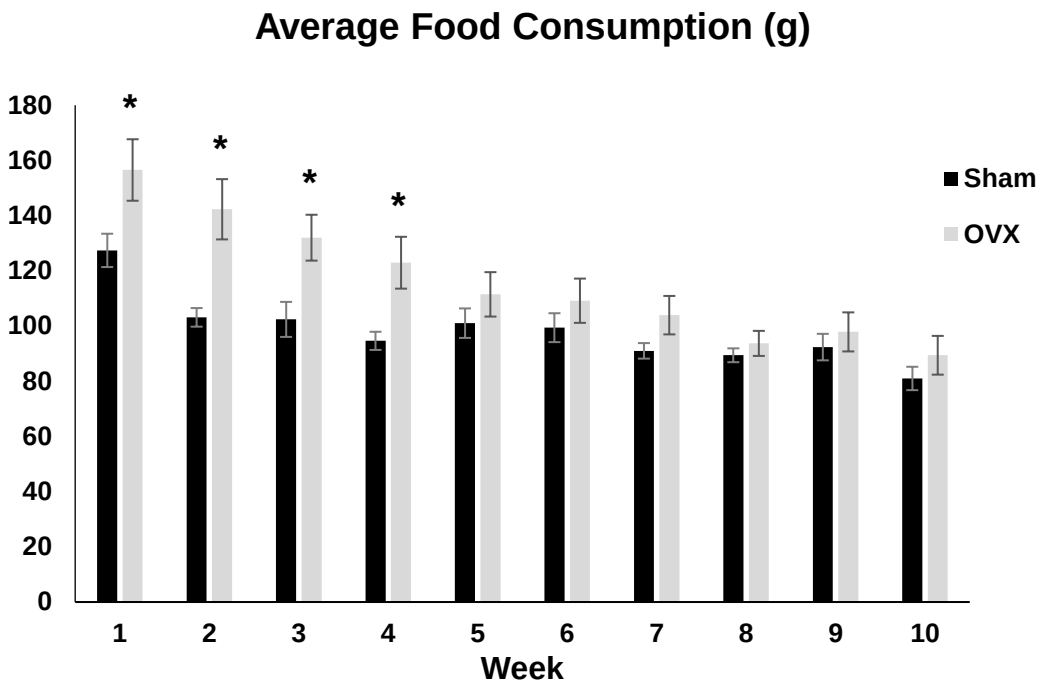

B

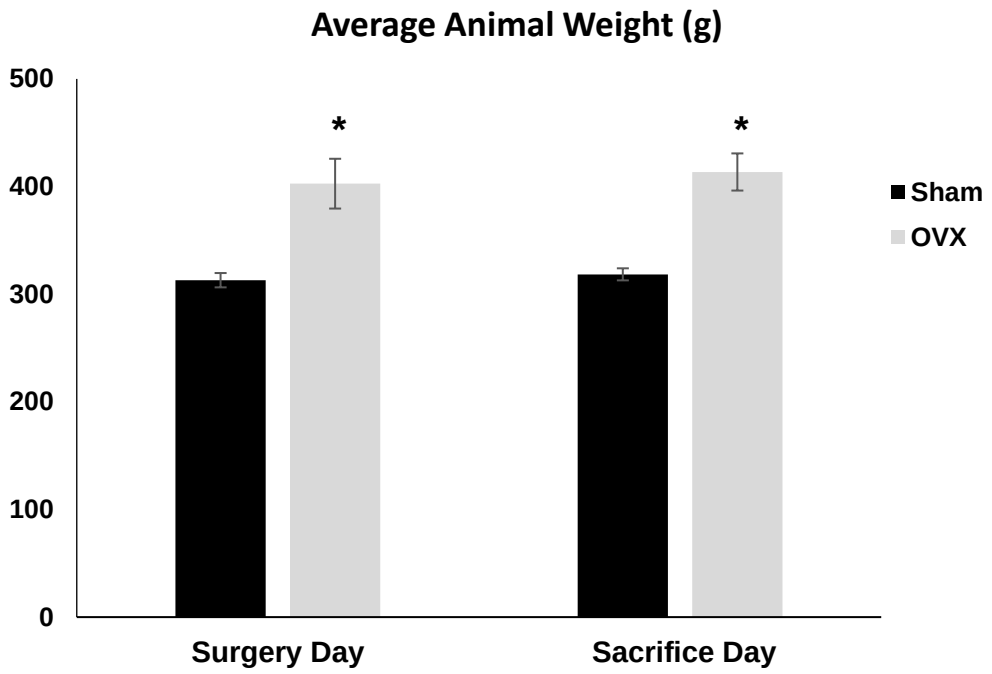

Figure 5.3. (A) Average consumption of low calcium diet between sham (n=6) and OVX (n=6) animals prior to surgery **(B)** Final weight of sham and OVX animals on the day of surgery and sacrifice; asterisk indicates statistical significance ($p<0.05$); error bars presented as SEM.

Table 5.1. Micro-CT analysis of control mandibles (non-defect side) of sham animals consuming either a standard chow diet or low calcium diet. Data presented is the average total volume (TV), bone volume (BV), bone volume/total volume (BV/TV), apparent bone mineral density (aBMD), tissue bone mineral density (tBMD), numbers of trabeculae (TB.N), trabecular thickness (Tb.Th), trabecular separation (TB.Sp), and connective density.

Parameter	Standard Diet	Low Ca2+ Diet	*P*-Value
TV (mm^3)	0.9263	0.9363	0.9554
BV (mm^3)	0.6252	0.5762	0.6121
BV/TV	0.6815	0.6237	0.2978
aBMD (mg HA/ccm)	679.7347	654.0386	0.5601
tBMD (mg HA/ccm)	975.9119	1005.0615	0.0761
Tb.N (1/mm)	6.9581	6.5129	0.5573
Tb.Th (mm)	0.1437	0.1399	0.5880
Tb.Sp (mm)	0.1657	0.1890	0.2984
Connective Density ($1/mm^3$)	103.1047	93.8882	0.6655

Data was analyzed using paired t-tests [n = 5 (standard diet) and 6 (low Ca2+ diet) sham rats).

Table 5.2. Micro-CT analysis of control mandibles (non-defect side) between sham and OVX animals. Data presented is the average total volume (TV), bone volume (BV), bone volume/total volume (BV/TV), apparent bone mineral density (aBMD), tissue bone mineral density (tBMD), numbers of trabeculae (TB.N), trabecular thickness (Tb.Th), trabecular separation (TB.Sp), and connective density.

Parameter	Sham	OVX	*P*-value
TV (mm^3)	0.9363	1.2147	0.3126
BV (mm^3)	0.5762	0.4388	0.1909
BV/TV	0.6237	0.3738	**0.0005**
aBMD (mg HA/ccm)	654.0386	434.8285	**0.0003**
tBMD (mg HA/ccm)	1005.0615	978.8372	0.0998
Tb.N (1/mm)	6.5129	4.0157	**0.0002**
Tb.Th (mm)	0.1399	0.1192	**0.0273**
Tb.Sp (mm)	0.1890	0.2906	**0.0030**
Connective Density ($1/mm^3$)	93.8882	82.7074	0.4466

Data was analyzed using paired t-tests (n = 5 sham and 6 OVX rats).

Table 5.3. Micro-CT results after comparing the average defect side: non-defect side of sham and OVX animals. Data presented is the total volume (TV), bone volume (BV), bone volume/total volume (BV/TV), apparent bone mineral density (aBMD), and tissue bone mineral density (tBMD).

Parameter	Sham	OVX	*P*-value
TV (mm^3)	1.00	0.99	0.3893
BV (mm^3)	0.32	0.38	0.5918
BV/TV	0.32	0.39	0.5547
aBMD (mg HA/ccm)	0.24	0.29	0.6867
tBMD (mg HA/ccm)	1.06	0.98	**0.0378**

Data was analyzed using paired t-tests (n = 5 sham and 6 OVX rats).

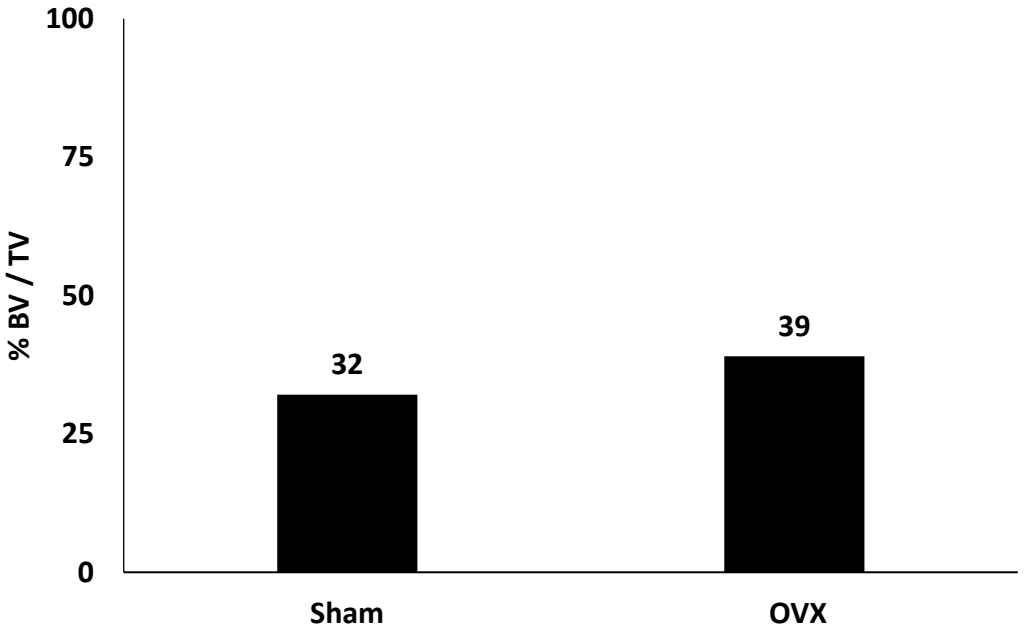

Figure 5.4. Average percentage of newly formed bone within the former defects as measured by micro-CT. For each animal group, the left-sided mandible (normal) served as a control to determine bone regeneration on the right-sided mandible (defect), which was treated with an rGO-cell construct. (n = 5 sham and 6 OVX rats).

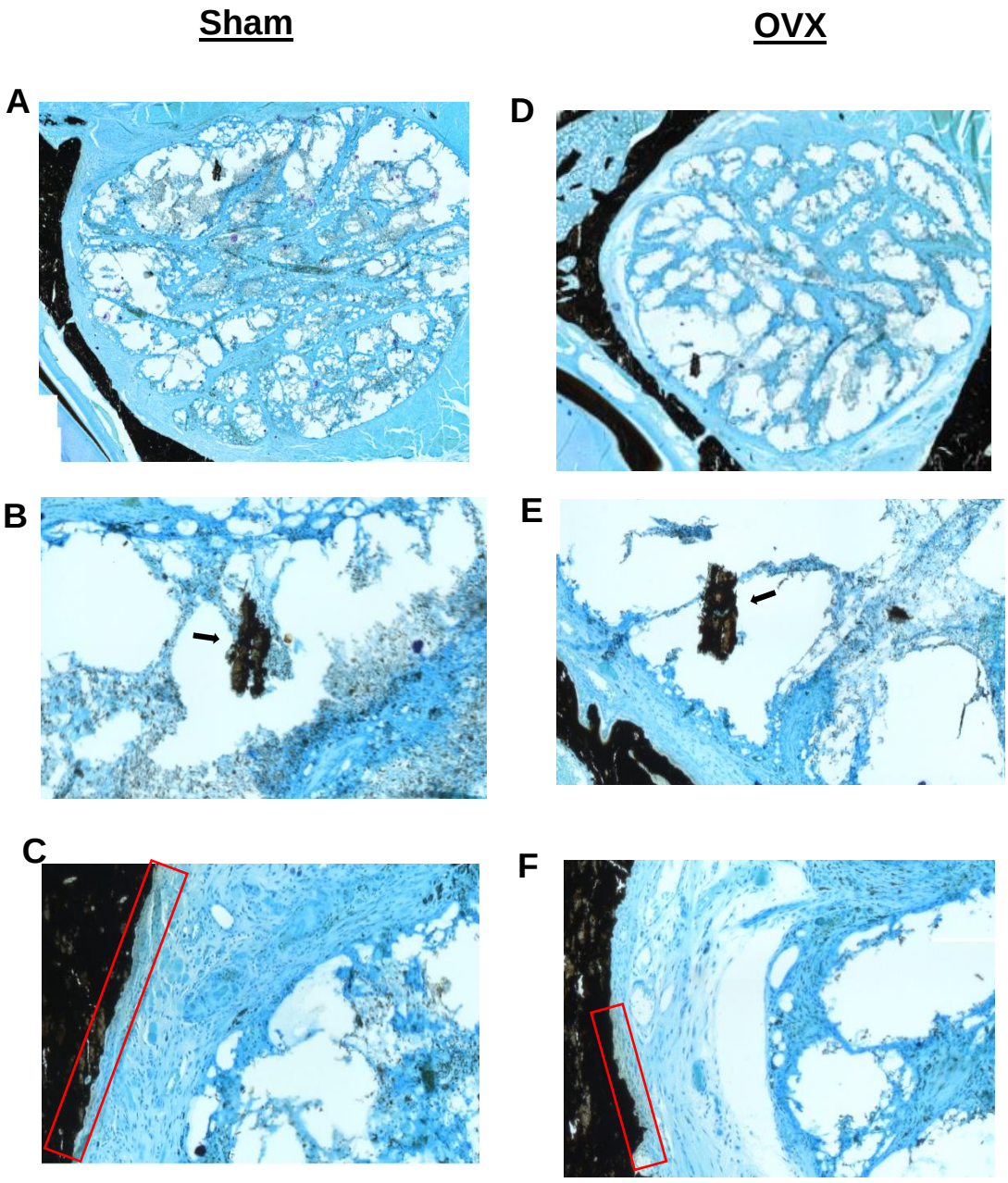

Figure 5.5. Representative von Kossa – MacNeal's tetrachrome staining images of mandibular defects treated with rGO-cell constructs in sham **(A-C)** and OVX **(D-F)** animals. **(A/D)** Image that includes all region of interest. **(B/E)** Region of mineralization, as indicated by black arrows. **(C/F)** Region of cellular integration between original bone and defect site, as indicated by red boxes. All images were taken under 10 X magnification.

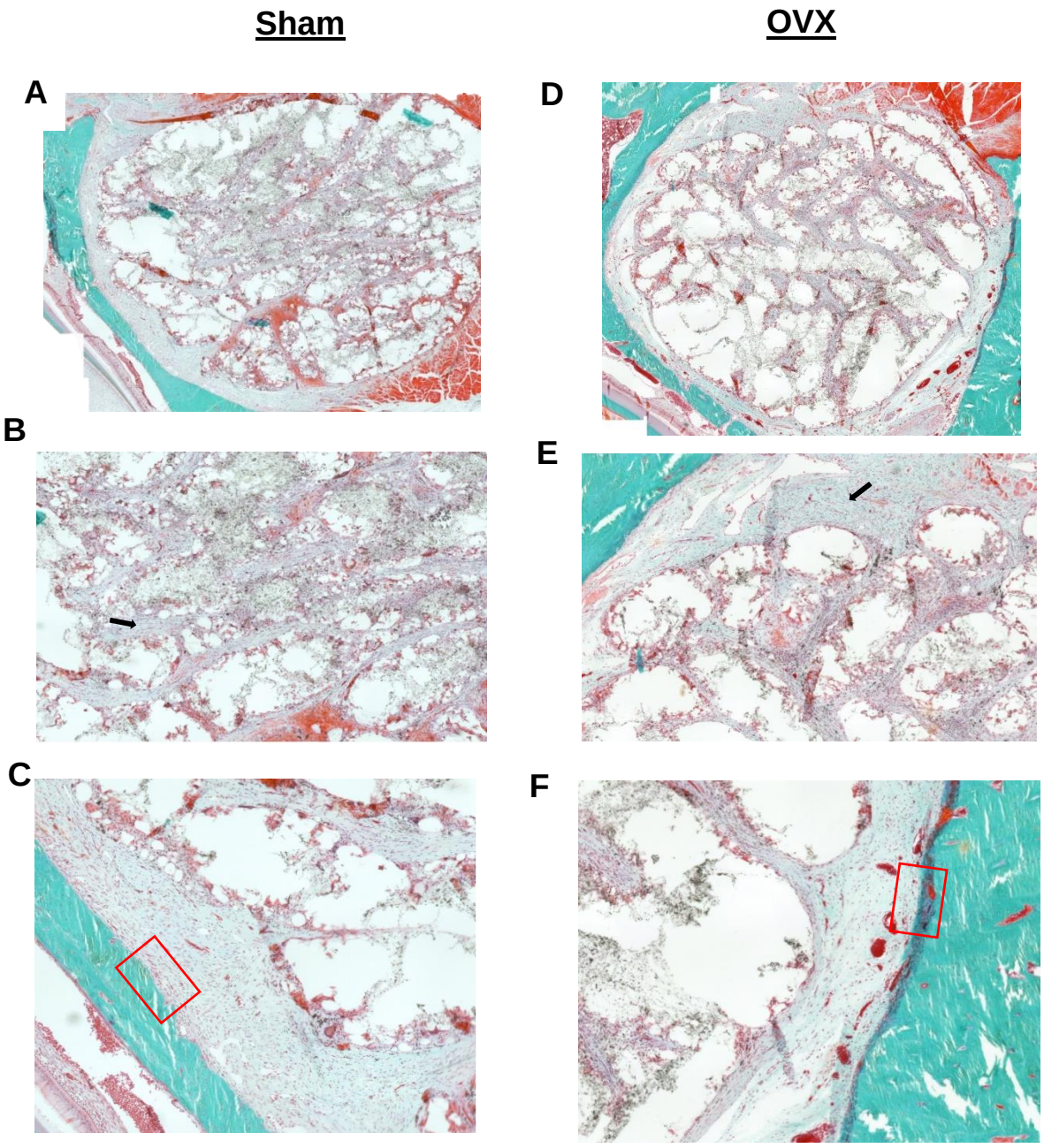

Figure 5.6. Representative Masson's Trichrome staining images of mandibular defects treated with rGO-cell constructs in sham **(A-C)** and OVX **(D-F)** animals. **(A/D)** Image that includes all region of interest. **(B/E)** Region of cells undergoing differentiation, as indicated by black arrows. **(C/F)** Region between original bone and defect site, as indicated by red boxes. All images were taken under 10 X magnification.

VITA

Amber F. MacDonald was born and raised in Beckley, WV to the parents of Macel Tolbert MacDonald and the late, Jack P. MacDonald on September 11th, 1989. She has three older brothers and three nieces. Amber graduated from Woodrow Wilson High School in 2008 and then attended Bluefield College, Bluefield, VA where she played softball and ran cross-country. In 2012, Amber graduated from Bluefield College, Magna Cum Laude with a Bachelor of Science degree in Exercise and Sports Science, concentrating in Sports Medicine. In 2014, Amber moved to Knoxville, TN to pursue a Master of Science degree in Cellular & Molecular Nutrition at the University of Tennessee (UTK), which was completed in 2017. During this time, Amber published four research articles, including a first-author report that studied an herbal supplement against prostate cancer. After finishing her degree, she worked full-time as a Research Assistant at UTK before pursuing a Ph.D. in Comparative & Experimental Medicine, also at UTK. Her research involves tissue engineering strategies for new bone development, using stem cells and biomaterials. So far, she has contributed to three publications, two of which are first-author reports and has been presented at several research conferences. Amber expects to finish her Ph.D. in Summer 2022.